Nanoimprint lithography as an alternative fabrication technique: towards applications in optics

(Die Nanoprägelithographie als eine alternative Technologie im Hinblick auf die Herstellung von optischen Bauelementen)

Im Fachbereich Elektrotechnik, Informationstechnik und Medientechnik der Bergischen Universität Wuppertal genehmigte Dissertation zur Erlangung des akademischen Grades eines

Doktors der Ingenieurwissenschaften

-Dr.-Ing.-

vorgelegt von

Dipl-Ing. Sergiy Zankovych

aus Nikolaev, Ukraine

Referent: Prof. Dr. rer. nat. Clivia M. Sotomayor Torres

Korreferent: Prof. Dr. rer. nat. Ludwig Josef Balk

Tag der mündlichen Prüfung: 04.06.2004

Wuppertal 2004

Hiermit versichere ich, die vorliegende Arbeit selbständig verfaßt und nur die angegebenen Quellen und Hilfsmittel verwendet zu haben.

Wuppertal, den 16. August 2004

Sergiy Zankovych

Abstract

The research work for thesis focuses on one of imprint-based techniques, namely, Nanoimprint Lithography, which relies on the pressing of a stamp into a printable polymer heated above the glass transition temperature. Of particular interest are the potentials of this technique to fabricate devices for optical applications. The general topic of this work is the development of a competitive fabrication process, starting from stamp fabrication up to the demonstration of a finished optical device. Beside process development, considerable attention is paid to the understanding of the physical concepts of printing, potentials and limitations of it, which are due to the material properties on nm-scale, and to the development of new polymers. Considering the key issues and challenges in becoming a competitive fabrication technology, the salient aspects of nanoimprint lithography addressed here are: printable materials, stamps, resolution, adhesion, reproducibility and throughput, among others.

Two kinds of stamps, metal-on-silicon and polymer-based, containing features of dimension controlled on the scale down to 20 nm are fabricated. It is shown that material properties, like the molecule size of used resist and the metal grain size, mainly limit the control of feature size.

The results of printing of number of polymers, like PMMA, PTFE, PS, mr-L 6000, are shown and discussed with respect to the feasibility of the control of feature size. It is shown that size of polymer molecule, i.e., viscoelestic properties, and

the mechanical recovery are a major limiting factor on the nm-scale, which affect both the adhesion to the stamp and the final feature shape.

The investigations of the luminescence properties of multiple quantum well substrates, in particular GaAs/$Al_{0.3}Ga_{0.7}As$ and $Ga_{0.47}In_{0.53}As$/InP, are carried out after being subjected to the nanoimprinting process. No degradation of optical properties is found for printing temperatures below 190°C and pressures up to 200 bar.

The process capabilities of nanoimprint lithography are exemplified here with the fabrication of passive polymer optical elements, such as PMMA diffraction grating and polystyrene-on-silicon oxide rib waveguide.

Contents

CHAPTER 1. INTRODUCTION 1

CHAPTER 2. PRINCIPLES OF NANOIMPRINT LITHOGRAPHY 5

2.1. Process description 5

2.2. Key issues 8

2.2.1. Throughput 9

2.2.2. Validation and standards 12

2.3. Complementary fabrication techniques 13

2.3.1. Electron beam lithography 13

2.3.2. Pattern transfer 18

CHAPTER 3. EQUIPMENT DESCRIPTION 22

3.1. Nanoimprinting machines 22

3.1.1. Small hydraulic press 22

3.1.2. Obducat Nanoimprinter 23

3.2. Scanning electron microscope and lithography module 25

3.3. Atomic force microscope 27

3.4. Optical spectroscopy setup 30

3.4.1. Excitation sources 34

3.4.2. Spectrometers 34

3.4.3. Detectors 35

3.4.4. Cryogenic equipment 37

3.5. Fibre coupling setup 37

3.6. Monochromator setup 37

CHAPTER 4. STAMP FABRICATION 39

4.1. Metal-on-silicon stamps 39

4.2. Polymer stamps 45

4.3. Feature size control 47

4.4. Summary 54

CHAPTER 5. PRINTING RESULTS 56

5.1. NIL model 56

5.2. Imprinting polymers 62

5.2.1. Process development 62

5.2.2. New printable materials 67

5.2.3. Printing small features 69

5.3. Adhesion effects 72

5.4. Summary 78

CHAPTER 6. EVALUATION OF IMPRINT INDUCED EFFECTS ON OPTICAL PROPERTIES 80

6.1. Samples 81

6.2. Experimental details 82

6.3. PL and PLE results 83

6.4. Electrical properties 86

6.5. Summary 88

CHAPTER 7. IMPRINTED PASSIVE OPTICAL DEVICES 89

7.1. Diffraction grating 90

7.2. Waveguides 92

7.3. Summary 96

CHAPTER 8. CONCLUSIONS 98

Acknowledgments 102

References 103

Annex A. List of publications and presentations appearing during this work i

Annex B. Curriculum Vitae vi

Chapter 1. Introduction

Nanoscience and nanotechnology promise to have major implications in next decades and knowledge in this field is growing constantly. Research in the nanometer scale combines such topics as materials science, physics, chemistry, biology, electronics and nano-optics, among others. It is not just the next step of miniaturization but new and unique properties and phenomena are becoming apparent, the understanding of which is one of major driving forces in nanoscience. Another one is to develop fabrication processes suitable for industrial applications. Progress in nanofabrication based on a recently developed ability to build, manipulate and measure structures in the nm-level. Several nanofabrication techniques have been developed over the last few decades in a laboratory environment, at the level of enabling nanofabrication techniques as tools for experiments to understand the underlying science and engineering in the nm- scale. These are, for examples, electron beam lithography, surface probe methods, where an atomic force microscope develops a resist in a liquid environment via current, SCALPEL (scattering with angular limitation projection electron beam lithography),

where the contrast is obtained by scattering of electrons out of the optical system, and ion beam projection lithography. All these techniques are suitable for small volume fabrication of nanostructures and are very time and cost consumable due to its sequential nature.

Recently, a number of imprint based alternative techniques have emerged during the last few years:

(a) Nanoimprint Lithography (NIL) also known as Hot Embossing Lithography (HEL), which relies on pressing a rigid template (stamp) into a heat-softened thermoplastic polymer [1]. This technique will be described in details in Chapter 2 below.

(b) Step-and-Stamp Imprint Lithography (SSIL), which is a sequential variation of NIL, where the stamp is pressed into polymer, then lifted, moved to the next site to make next imprint and so forth [2].

(c) Mold Assisted Lithography (MAL), which relies on the imprinting into a low viscosity monomer or prepolymer fluid precursor and then curing the film inside the mould cavities by thermal heating or UV illumination [3,4].

(d) Step-and-Flash Imprint Lithography (SFIL), which is based on the step-and-repeat sequence and uses the photo-curable, low-viscosity organosilicon precursor [5].

(e) Microcontact Printing (μCP), which relies on the forming of self-assembled monolayers in regions of a substrate that come into contact with the raised features of a polymeric stamp [6].

The big advantage of all these techniques is its parallel character and, therefore, potentially combine high resolution, high throughput and low-cost. Despite much research done in this field, imprint-based techniques as potential industrial nanotechnologies are still in their infancy. Stringent nanofabrication specifications have

to be met in industrially-relevant processes due to manufacturability and reproducibility needs. Thus, several issues need to be explored, such as multilevel capability, alignment, instrumentation, throughput, validation and standards.

This thesis work concentrates on one of imprint-based techniques, namely, Nanoimprint Lithography. Of particular interest are the potentials for the fabrication of devices for optical and opto-electronic applications. The general topic is the development of a competitive process, starting from stamp fabrication up to the demonstration of a finished optical device. Of course, beside process development, a considerable attention will be paid to understand the physical concepts of printing, potentials and limitations due to the material properties on nm-scale and to the development of new polymers.

The thesis is divided in few parts. In Chapter 2 an overview of the basic ideas and principles of nanoimprint lithography is given, as well as the key issues and the complementary fabrication techniques. Chapter 3 describes shortly the equipment used for fabrication, imaging and optical characterisation.

In Chapter 4 the development of stamp fabrication process by means of electron beam lithography and metal lift-off is described. The problem is considered from two points of view: to develop a competitive process to fabricate stamps with nm-features and with nm-accuracy, which includes optimisation of exposure and development steps and new materials; and to explore the limits of materials used with respect to resolution and control of critical dimension.

Chapter 5 will deal with development of printing process, describing results of imprinting on micro- and nano-scale using a number of polymers, which demonstrate the quality of the replicated structures and their fidelity towards the stamp. The

mechanical properties of polymers are discussed highlighting the polymer flow during printing and its temperature dependence. Other important aspects are the printing of very small feature, where polymer recovery plays a significant role, and adhesion effects.

The issue whether nanoimprinting induce defects in the underlying semiconductor substrate is addressed in Chapter 6. This is done investigating luminescence properties of quantum wells substrate subjected to the NIL cycle over wide range of printing temperatures and pressures.

The examples of passive simple polymer optical devices are treated in Chapter 7. A diffraction grating and a rib waveguide for visible range were made by nanoimprinting in one step. Basic characterisations are performed.

Finally, Chapter 8 gives the conclusion and outlook. The list of publication, conference presentations and talks appearing during this work is given in Annex A.

Chapter 2. Principles of nanoimprint lithography

Imprint technology using compression moulding of thermoplastic polymers has been known for several decades, when features sizes above 1 μm have been routinely imprinted in plastics. In 1995 Chou et al. demonstrated for the first time that imprint techniques could be used to fabricate nm-structures in polymers [1]. In this chapter a brief description of nanoimprint lithography (NIL) is given as a potential cost-efficient fabrication technology. Key issues, which may serve the technological demands of nano- and optoelectronics and related areas, are also discussed.

2.1. Process description

NIL relies on the patterning of a thin polymer layer by a stamp under controlled temperature and pressure. Thus, this technique needs: (a) a stamp with the desired nm-range features usually fabricated by, for example, optical lithography and or electron beam lithography and dry etching; (b) material to be printed, for example, a

polymer film; and (c) a printing machine with sufficient control of process parameters like temperature and pressure. Both stamp and substrate, coated with an appropriate polymer, are brought in contact at ambient temperature and heated up (see Fig.2-1). At a temperature above the glass transition temperature (T_g) a pressure is applied and held for several minutes, during which the polymer can flow to fill in the volume delimited by the surface topology of the stamp. After cooling down, demounting and separation of the stamp and substrate take place, usually when both are at a temperature of "just

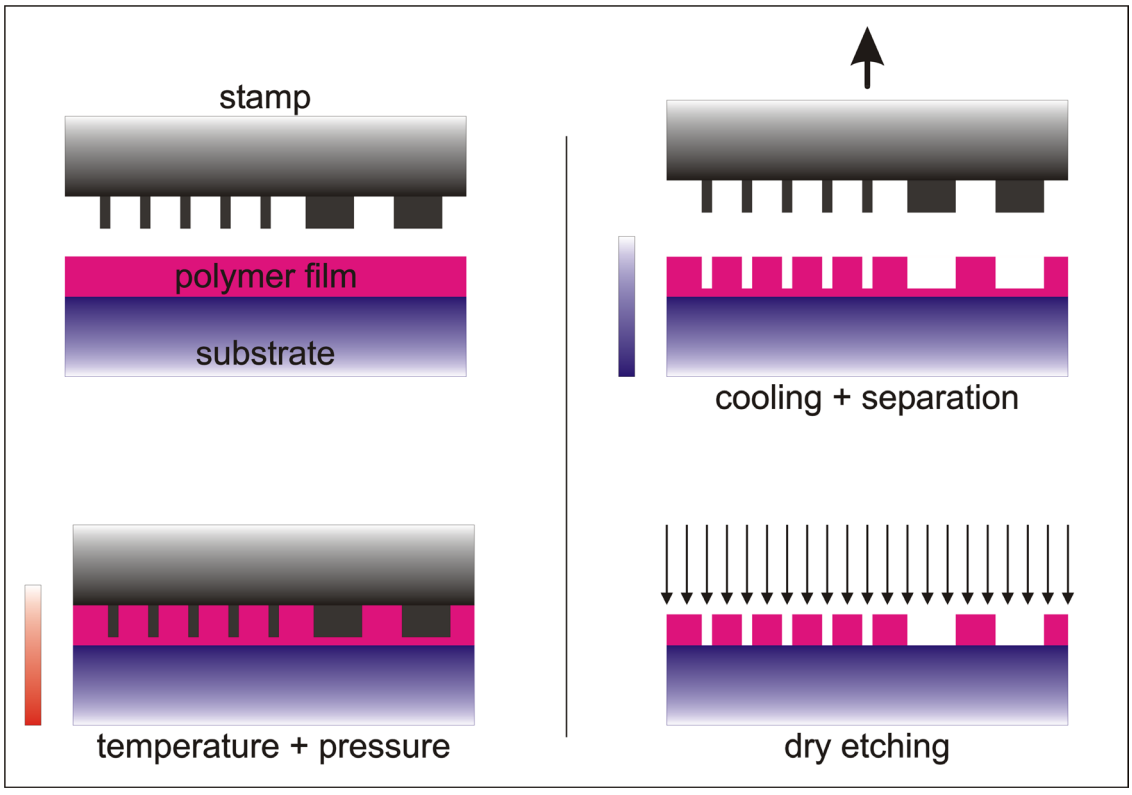

Fig.2-1. Schematics of the nanoimprinting process. The stamp and the substrate are brought in contact. After heating up to the imprint temperature (T_{imp}), the pressure (P_{imp}) is applied and held for several minutes at this temperature. After cooling below glass temperature (T_g), the stamp and substrate are separated. The remaining polymer at the bottom of imprinted features (residual layer) is removed by plasma etching.

under" T_g. The time diagram of temperature and pressure during nanoimprinting is shown schematically on Fig.2-2. The temperature rise time (t1) and the rise time for force (t2) are usually fixed and are defined by construction of press ranging from 10s of seconds up to few minutes. The temperature and pressure hold times, t3 and t3+t4, correspondingly, depend on several factors and are typically in the few minutes regime. The value of pressure lies in the range from 10 to 100 bar and the imprint temperature is usually around 70-90°C above T_g. The typical values of glass temperature for several polymers are given in Table 1. The polymer thickness contrast left on the substrate after printing can be used as: (a) a mask for dry etching, if the imprinted polymer is resistant enough, or (b) a step in a lift off process, or (c) assuming the printed polymer has a functionality (conductivity, optical linear or non-linear response, among others) as a device itself.

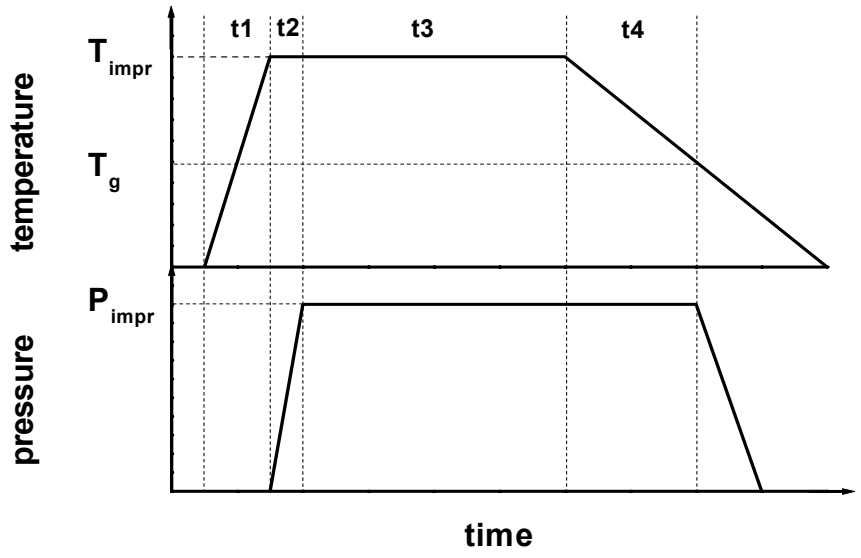

Fig.2-2. Schematical diagram of temperature and force profiles during imprinting.

Table 1. The value of glass transition temperature (T_g) for different polymers.

Polymers	Trademark	Glass temperature, T_g	Remarks
PMMA	AR-P 669.04	95-105	Thermoplastic
Polystyrene	168N (BASF)	110	Thermoplastic
PTFE	Teflon AF1601S	160	Thermoplastic
PPM	mr-I8000	107	Thermoplastic
PDAP	mr-I9000	63	Duroplastic
	mr-L6000	-	UV-crosslinking

2.2. Key issues

There are several key issues, which have to be considered for nanoimprint lithography to make it as a competitive nanofabrication technology. A main criticism levied at imprint lithography is the multilevel issue. For this to be overcome the first step is to develop approaches for in-plane alignment. The target is alignment or overlay accuracy better than 10 nm, at least for VLSI applications. In general, the stamp is considered the functional equivalent of the photo-mask in conventional projection lithography. At present the limit is ~ 1 μm, as shown by the step-and-stamp process, using a commercially available stepper [2]. In first approximation, alignment depends on the stamp size, the thermal and mechanical stability of the polymer during alignment and the choice of stamp and substrate material. Optical alignment techniques are also limited to about 1 μm. Today's instrumentation, which equipped with piezo-drivers for fine positioning and laser interferometer feedback position adjustment, allows a much better precision (down to 5 nm for 6" wafer), as for example laser interferometer stage from Raith GmbH (www.raith.de), however, only at stable temperature. In

nanoimprinting, the thermal effects, which are imprescriptible properties of NIL, bending and specifications of equipment, have to be considered together. An effort has been recently put forward [7] for an alignment system suitable for printing with UV-curing, which combines an adaptive wafer holder with optical detection of diffraction fringes. It is estimated that this approaches could provide an alignment of about 30 nm over 50 mm.

Using an in-house developed printing machine aided by a commercially available aligner and matching the thermal expansion coefficients of stamp and substrate, alignment to within just under 1 μm over a 4" wafer has been demonstrated printing gratings with 100 nm features [8].

Printing experiments carried out in the laboratory are single-level and, therefore, no alignment was needed and the development of instrumentation and alignment capabilities are not the issue in this work.

2.2.1. Throughput

Whereas a working definition of throughput as understood in conventional lithography is still lacking, a rough approximation would consider the actual printing and alignment times, both currently in the range of a few minutes. Then the time required for stamp cleaning and replacement and, if needed, coating with an anti-adhesion layer after a number of prints will all have to be included, although at present these values differ substantially as most results are obtained using non-automated processes. Factors leading to an increase of throughput include:

(f) *Large stamp size.* The stamp size determinates the area to be printed each time. Ideally this will have a size compatible with standard production and process handling.

Potential drawbacks include the parallelism of the wafer given thermal gradients in printing, which can in principle be addressed with a suitably designed printing machine. Recently, 6" wafers have been printed in a compact disc-like production setting. The 6" stamp had representative areas with feature sizes down to 50 nm, separated by several 100s of nm from the next feature [9]. One technique which addresses the large area stamp issue and other factors is Step and Flash Imprint Lithography or SFIL, which has been tested with stamps up to 2" and a test-bed machine for 8" wafers developed [5]. The stamps used during this work are usually 2 x 2 cm^2, which is limited by the specifications of available nanoimprinting machines. These stamps are: silicon stamps with patterned area of 2 x 2 cm^2, or metal-on-silicon and polymer-on silicon stamps, which have several areas of features with size down to 20 nm, thus the patterned area of up to 2.5 x 2.5 mm^2. It will be described in Chapter 4. "Stamp fabrication".

(g) *Stamps with high feature density.* Depending on applications, one of the limits is the flow of the displaced polymer. To date, precise design rules are still under development as far as negative and positive features in a given stamp. In the Step-and-Stamp Imprint Lithography or SSIL variation of printing 150 mm^2 were printed with features of 400 nm separated by 400 nm spaces in 36 consecutive stamping steps [2]. Imprint tests on areas of 200 x 200 μm^2 containing 50 nm features separated by 50 nm spaces are discussed in details in Chapter 5 "Printing results".

(h) *Adhesion.* Ideally, the use of an anti-adhesion layer in the printing process is to be avoided. Much research is in progress to investigate polymers and define processing windows, which make the use of an anti-adhesion layer redundant. Here the choice of printing temperature, of the visco-elastic properties of the polymer and the interfacial energy between polymer and substrate and between polymer and stamp are among the

key factors [10]. This issue is one of the objects of investigation in this work and will be addressed in Chapter 5 “Printing results”.

(i) *Curing.* If curing the polymer is necessary, then reduction of the curing time is important. The aim here is to move away from a curing step, either by temperature or UV illumination, unless (i) it takes place in combination with another nanofabrication technique, which would then compensates for the extra time, or (ii) it adds flexibility to the process [11]. Such flexibility could be the result of the use of bi- or tri-layers of polymers with different printing and curing behaviour.

(j) *Printing temperature and pressure.* Both parameters should be as low as possible in view of the time needed for temperature and pressure cycling. Current research in polymers suitable for printing has yielded two new polymers, which are commercially available from mrt GmbH for printing (www.microresist.de). These are mrI-8000 and mrI-9000, having a glass temperature of 107°C and 63°C, respectively. Other specifications are available from the suppliers. At present the knowledge base is not sufficient to have a fixed window of parameters, as medium term mechanical recovery of sub-20 nm features, has not been systematically studied. Pressure is less important, as its application takes a minute or so. More significant may be the rate at which pressure is increased, again with respect to the mechanical recovery of the polymer [12].

(k) *Stamp lifetime.* This issue has not been explored to its limits because most tests take place in a laboratory environment and are non-automated. Manually controlled experiments reported up to 36 times using a Flip-chip bonder [13]. One aspect, which merits attention, is the possibility to use printing to fabricate or replicate stamps. This approach has been recently investigated [14,15] showing that using a thermoset polymer in its pre-polymer state, subsequently followed by thermal cross-linking, stamps with 400 nm features has been successfully replicated.

2.2.2. Validation and standards

Other aspects affecting all technologies are validation and standards. Standards depend strongly on design rules and it is too early to expect definitive statements for nanoimprint techniques. Validation, or the quality control issue, needs agreement as to what counts as tolerances for a good print. Optical diffraction techniques lend themselves to monitor the quality of periodic structures, but there is a gap in fast quality control methods for printing.

Recently, the first attempt to use the fluorescence spectroscopy as a fast quality control routine for the inspection of the stamps was made [16]. The presented method is based on a fluorescence microscope coupled with a digital imaging system giving a spatial resolution around 500 nm. A standard polymer for nanoimprinting mrI-8000 was labelled with a fluorescent dye, which did not affect the printing behaviour of the polymer. The fluorescent dye helped to detect polymer particles of lateral size down to 100 nm. The quality of a stamp is related to the amount of sticking polymer residues per unit area. Changes in the area of the stamp covered with polymer as a function of the number of imprints could be summarised in a statistical process chart. The method was tested with two different types of stamps: silicon and polymer stamps with features down to 30 nm. For both stamps, the self-cleaning phenomenon was detected and monitored: in the beginning of the process, as well as after artificially inducing adhesion, severe sticking was noticed, which disappeared after the third printing steps. Potentially, in an industrial environment a 4” stamp could be inspected for a few minutes. In addition to the quality control of the stamp surface the method has the potential to inspect and examine imprints. Since the experimental set-up allows a non-contact assessment of the whole stamp surface without additional sample

preparation, serial measurements can be performed easily and this method could be easily adapted to the nanoimprint process.

2.3. Complementary fabrication techniques

Nanoimprint lithography is not a self-contained technique. First of all stamps with nanometer features have to be fabricated. This can be done by UV-lithography, for micrometer and sub-micrometer features over large area, or electron beam lithography, if features below 200 nm are needed. After imprinting, polymer relief may be required to be transferred to the substrate by metal lift-off or dry etching, if the printed polymer is to be used as an etch mask to fabricate semiconductor devices. In the following the key points, achievements and limits of EBL and lift-off are described.

2.3.1. Electron beam lithography

Electron-beam lithography (EBL) is the most developed of the nanofabrication processes and the most practical and widely used direct pattern generation technique to date in the nanometer regime. EBL is a technique for creating the extremely fine patterns required by the modern electronics industry for integrated circuits. Derived from the early scanning electron microscopes, the technique in brief consists of scanning a beam of electrons across a surface covered with a resist film sensitive to those electrons, thus depositing energy in the desired pattern in the resist film. With computer control of the position of the electron beam it is possible to write arbitrary structures onto a surface, ranging from <10 nm to several micrometers.

The main characteristic of this technology are: (a) it is capable of very high resolution; (b) it is a flexible technique that can work with a variety of materials; (c) it is slow, being one or more orders of magnitude slower than optical lithography; and (d) it is expensive and rather complicated. The first electron beam lithography machines, based on the scanning electron microscope (SEM), were developed in the late 1960s. Shortly thereafter came the discovery that the common polymer PMMA (polymethyl methacrylate) made an excellent electron beam resist [17]. It is remarkable that even today, despite sweeping technological advances, extensive development of commercial EBL, and a myriad of positive and negative tone resists, much work continues to be done with PMMA resist on converted SEMs.

Electron-beam lithography using organic polymer resists uses the same pattern definition technique used by optical lithography in integrated circuit production as illustrated in Fig.2-3. In this process, a radiation-sensitive thin film, conventionally an organic polymer, is used as a pattern definition medium, or resist. The substrate is first coated with a thin layer of resist by spin coating, followed by the selective exposure of the resist by a focused electron beam. After being irradiated, chemical reactions and physical changes occur in the resist. The exposed areas have a different solubility than the unexposed parts in a suitable solvent (developer). The more soluble part can be removed selectively in the development stage so a pattern is obtained in the resist film, which can then be used as a mask for transferring the pattern to the substrate. There are two types of resists: positive resist where the electron-beam irradiated part becomes more soluble, and negative resist where the electron-beam irradiated part becomes less soluble.

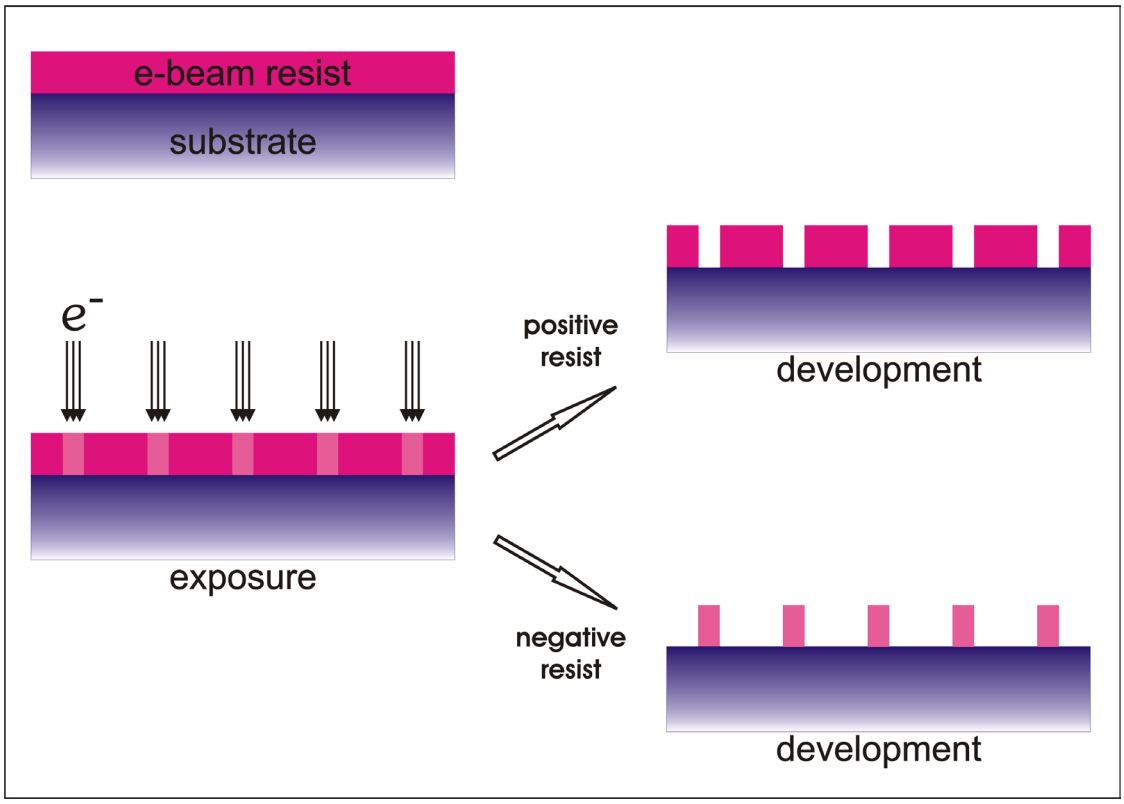

Fig.2-3. Electron beam lithography process. The substrate is coated with a thin layer of electron sensitive film (resist). The desired structure is exposed to a certain dose of electrons. The exposed area changes its solubility in the developer. After development, the written pattern is revealed in the film.

Although electron beam lithography tools are capable of forming extremely fine probes, things become more complex when electrons impinge upon the resist. As the electrons penetrate the resist, they experience many small angle scattering events (forward scattering), which tend to broaden the initial beam diameter. As the electrons penetrate through the resist into the substrate, they occasionally undergo large angle scattering events (backscattering). The backscattered electrons cause the "proximity effect", where the dose received by a pattern feature is affected by electrons scattering from other features nearby. During this process the electrons are continuously slowing down, producing a cascade of low voltage electrons called secondary electrons. These electrons may return back through the resist at a significant distance from the incident beam, causing additional resist exposure.

Many different schemes have been devised to minimise the proximity effect [18]. If a pattern has fairly uniform density and linewidth, all that may be required is *to adjust the overall dose* until the patterns come out the proper size. This method typically works well for isolated structures. Using *higher contrast resist* can help minimise the linewidth variations. *Multilevel resist*, in which a thin top layer is sensitive to electrons and the pattern developed in it is transferred by dry etching into a thicker underlying layer, reduce the forward scattering effect, at the cost of an increase in process complexity. *Higher beam voltages* also minimise forward scattering, although this can increase the backscattering. By going to *very low voltages*, where the electron range is smaller than the minimum feature size, the proximity effect can be eliminated. The penalty is that the thickness of a single layer resist must also be less than the minimum feature size. The most common technique of proximity correction is *dose modulation*, where each individual shape in the pattern is assigned a dose such that written pattern reveal at its desired size. The calculations needed to solve the shape-to-shape interactions are computationally very time consuming. A computationally similar approach is *pattern biasing*. In this approach the extra dose that dense patterns receive is compensated by slightly changing their size [18].

In electron beam lithography, a thin resist layer and a high electron acceleration voltage are normally used to reduce the effect of forward scattering of electrons in the resist. It was demonstrated that sub-20 nm structures can be fabricated in PMMA resist on thin-membrane substrates [19]. A thin resist layer was used to reduce the forward scattering of electrons, and a membrane substrate was used to reduce the backscattering of electrons. Although thin membranes are very useful for resolution studies, most technological applications, e.g., in case of stamp fabrication in nanoimprint lithography, require the use of solid substrates rather than electron-transparent membranes. Usually

the resolution on solid substrates is worse than that on thin substrates, where the limitations imposed by the forward and backward scattering are substantially overcome. In solid substrates the "proximity effect" becomes severe, when the size of the structure is comparable with the scattering range of electrons. However, for isolated structures in the nanometre regime, the range of electron backscattering becomes much larger than the size of the structures so it will not so much affect the resolution as enlarges the exposure time. Using a tri-level resist, which separates the thin layer of high-resolution PMMA resist from the substrate, 25 nm metal structures were produced [20]. Recently, it was demonstrated that by carefully controlling the development process even smaller isolated structures can be fabricated in PMMA resist. A 7 nm wide monogranular lines were obtained after lift-off of a 3 nm thick pure gold granular film [21,22]. It was suggested that the intermolecular forces between the PMMA molecules and resist swelling during development limit the minimum structure achievable in experiments.

Thus, conventional EBL is the most versatile tool in nanostructure fabrication and is the natural choice to fabricate stamps for nanoimprinting. Some limitations of demonstrated processes, like feature density in multi-level process, aspect ratio after pattern transfer, control of feature size and shape etc., still have to be overcome. The ultimate resolution of the technique is believed to be limited by the molecular size of the resist, the delocalised range of scattered electrons and secondary electrons in the resist and, probably, by the intermolecular forces during development process. Because of this resolution limit, researchers began to look for other resists with higher resolution, which is also one of the aims of this work.

2.3.2. Pattern transfer

One of the purpose of producing high-resolution patterns in resists is to use the resulting pattern as masks to fabricate nanostructures in solid substrates, although in rare instances the pattern in the resist may be the main purpose of lithography. The most practical and versatile method of nanofabrication to date has been the planar method employing electron-beam lithography and, more recently, nanoimprinting to make patterns in organic resists. The many ways of utilising the patterns as masks to fabricate structures in solid substrates can be categorised into two main types of pattern transfer methods: subtractive and additive. Subtractive methods employ different types of wet or dry etching techniques, and additive methods include electroplating and metal deposition followed by lift-off. These processes are described schematically in Fig.2-4.

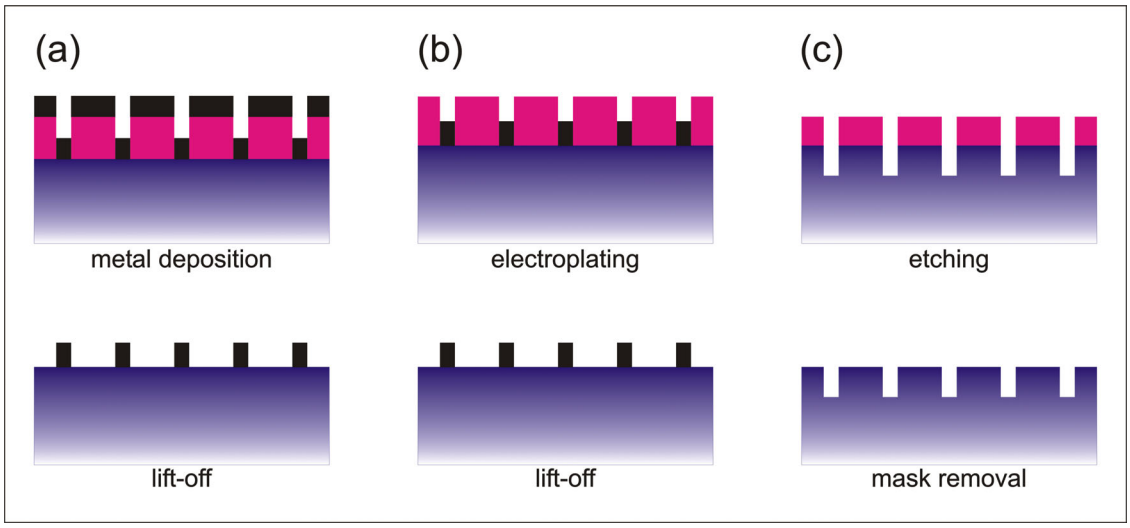

Fig.2-4. Pattern obtained in polymer film by EBL or NIL can be transferred using (a) deposition, (b) growth or (c) etching.

The lift-off technique is often used for the delineation of very high-resolution metal patterns. The process is described schematically in Fig.2-4a. A substrate is coated with a layer of resist and a pattern is defined in the resist using one of the pattern

formation techniques. The substrate with the patterned resist layer is placed at some distance away from a metal evaporation source. The metal is evaporated by means of thermal evaporation or other evaporation methods and deposited over the entire substrate. If the resist has an undercut or vertical profile, there will be no connecting material between the desired metal pattern and unwanted metal that lies on the surface of the resist. Stripping off the resist in a suitable solvent leaves only the desired metal pattern on the substrate. The lift-off process can be successful only when there is an undercut in the resist pattern or when the resist pattern has a straight sidewall and the thickness of the material to be deposited is much less than the thickness of the resist. A ratio of 3:1 between the thickness of the resist and that of the metal is usually enough for successful and reliable lift-off in the case of thick resists (>100 nm). For thinner resists, the ratio has to be increased to obtain successful lift-off.

The lift-off technique has been successfully used to produce metal structures of lateral sizes less than 20 nm. In [19] was shown that metal lines as narrow as 17 nm can be fabricated on membrane substrates by the lift-off method with electron beam lithography and PMMA resist. On solid substrates the resolution is usually poorer due to the effect of backscattered electrons from the substrate. However, structures with lateral sizes similar to those obtained on membrane substrates can be fabricated if the layout of the pattern is chosen such that the backscattered electrons can only generate a background exposure and reduce the contrast but no affect the resolution. In [23] was demonstrated that metal lines down to 10 nm in width can be made on solid substrates. Electron energies ranging from 20 to 200 keV were used in the experiment and it was shown that higher electron energies improve process latitude. More recently, monogranular gold lines as narrow as 5 nm have been obtained [22].

The resolution of transferred patterns is usually determined by the resolution of the resist. As the best resolution is obtained with thin resist and the thickness of metal has to be thinner than that of resist, the aspect ratio of the resulting metal pattern cannot be high for successful lift-off if only a single layer of resist is used: for example, in the experiment of [19] the thickness of the metal film was only a few nanometers. Even in this case, some part of the metal failed to lift-off. To improve the quality of lift-off and to obtain higher aspect ratio patterns, multiple-layer resists consisting of a thin imaging layer on top of thicker underlayers can be used to create an undercut profile. The resolution of the resist pattern is then determined by the thin imaging layer. In this way a high resolution as well as high aspect ratio can be achieved.

Several stages are usually needed to develop multilayer resists. More reliable and easier processes can be obtained if both layers can be exposed with a single exposure and developed with one development step. Double-layer PMMA resist approach with a low molecular weight resist at the bottom and a high molecular weight resist as the top layer is one example. The dissolution rate of PMMA resist is a function of its molecular weight in a given developer. The dissolution rate of lower molecular weight resist is higher than that of higher molecular weight resist; and higher molecular weight resist has a higher resolution. The difference in dissolution rate results in an undercut pattern profile in the resist after development while at the same time maintaining a high resolution.

In comparison with the lift-off method, where vacuum deposition equipment is needed, electroplating (Fig.2-4b) is much simpler and less expensive. Electroplating is essentially a process of electrolytic deposition of metal from a solution and there are two basic variants: electrolytic and electroless. With electrolytic deposition, the surface on which the metal is to be deposited is used as the cathode and deposition occurs when

the metal ions travel under the influence of the electrical field in the aqueous solution of metal salts. A DC voltage is applied between the substrate and the metal to be deposited. The deposition rate can be controlled by the current density in the bath. The electroless process is a technique for deposition through the catalytic action of the deposit itself, without the use of a source of external current. Electroless deposition of gold, platinum, and nickel has been used in nanostructure fabrication. It is necessary to have a conducting substrate to enable the plating process and in many cases the plating base must be removed after plating. These shortcomings limit the range of its application. However, this process does have certain advantages over the lift-off technique, such as in the fabrication of very high aspect ratio structures. Using electron beam lithography and electroplating, arrays of Ni pillars of 35 nm diameter and 120 nm height on 100 nm pitch were fabricated [24]. One of the problems associated with electroplating is end-point detection. The deposition rate cannot be easily controlled, so it is necessary to develop an in situ end-point detection system that can be used to determine the optimum electroplating time.

Chapter 3. Equipment description

3.1. Nanoimprinting machines

The following nanoimprinting machines are constructed to meet the requirements of NIL process, as described in section 2.1 above, which includes the needs to heat up the sample and the stamp, apply a pressure and cool down with satisfactory control of temperature and pressure.

3.1.1. Small hydraulic press

Several imprints reported here were made using a small *hydraulic press* cooled by oil (Fig.3-1). Sample and stamp are placed between two thick metal plates. These can be heated up to 240°C and the pressure can be stabilised manually between 20 and 200 bar. The time required for one cycle (heating, cooling, separation) is between 10 and 30 min, depending of imprint temperature and the temperature at which the stamp is

separated from the substrate. The size of stamps is limited to 2 x 2 cm^2 in this equipment. The disadvantages of this equipment are long cycling time, poor temperature control and insufficient parallelism between stamp and substrate.

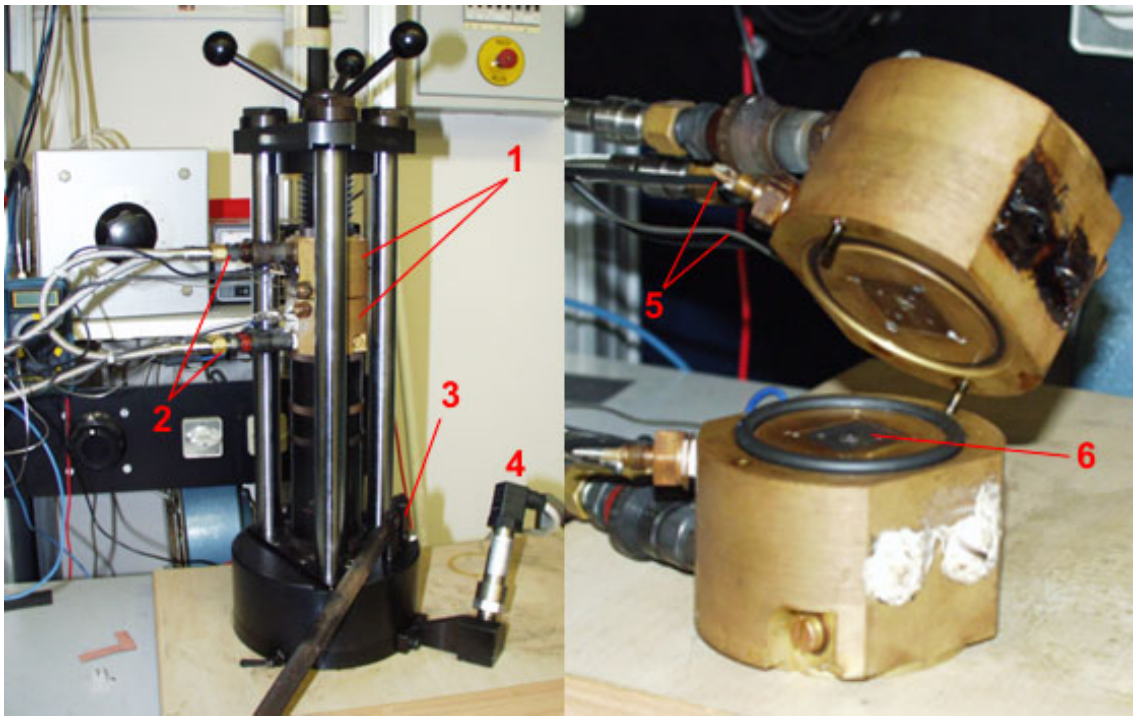

Fig.3-1. Hydraulic press. (1- metal plates, 2- radiator hose, 3- manual oil pump, 4- pressure measurement unit, 5- connections to the heater and thermometer, 6- space, where the stamp and the sample are placed, one on the other, during printing).

3.1.2. Obducat Nanoimprinter

Another press used in this work is the *Obducat 2.5" Nanoimprinter* machine (Fig.3-2), which allows imprinting on any stamp and substrate size up to 2.5 inch in diameter. This equipment is optimized for replication of small series structure on, for example, Si, GaAs and InP substrates, as well as on polymers, ceramics and metal substrates.

The heater of the press provides uniform heating of the substrate over a wide range of temperatures, making it possible to use any thermoplastic materials. Moreover,

it has the ability to be heated up to 250°C and the pressure can be established automatically between 5 and 70 bar. The time required for one cycle (heating, cooling, separation) is approximately 25 min, depending on the imprinting temperature and on the temperature at which the stamp is separated from the substrate.

The unique feature of the press is that the pressure is applied to the stamp without any rigid piston (soft press). For thin stamps (150-300 μm) this feature practically excludes effects of stamp/substrate thickness variation or waviness. For instance, with a substrate waviness of ~5 μm it is possible to achieve ~20 nm variation of resist thickness in the imprinted area.

Fig.3-2. Obducat 2.5" Nanoimprinter. (1– base-plate with heater, 2- space, where the stamp and the sample are placed, one on the other, during printing, 3- upper part with gas volume and membrane, 4- hose with cooling air).

3.2. Scanning electron microscope and lithography module

The Scanning Electron Microscope (SEM) is one of the most versatile and widely used tools of modern science and designed for direct studying of the surfaces of solid objects. In the SEM, the image is formed and presented by a very fine electron beam, which is focused on the surface of the specimen. The beam is scanned over the specimen in a series of lines and frames called a raster, just like the electron beam in an ordinary television. The raster movement is accomplished by means of small coils of wire carrying the controlling current (the scan coils). At any given moment, the specimen is bombarded with electrons over a very small area. These electrons may be elastically reflected from the specimen, with no loss of energy, they may be absorbed by the specimen and give rise to secondary electrons of very low energy, together with X-rays, they may be absorbed and give rise to the emission of visible light (an effect known as cathodoluminescence) and they may give rise to electric currents within the specimen. All these effects can be used to produce an image. The most common is image formation by means of the low-energy secondary electrons.

The secondary electrons are selectively attracted to a grid held at a low (~50 V) positive potential with respect to the specimen. Behind the grid is a disc held at about 10 kV positive with respect to the specimen. The disc consists of a layer of scintillant coated with a thin layer of aluminum. The secondary electrons pass through the grid and strike the disc, causing the emission of light from the scintillant. The light is led down a light pipe to a photomultiplier tube, which converts the photons of light into a voltage. The strength of this voltage depends on the number of secondary electrons that are striking the disc. Thus the secondary electrons produced from a small area of the specimen give rise to a voltage signal of a particular strength. The voltage is led out of

the microscope column to an electronic console, where it is processed and amplified to generate a point of brightness on the screen. An image is built up simply by scanning the electron beam across the specimen in exact synchrony with the scan of the electron beam in the cathode ray tube [18].

The SEM does not contain objective, intermediate and projector lenses to magnify the image as in the optical microscope. Instead magnification results from the ratio of the area scanned on the specimen to the area of the television screen. Increasing the magnification in an SEM is therefore achieved quite simply by scanning the electron beam over a smaller area of the specimen. This description of image formation in the SEM is equally applicable to elastically scattered electrons, X-rays, or photons of visible light, except that the detection systems are different in each case. Secondary electron imaging is the most common because it can be used with almost any specimen.

Scanning electron microscopy is also a part of electron-beam lithography (EBL) systems, which in brief consists of scanning a beam of electrons across a surface covered with a resist film sensitive to those electrons, thus depositing energy in the desired pattern in the resist film. With computer control of the position of the electron beam it is possible to write arbitrary structures onto a surface, ranging from <10 nm to several micrometers, as described in section 2.3.1 above.

The scanning electron microscope used in the laboratory for imaging and electron beam lithography is a *Philips XL30S FEG* equipped by *RAITH ELPHI-Plus* attachment system. Key system parameters are:

- Filament Type: Schottky Thermal Field Emission
- Acceleration Voltage (HV): 200 V – 30 kV
- Probecurrent Range: 2 pA – 300 pA

- Resolution: 1.5 nm at HV >10 kV and 2.5 nm at HV<10 kV
- Writing Field Size: Variable 0.5 μm – 800 μm (magnifications from x50 up to $x10^6$ with accuracy <3%)
- Exposure Step Size: Write Field / 65536
- Writing Speed: 2.6 MHz area mode, <10 ns resolution
- Current Stability: < 0.5 % per hour
- Automatic Stage: 2 nm resolution (0.5 nm optional)
    - Sample Handling: Full 2" wafer capability
    - Working Distance: Variable 2 – 12 mm
    - Reproducibility: <3 μm
    - Position drift: < 10 nm/min

The *RAITH* equipment attached to the SEM is used for electron beam lithography, while the electron beam is controlled by external scan generator and the ELPHY Plus software to generate the pattern to be written. In addition, it is used for alignment of the write field and alignment of pattern on the wafer. This equipment allows alignment and exposure of features 2000-4000 times smaller than the size of the scan field.

3.3. Atomic force microscope

Since the invention of atomic force microscopy (AFM) in 1986 by [25], it has rapidly developed into a powerful and invaluable surface analysis technique on micro- and nanoscales and even on atomic and molecular scales. The AFM is an offspring of the scanning tunnelling microscopy (STM). Early on in the development of STM it became evident that relatively strong forces act between a tip in close proximity to a

sample. These forces can be classified by their range and strength: van-der-Waals, electrostatic and magnetic forces with a long rage (up to 100 nm) and chemical forces with a short range (fraction of nm). These forces could be put to good use in atomic force microscope. Forces between the tip and sample are typically measured by recording the deflection of a cantilever beam, which has a tip mounted to its end. Today's techniques use optical (interferometer, beam-bounce) or electrical (piezoresistive, piezoelectric) methods for measuring the cantilever deflection. In traditional contact AFM the force translates into a deflection of the cantilever, while the force is kept constant. At the moment besides contact mode (static), several other dynamic (when a cantilever is deliberately vibrating) AFM modes are used. The basic ones are: TappingMode AFM, non-contact AFM with either amplitude or phase modulation detection method.

AFM imaging for this work was done using TappingMode™ AFM (www.veeco.com). One advantage of this mode is an absence of frictional forces, which exert torque on the cantilever. By lightly "tapping" the tip on the surface during scanning, TappingMode eliminates lateral, shear forces, which does not damage our soft samples. Unlike contact AFM, the feedback loop keeps a vibrating cantilever at a constant amplitude rather than keeping a cantilever at a constant deflection. The tip on the cantilever is modulated through mechanical excitation at its resonance. A laser beam is reflected from the cantilever onto a photodiode array. The laser spot oscillates across the array as a result of the vibrating cantilever. The signal from the photodiodes is converted to a root mean square (RMS) amplitude value, the magnitude of RMS amplitude is proportional to the amount of cantilever motion.

The feedback compares the RMS amplitude with the setpoint voltage, and both are kept equal by controlling of cantilever movement. The sample surface is in close

proximity to the cantilever. The distance is such that the tip touches the surface only at the lowest point of its oscillation. The RMS voltage is reduced to the setpoint voltage by the feedback loop moving the tip into the sample. The sample restricts the cantilever movement until the desired RMS voltage is reached. The damping of the cantilever is held constant by moving the tip in z as it is simultaneously translated in x and y directions. Thus, although the piezo stack continues to excite the cantilever with the same energy, the tip is deflected in its encounter with the surface. The reflected laser beam reveals information about the vertical height of the sample. The engagement of TappingMode AFM requires that the setpoint voltage b smaller than the RMS voltage. The tip is lowered until the RMS reaches the setpoint, thus that prevents hard collisions between the probe and sample surface

The AFM used in this work is a *MultiMode™ SPM MMAFM-2* of *Digital Instruments*. This is designed for imaging small samples up to 1.5 cm size Samples are fixed to a round metal disk, then magnetically attached to the top of the scanner tube. Key MMAFM-2 specifications are:

- noise: <0.3 A RMS in vertical dimension
- sample size: <15 mm diameter, <5 mm thick
- scan range: <125 μm lateral, <5 μm vertical
- tip/cantilever holders: tapping mode / contact mode in air
- vibration and acoustic isolation: silicone vibration pad and acoustic cover, vibration isolation tripod
- scanner: AS-05, 125 μm x 125 μm lateral (X-Y) range, 5 μm vertical (Z) range.

AFM tips used in this work were *RTESP* of Veeco Metrology Group (www.spmprobes.com). The SEM image and schematics of these tips are shown in

Fig.3-3. The tip convolution effect on the images of the samples was not taken into account. Specifications of this tip are:

- Force (or Spring) Constants: 20 - 80 N/m
- Resonant Frequency: 200-400kHz
- Nominal Tip Radius of Curvature: <10nm
- Cantilever Lengths: 125µm
- Tip Height: 15-20µm
- Cantilever Configuration: Single Beam
- Cone Half Angle: 17.5 on each side, 15.0 front, 25.0 back

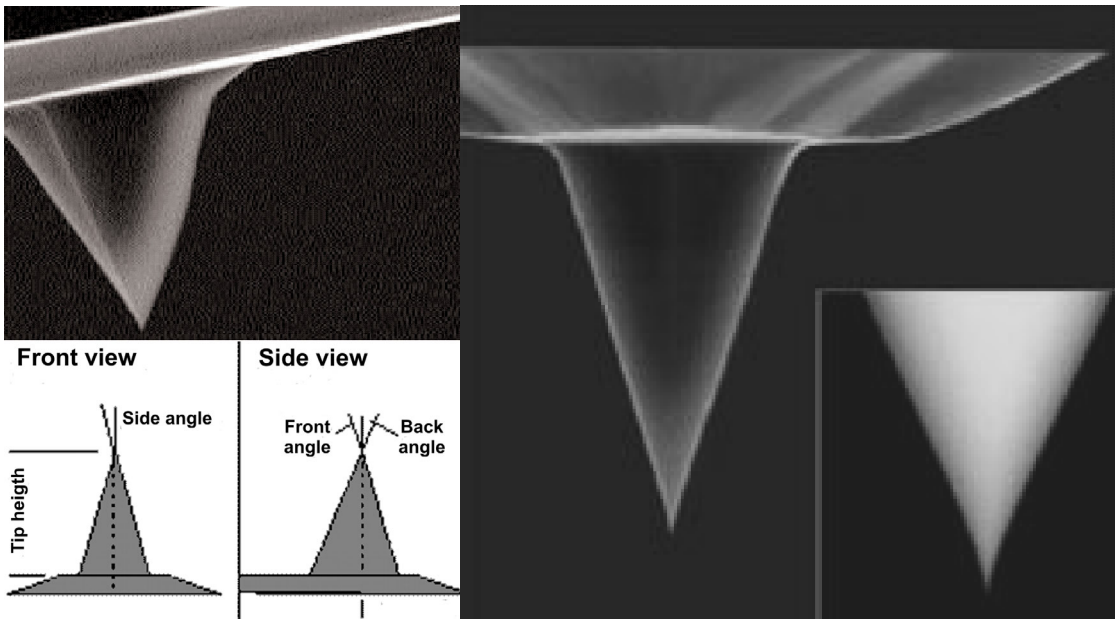

Fig.3-3. Schematics and SEM micrograph of RTESP AFM tip used for TappingMode AFM imaging.

3.4. Optical spectroscopy setup

Photoluminescence (PL) spectroscopy is a contactless, non-destructive method of probing the electronic structure of materials. Light is directed onto a sample, where it

is absorbed and imparts excess energy into the material in a process called photo-excitation. One way this excess energy can be dissipated by the sample is through the emission of light, or luminescence. In the case of photo-excitation, this luminescence is called photoluminescence. The intensity and spectral content of this photoluminescence is a direct measure of various important material properties. The special features are of PL spectroscopy are: various excitation wavelengths allow for varying penetration depths into the material, and thus, varying levels of volume excitation.; detection of photoluminescence from 0.4 to 2.8 μm using diffraction and Fourier-transform-based systems.; mapping capabilities; sample temperatures of 4 to 300 K; sensitivity down to the level of parts per thousand, depending on impurity species and host.

Specifically, photo-excitation causes electrons within the material to move into permissible excited states. When these electrons return to their equilibrium states, the excess energy is released and may include the emission of light (a radiative process) or may not (a non-radiative process). The energy of the emitted light, or photoluminescence, is related to the difference in energy levels between the two electron states involved in the transition that is, between the excited state and the equilibrium state. The quantity of the emitted light is related to the relative contribution of the radiative process. The possible applications of this technique are:

(a) Bandgap determination. The most common radiative transition in semiconductors is between states in the conduction and valence bands, with the energy difference being known as the bandgap. Bandgap determination is particularly useful when working with new compound semiconductors.

(b) Impurity levels and defect detection. Radiative transitions in semiconductors involve localized defect levels. The photoluminescence energy associated with these

levels can be used to identify specific defects, and the amount of photoluminescence can be used to determine their concentration.

(c) Recombination mechanisms. As discussed above, the return to equilibrium, also known as "recombination," can involve both radiative and nonradiative processes. The amount of photoluminescence and its dependence on the level of photo-excitation and temperature are directly related to the dominant recombination process. Analysis of photoluminescence helps to understand the underlying physics of the recombination mechanism.

(d) Material quality. In general, nonradiative processes are associated with localized defect levels, whose presence is detrimental to material quality and subsequent device performance. Thus, material quality can be measured by quantifying the amount of radiative recombination.

Apart from PL spectroscopy, photoluminescence excitation (PLE) spectroscopy involves detecting luminescence intensity at a selected wavelength within a luminescence band as a function of the wavelength of the exciting light, thus isolating one luminescence band and providing information about the absorption energies required to excite that luminescence band. Thus, PLE spectroscopy allows detect the presence and magnitude of the internal strain of the material, which is expected to manifest as changes in the splitting between the heavy-hole (hh) and the light-hole (lh) exciton.

PL and PLE measurements were curried out either with a standard lock-in detection based system equipped with the *SPEX 1680* 0.22 m double spectrometer and *EO-817* Ge detector for measurements in 800-1700 nm range or in a photon counter system equipped with the *Dilor XY800* triple spectrometer and *HAMAMATSU R1617*

GaAs photomultiplier tube for measurements in 300-850 nm range. The arrangement is shown in Fig.3-4. The systems provide the resolution of about 0.6 meV and 0.1 meV, respectively. A *BeamLok 2080* Ar-ion laser, at 514.5 nm and power levels between 1 and 200 mW, was used as the excitation source. Photoluminescence excitation (PLE) measurements were performed using a Ti:Sapphire tuneable laser as the excitation source. During optical measurements the samples were kept at 20 K in an *Oxford Instruments* continuous-flow cryostat system.

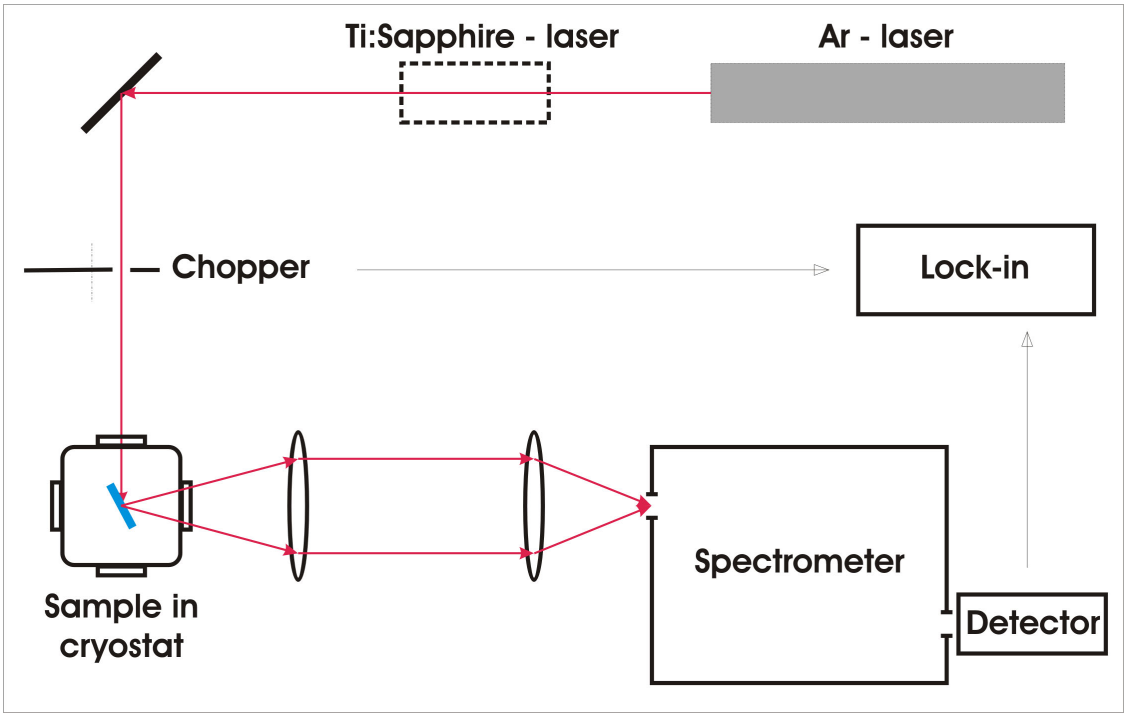

Fig.3-4. Layout of photoluminescence experiments. Sample placed in the cryostat is excited by Ar- or Ti:Sapphire laser. The luminescence signal is focused on the entrance slit of the spectrometer. Chopper modulates the exciting beam for lock-in detection at frequency of 1447 Hz (not used in photon counter system). The width of both entrance and exit slits are 50 μm. The tunable Ti:Sapphire laser (dash line) is used for photoluminescence excitation experiments.

3.4.1. Excitation sources

3.4.1.1. Ar-laser

A *BeamLok 2080 Spectra Physics* Ar-ion laser operated on a 514.5 nm line was used for photoluminescence experiments. The laser provides a low noise (<0.4%) light beam of 1.9 mm diameter with the maximum power output around 10 W. The power stability is about 0.5%. To pump the Ti:Sapphire laser the multi-line mode (454.5-514.5 nm) with power up to 20 W was used.

3.4.1.2. Ti:Sapphire laser

A *CW Spectra Physics Ti:Sapphire 3900* laser pumped by the Ar-laser was used for photoluminescence excitation experiments. The generated wavelength can be tune over a wide range of about 650 nm to 1.1 μm. The laser provides a low noisily (<1%) light beam of 0.95 mm diameter. The output power depends of pump power and 2 W could be reached. With the standard long mirror set the wavelength range from 830 nm to 1020 nm is available. The laser is equipped with a motor actuator controlled by electronics that provides the control and the hold of the wavelength with accuracy better than 0.1 nm. Both thin and thick etalons are installed.

3.4.2. Spectrometers

3.4.2.1. SPEX double spectrometer

The *SPEX 1680* 0.22 m double spectrometer with 600 gr/mm gratings was used. The spectrometer can work in a spectral range of 370-1800 nm. Both entrance and exit slits are manually controlled with an accuracy of 50 μm. This gives a dispersion of 3.6 nm/mm and a resolution of about 0.4 nm (at 1000 nm). The computer control of the

gratings driver provides a repeatability of ± 0.4 nm and an accuracy of ± 0.8 nm. The optical layout of SPEX 1680 is shown in Fig.3-5, left.

3.4.2.2. Dilor triple spectrometer

The *Dilor XY800* triple spectrometer with 1200 gr/mm gratings was used in single channel mode. The spectrometer can work in a spectral range of 310-1100 nm. Both entrance and exit slits are electronically controlled with an accuracy of 5 μm. The computer control of the gratings driver provides an accuracy of 0.01 cm^{-1} with a repeatability of ± 0.1 cm^{-1}. The resolution is around 0.2A with 50 μm slit. The optical layout of XY800 is shown in Fig.3-5, right.

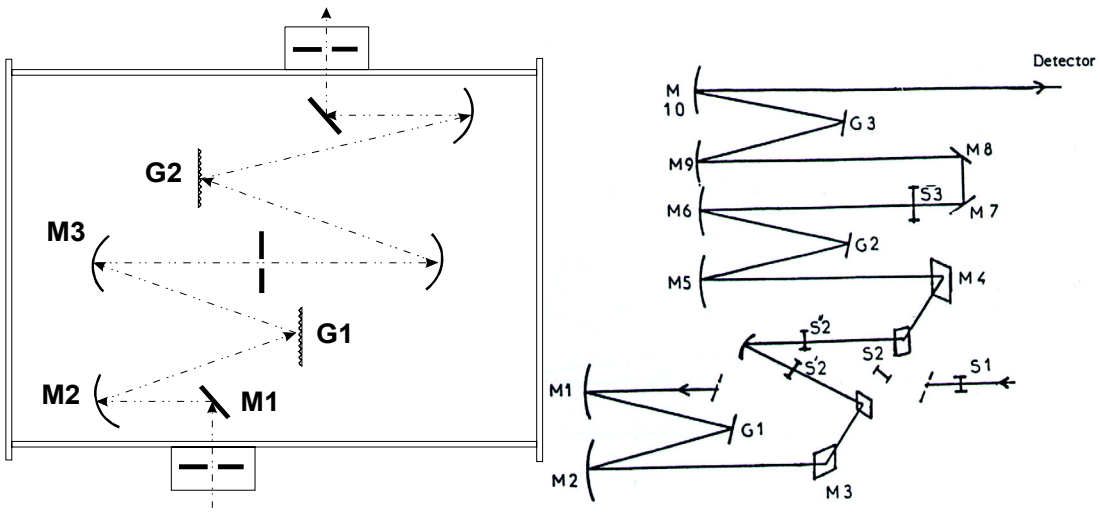

Fig.3-5. Optical layout of the SPEX 1680 0.22 m Double Spectrometer (left) and Dilor XY800 (right).

3.4.3. Detectors

3.4.3.1. Photomultiplier Tube

A *HAMAMATSU R1617* photomultiplier tube (PMT) was used in conjunction with the Dilor XY800 spectrometer in photon counting mode. This PMT provides a spectral response in the visible and near-infrared ranges (300-850 nm), it is

characterised by high sensitivity (120 μA/lm), low dark current (4 nA), fast time response (rise time of 2.5 ns) and low noise. The PMT was kept at about –40°C in order to reach the minimum dark current. The spectral response characteristic of R1617 is shown in Fig.3-6, left.

3.4.3.2. Germanium detector

A *North Coast Optical systems & Sensors EO-817* Germanium detector was used in conjunction with the *SPEX 1680* double spectrometer. It has an extremely high performance in the near-infrared range (0.8-1.7 μm). Cooling the Ge photodiode to 77K results in a very high shunt impedance for noise equivalent power below 0.04 pW/Hz$^{1/2}$, responsivity of 0.64 A/W, dark current of 0.08 μA and rise time of 10 μs. The spectral response characteristic of EO-817 is shown in Fig.3-6, right.

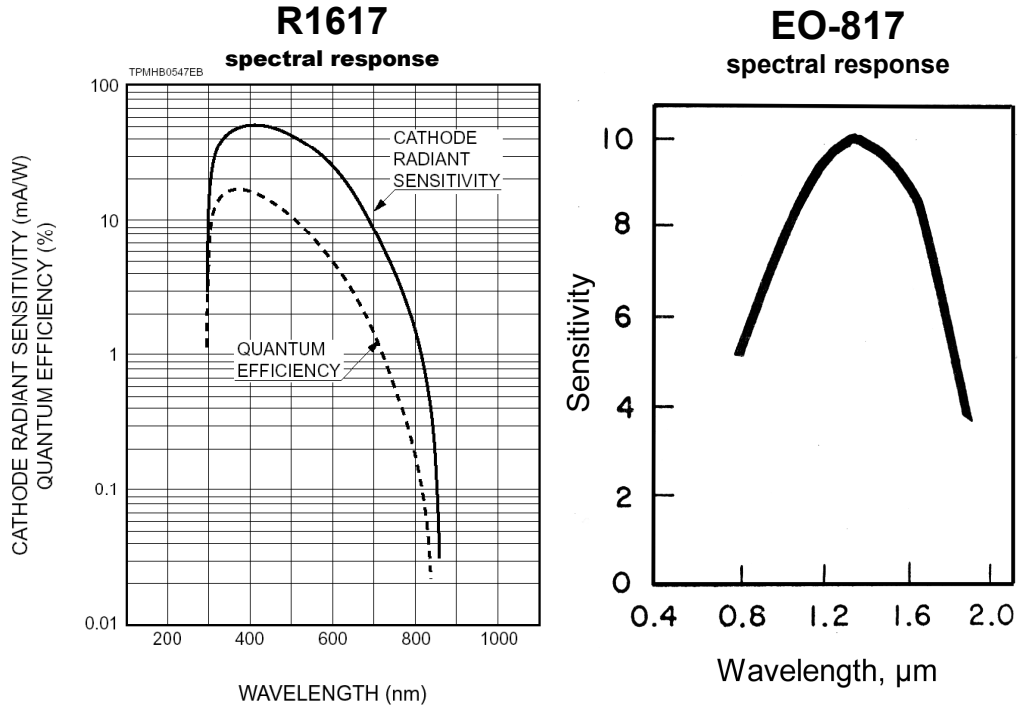

Fig.3-6. The spectral response characteristics of (left) HAMAMATSU R1617 photomultiplier tube (red line marked by 500K) and (right) EO-817 Germanium detector.

3.4.4. Cryogenic equipment

The cryogenic equipment used in this work is an *Oxford Instruments CCC1204* closed-cycle cooler system, which consist of an optical cryostat built on an *Edwards* model cold head, a water-cooled compressor unit and integral control unit, a pair of flexible helium lines and a temperature controller. The system can hold the sample temperature within 0.1K within the range from 15K to 300K.

3.5. Fibre coupling setup

Fibre coupling system consists of optical system and mechanical positioning system. A monomode fibre with a mode field diameter of about 4 μm is used to couple in 514 nm light from Ar-laser. The light passing the devices under test is collected by a multimode fibre with a core diameter of 200 μm. The sample is placed on the three-axis positioning stage of *Melles Griot*, and both entrance and exit fibres are mounted on the two-axis positioning stage. These stages were equipped with micrometer screws that allow the movement and positioning with accuracy of 0.5 μm. The light on the exit is detected by a Si diode.

3.6. Monochromator setup

The printed gratings were characterised using light from a tungsten halogen lamp. The collimated light is directed through the 5 mm aperture to the grating, which is placed 30 cm away. The geometry at the sample is sketched in the inset of Fig.3-7. The diffracted light exits through a 20 mm aperture at the distance of 30 cm, which is the

entrance slit of monochromator, and it is detected by single monochromator *ISA 270M* equipped with a Si diode at the exit slit. The overall spectral resolution of the set up is of the order of 2 nm in the spectral region tested.

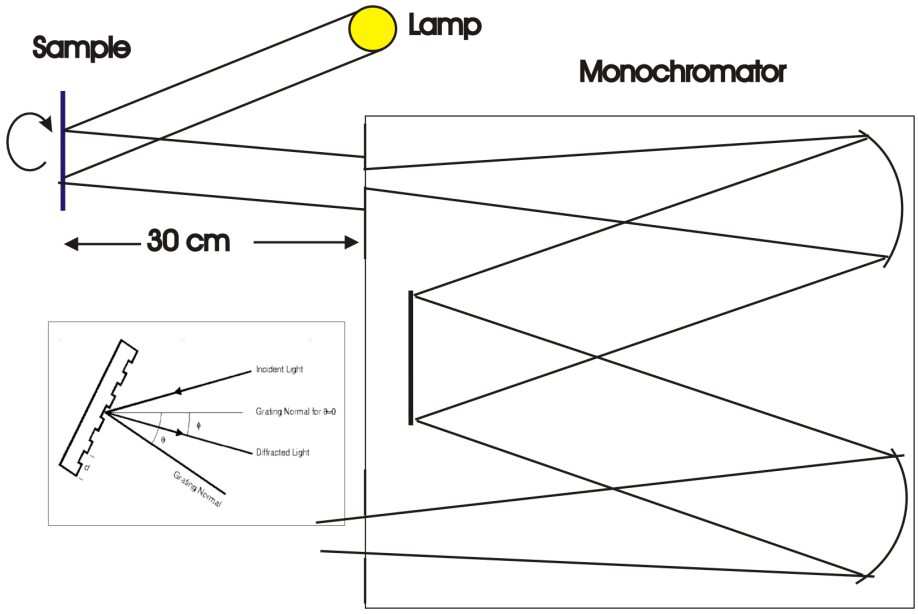

Fig.3-7. Schematics of a monochromator setup used for characterisation of diffraction gratings. The inset sketches the geometry used for measurements.

Chapter 4. Stamp fabrication

In this chapter the issue of stamp fabrication is considered from two points of view: to explore the limit of used materials concerning resolution and control of critical dimension and to develop a competitive process for fabrication of stamps with nm-features and with nm-accuracy, which includes optimisation of exposure and resist development steps as well as providing feedback in the development of new materials.

4.1. Metal-on-silicon stamps

The metal-on-silicon stamps are useful if nm-features are needed. To fabricate such stamps, electron beam lithography together with metal deposition and lift-off is probably the most suitable method. As one of the first attempt in the laboratory, small "isolated" metal pattern with low aspect ratio were fabricated with relative ease using standard electron beam (e-beam) resist and process [26], as shown with the example of 60 nm high Cr-columns of 120 nm diameter and 1 μm period (see Fig.4-1). However,

stamp fabrication becomes much more complicated, if high feature density and/or high aspect ratio are needed, for example, to fabricate stamps for magnetic storage devices, photonic crystals, etc. In these cases, the broadening of electron beam due to the scattering in the resist, irradiation by secondary electrons and proximity effect play a significant role (see Section 2.3.1). The standard process was optimised in this work, pushing the known limits as far as obtaining smaller features with as high as possible density and high aspect ratio.

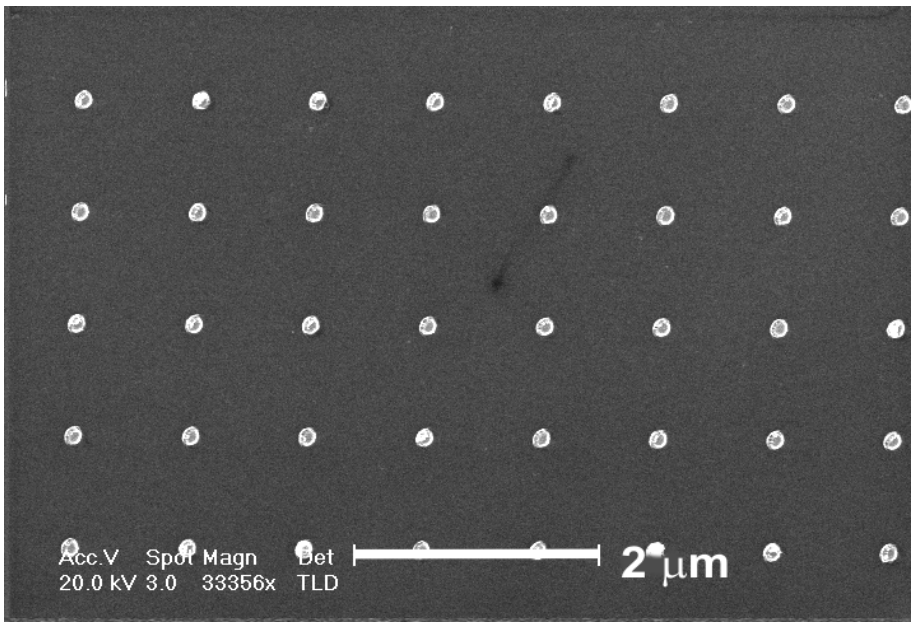

Fig.4-1. SEM micrograph of chromium-on-silicon stamp. The stamp was fabricated by electron beam lithography and Cr lift-off. Features were written in a 100 nm thick 950K PMMA resist with area dose of 400 $\mu C/cm^2$, resulted after development and lift-oft in a 60 nm high Cr-columns of 120 nm diameter and 1 µm period.

In order to fabricate a high aspect ratio stamp the double layer resist was chosen. The idea is to separate from the substrate the top thin layer of high resolution and high contrast resist (imaging layer) with a low contrast bottom resist layer. In this case, the primary scattering of the electron beam takes place mainly in bottom layer and thus does not decrease the resolution of the upper resist layer. The high electron scattering in

the bottom layer leads to an undercut vertical profile after development, which facilitates the lift-off procedure (Fig.4-2, left). An example of a stamp fabricated using two-layer resist is shown in Fig.4-2, right. A 60 nm thick 950K PMMA was used as the top layer and a 160 nm thick 200K PMMA- as the bottom layer. The features were written by Electron Beam Lithography (EBL) system consisting of Philips XL30S FEG scanning electron microscope equipped with a Raith lithography module (see Section 3.2). The resist was spun onto the silicon substrate and baked at 150°C for 30 min after spinning each layer. A 10 μm x 100 μm area with 670 parallel lines with length of 10 μm each, resulting in an one-dimensional grating of single pixel lines with period of 150 nm was written at 20 kV and line dose of 2.7 μC/cm. After development in 1:3 MIBK:IPA during 30 s, a 100 nm thick chromium film was deposited following by lift-off in AR 600-70 remover, which resulted in 30 nm linewidth.

To fabricate stamps with higher feature density the total resist thickness should be decreased. In this case, a single layer resist is found to be more practical. One of the disadvantages is the limitation on the aspect ratio: results published so far describe the thickness of deposited metal to be at least tree times less than the resist thickness in order to perform reliably lift-off [21]. But in general this does not satisfy the requirements for stamps, because the thickness contrast after printing with such stamp will not be sufficient for further processing. Thus, the single layer fabrication process has to be optimised, i.e. to find a way to obtain metal structure with thickness up to two thirds of the initial resist thickness.

In this context, an optimal fabrication procedure was undertaken in which all process steps and parameters, including polymer spin-coating, baking, exposure dose, and distribution of dose over feature area, development, metal deposition and lift-off,

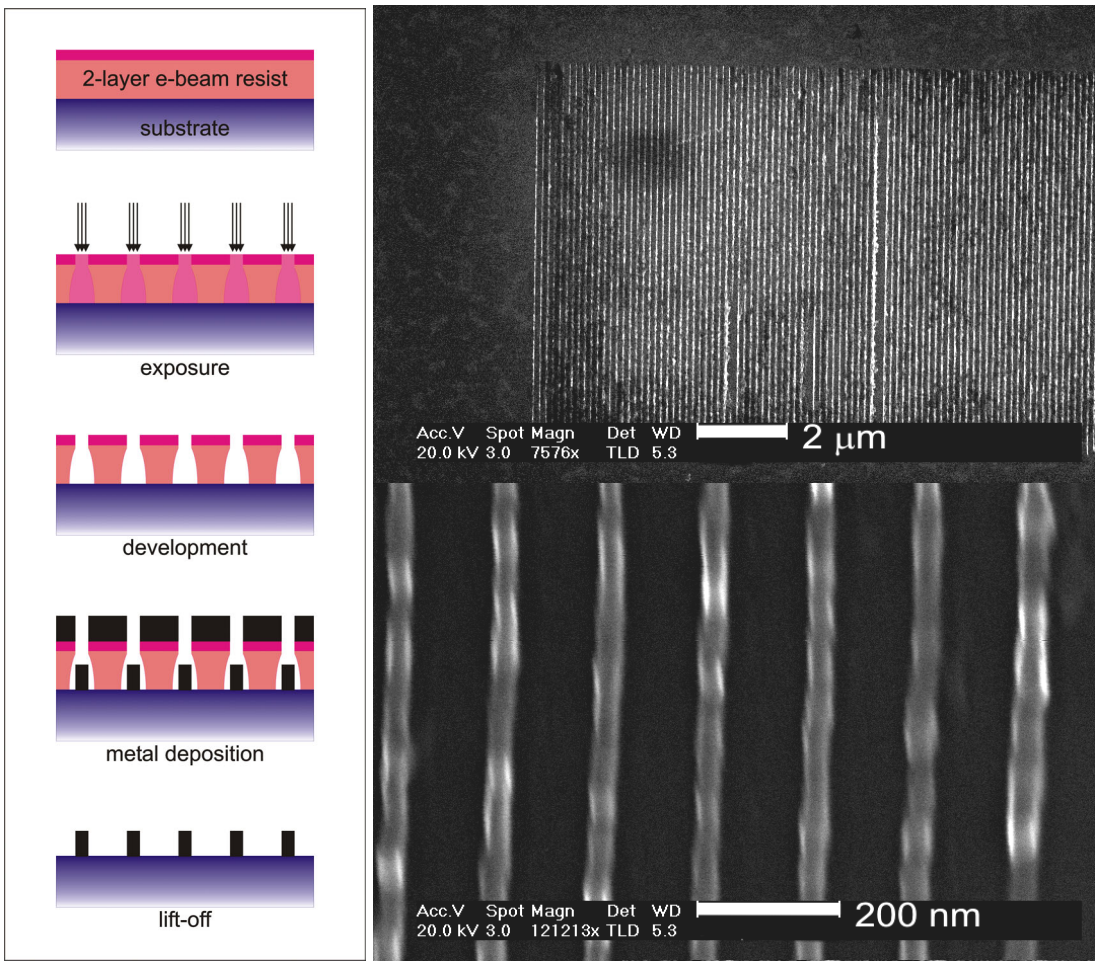

Fig.4-2. (left) Schematics of stamp fabrication process using a double layer resist. (right) SEM micrograph of a 100 nm high chromium grating consisting of 30 nm wide lines with 150 nm period.

had to be precise controlled. The strategy was based on fine dose tuning for a particular stamp design, considering the whole process rather than separate steps. For this purpose test exposures were carried out varying the dose in small steps along one axis. In this way the necessary dose can be defined as the dose for a given feature, which appears having the desired size/shape and has no problems to lift-off. A set of experiments was performed to define the optimum process, while different conditions of resist film preparation, development and used developers were tested. As a resist the 950K PMMA was used, which is known as a high resolution and high contrast electron beam resist.

The film thickness was varied from 55 nm up to 100 nm. The resist was spin-coated on a silicon substrate and baked out at 150°C for 30 min. Decreasing of the baking time and temperature seemed to decrease the resolution. Few developers were tested and no advantages were found compared to the standard 4-methyl-2-pentanone:2-propanol (MIBK:IPA). Moreover, no advantages could be identified by changing the development time or using of ultrasonic agitation. Therefore, in this work preference

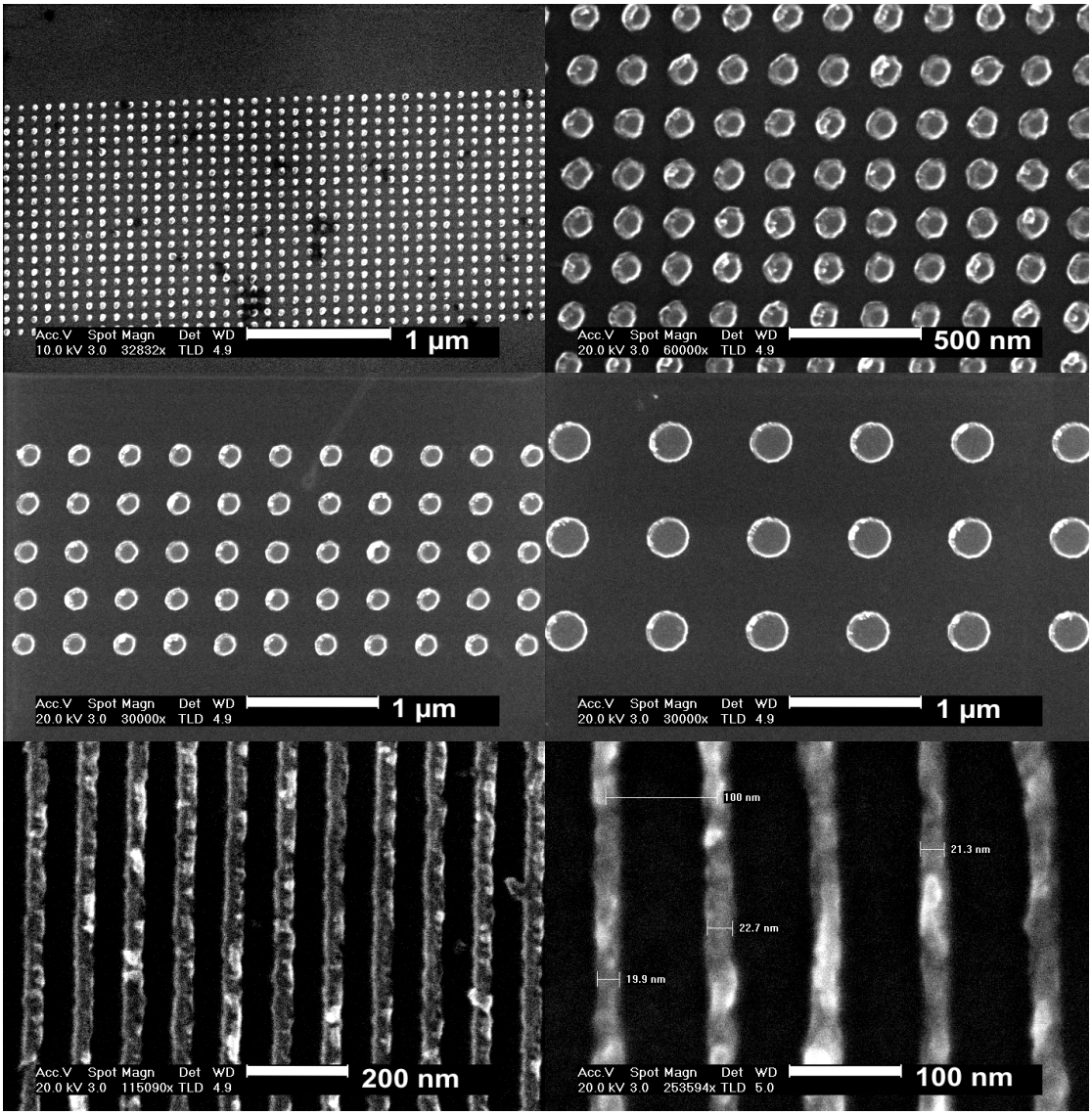

Fig.4-3. SEM images of metal-on-silicon stamps: (a) 50 nm dots/spaces, (b) 100 nm dots/spaces, (c) 200 nm dots/spaces, (d) 400 nm dots/spaces, (e) 40 nm line with 60 nm spaces, (f) 20 nm lines with 80 nm spaces. All stamps are 60 nm thick Cr on silicon.

was given to development in 1:3 solution of MIBK:IPA for 30 s. With this procedure stamps containing feature with sizes down to 20 nm were fabricated with sufficient reproducibility by e-beam lithography and metal lift off characterised by good uniformity of feature size and shape over the whole area. The variation of the feature size was ~1% for pattern down to 100 nm in lateral size and ~10% for 20 nm pattern. Examples of such stamps are shown in Fig.4-3. The summary of corresponded process sheet is given in Table 2. For e-beam exposure high accelerating voltage was chosen.

Table 2. Process details to fabricate metal-on-silicon stamp containing features with lateral size down to 20 nm.

Feature	**50 nm dots**	**100 nm dots**	**200 nm dots**	**400 nm dots**	**40 nm lines**	**20 nm lines**
Resist	950K PMMA					
Resist thickness	100 nm					55 nm
Exposure mode	Single dot	Area with step of 3 nm			Single pixel line with step of 0.1 nm	Single pixel line with step of 1 nm
HV / beam current	20 kV / 26 pA					30 kV / 24.7 pA
Dwell time	50 µs	1.5 µs	3.75 µs	3.75 µs	1.8 µs	1.75 µs
Development	1:3 MIBK:IPA for 30 s					
Metal thickness	up to 75 nm					up to 30 nm
Lift-off	AR 600-70 remover, ultrasonic agitation					

The reason is that in this case much less forward scattering in the resist occurs (as described in section 2.3.1) and thus smaller pattern can be defined. For the examples given in Table 2 the resist thickness of 100 nm was used for fabrication of stamps with feature size down to 50 nm, i.e., aspect ration up to 2:1. It was found that here is not considerable difference between exposure at 20 kV and 30 kV, because the range of the forward scattered electrons is smaller than desired feature size even at 20 kV. Therefore, it is not necessary to use higher voltages. On the other hands, when fabricating stamps with feature size of 20 nm, forward scattering becomes more crucial even if thinner resist (55 nm) is used. In this case, a higher accelerating voltage is necessary, i.e., the highest available in our SEM voltage of 30 kV was used. The exposure dose was defined by test exposures as described above. Therefore, to write features of 20 nm or less a combination of thin resist and high acceleration voltage is needed.

4.2. Polymer stamps

Polymer stamps are known only since few years, when a stamp containing μm-features was fabricated by NIL using a thermoset polymer in its pre-polymer state, subsequently followed by thermal cross-linking [14]. A more promising development, with potential impact in a range of applications, is the synthesis of new cross-linkable polymers, which are also electron- and/or UV-sensitive. Such polymer, mr-L 6000, was recently synthesized and a competitive process to write directly polymer stamps with nm-features was developed in the laboratory in collaboration with *mrt GmbH* [15]. The mr-L 6000 is based on a novolak-derived multifunctional epoxy resin, an onium salt as photo-acid generator (PAG) and safer solvents. Under illumination by electron beam or

UV the PAG initiates a chain reactions resulting in cross-polymerisation. Thus, it is a negative e-beam and UV resist, which has high sensitivity, ~5 μC/cm^2, compared to 80-200 μC/cm^2 for PMMA. The next consequence is much shorter writing times. After cross-linking, the written structure can be used as a stamp, i.e., stamps are fabricated in one step: the lift-off step necessary for the production of metal on Si stamps or the production of metal etch mask is then no longer necessary for polymer stamp fabrication using mr-L 6000.

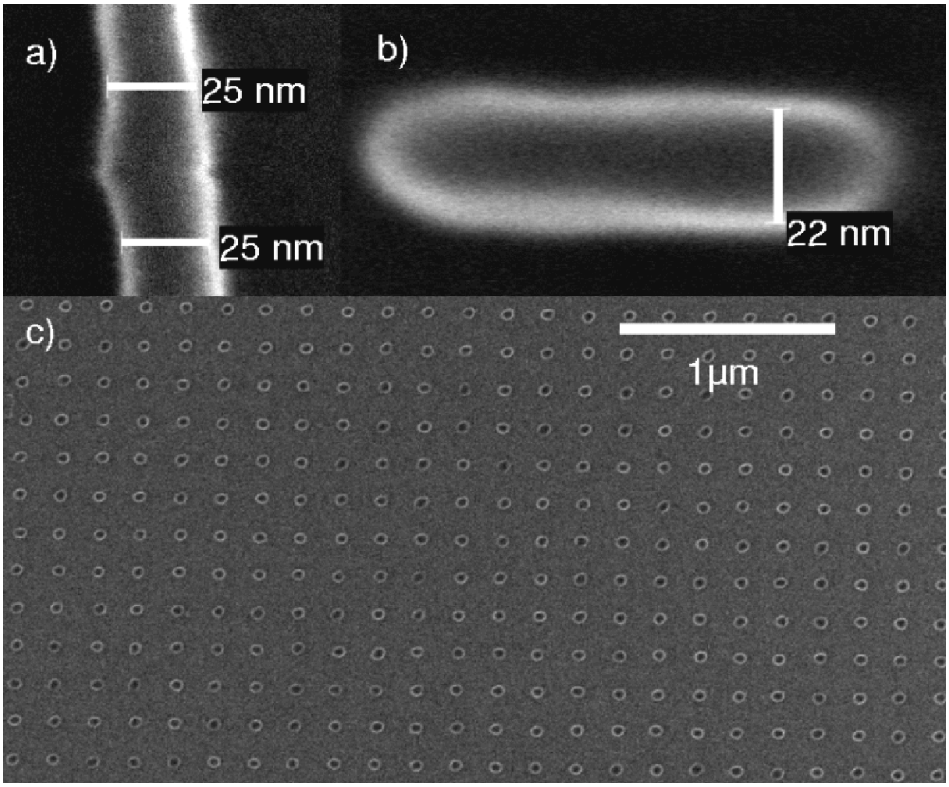

Fig.4-4. SEM micrograph of the stamp directly written in mr-L 6000 with electron beam lithography: (a) wires of 25 nm width, (b) an array of dash of 22 nm width and (c) an array of dots of 50 nm diameter.

An mr-L 6000 films with thickness of 100-130 nm were obtained by spin coating on silicon substrate. The films were prebaked for 180 s at 120°C at hot plate. Patterns were written by electron beam lithography at 30 kV. After exposure the samples were postbaked for 300 s at 100°C and developed in PGMEA. This was

followed by near UV flood exposure and hard bake on a hot plate for 300 s at 120°C to improve the thermal and mechanical pattern stability. Samples were kept in dark during whole process from the preparation of the film until UV exposure and hard bake. An example is shown in Fig.4-4, where several patterns were written by electron beam, e.g., (a) wires of 25 nm width, (b) an array of dashes of 22 nm width and 500 nm period and (c) dots of 50 nm diameter and 200 nm period. This polymer can also be imprinted, which offers the possibility for low-cost replication of master stamp as described in Chapter 5.

4.3. Feature size control

In first approximation the ultimate resolution of nanoimprint lithography depends on the minimum feature size in the stamp. Moreover, the shape of features on the stamp also affects the shape of imprinted features. In this context, the limit of fabrication process and used materials concerning the control of feature size needs to be explored. Here, the resist surface roughness and resist line-edge roughness play a role.

Recently, several studies concerning resist surface roughness and line-edge roughness (LER) of the resist after exposure and development steps have been reported [27,28,29]. As the pattern size becomes smaller, the resist surface roughness becomes the critical issue for strict control of feature size. It was shown that a non-uniform energy distribution of the electron beam and the high dissolution contrast (difference between development rates of exposed and unexposed resist) during development increase the surface roughness [27]. In order to reduce the resist surface roughness, one needs to optimize the dissolution contrast or, alternatively, optimize resist properties.

One of the possible alternative resists is mr-L 6000, which is described in section 4.2. Its limits concerning the minimum feature size will be explored below in this section.

In [28] the line-edge roughness of a developed resist pattern has been calculated in the case of low-dose, i.e., low accelerating voltage electron beam lithography of chemically amplified resist. A low energy electron beam has a high energy loss rate and it gives sufficient energy density to expose a resist with a very low dose, eg., less than 1 $\mu C/cm^2$. Thus, every trajectory of the electron beam might be resolved as the resist structure after development. Under this condition, it is a concern that the statistical fluctuation of the exposure, the so-called shot noise, becomes important. In spite of these concerns, however, it was verified experimentally that the edge roughness observed at the resist surface after development is smaller than the statistical fluctuation, which is expected by a simple consideration of the number of electrons incident on the resist. This decreased fluctuation may be due to the following factors. The energy deposited in the resist is not only from incident primary electrons, but also from the many secondary electrons generated in the resist. It is the latter which excite the resist molecules with higher efficiency. Consequently, the influence of the exposure is spatially smoothened by the secondary electron diffusion volume. In chemically amplified resists the acid is generated from a photo-acid generator (PAG) by electron exposure and diffuses spatially during the post exposure baking process. In this case the influence of the electron beam exposure is broadened and spatially smoothened. Furthermore, by using a strong developing solvent, which dissolves the resist with less sensitivity to the electron exposure dose variation, unexposed parts of the resist can be dissolved and the resist structure can be spatially smoothened. It was shown [28] that the LER can be decreased by choosing a large acid diffusion length, a moderate exposure dose, a gentle solubility rate variation with dose and thick resist. In all cases, if

the acid diffusion length is larger than 20 nm, the LER of the 100 nm wide line pattern after development will be less than 5 nm on average at an accelerating voltage below 2 kV.

The experimental results following prediction of [28] indicated that there is no clear difference in LER of 100 nm lines/spaces in chemically amplified resist written with exposure dose varied from 2 keV to 50 keV [29]. On the other hand, it is expected that at high accelerating voltage the PAG will be generated in the unexposed area due to proximity effect. This may result in the appearance of undesired resist features over unexposed area.

In this section the limitations of stamp fabrication process concerning feature size are explored. This considers, in contrast to the above described studies, the study of "finished products", i.e., stamps, and includes not only EBL but also lift-off or UV- and thermal hardening steps.

Set of exposures was made writing structures with very low exposure dose, when the written structures just become detectable. Firstly, EBL and lift-off was performed using the same process and resist as described above (section 4.1). Thus, exposures were carried out at an accelerating voltage of 30 kV and a beam current of 24.7 pA. The structures were written in a 100 nm thick film of PMMA with a molecular weight of 950K. An array of dots with period of 100 nm was generated by point exposures of duration of 30 μs. After exposure and development in 1:3 MIBK:IPA a 60 nm thick Cr layer was deposited. The lift-off was performed in acetone under ultrasonic agitation at room temperature. A SEM micrograph of a stamp is shown in Fig.4-5. The patterns on the stamp, having lateral sizes below 10 nm, have a well-defined periodicity, no absence of features was notified over whole stamp area, but they exhibit a non-regular circular shape and large dispersion of lateral size (~50%).

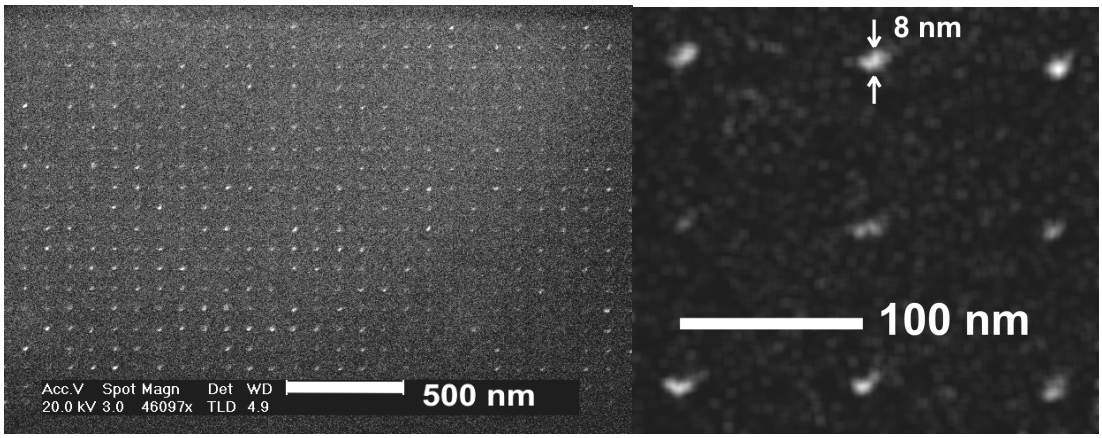

Fig.4-5. SEM micrograph of a stamp containing sub 10 nm Cr features. The big variations of feature size and shape are due to large size of polymer molecule and evaporated metal.

The variation of the shape and the height of the pattern fabricated by e-beam lithography and Cr lift-off is due to material properties of the Cr evaporated. In Fig.4-6, left the 400 nm diameter column shows a surface texture with sizes of several nm. This texture already causes significant deviations from the circular shape of 50 nm diameter columns (Fig.4-6, right).

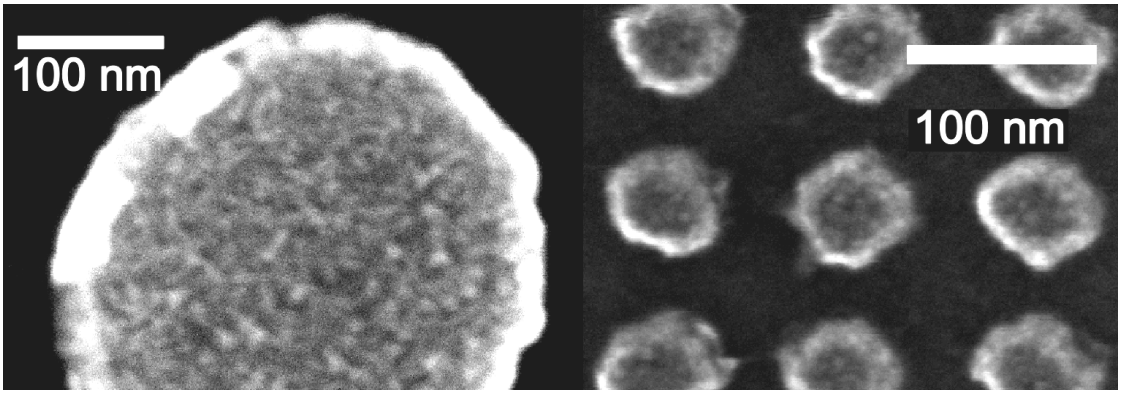

Fig.4-6. SEM micrographs of Cr stamp consisting of structures with sizes of 400 nm (left) and 50 nm (right). Small features with sizes up to 10 nm on the edges and on top of metal column are present.

Thus, the reason for the shape variation of sub 10 nm features, as depicted in Fig.4-5, is the “roughness” induced by the stamp-material properties such as grain size or polymer molecule size. The later influences the mask defined by EBL. Fig.4-7 shows

a typical surface of a 950K PMMA film after an e-beam exposure and development steps for a 50 nm (left) and 10 nm (right) diameter dot patterns. The surface shows surface and line-edge roughness in the nm scale and, therefore, it becomes more critical for 10 nm features. The aperture in the resist is not circular any more. Moreover, as the minimum size of patterned structures approaches the 10 nm regime it often becomes comparable to the grain size of the metal to be deposited. It appears that during lift-off grains are removed as a whole, leading to gaps appearing in the structures. Thus, the metal grain size becomes one of the factors limiting the minimum feature size achievable by lift-off.

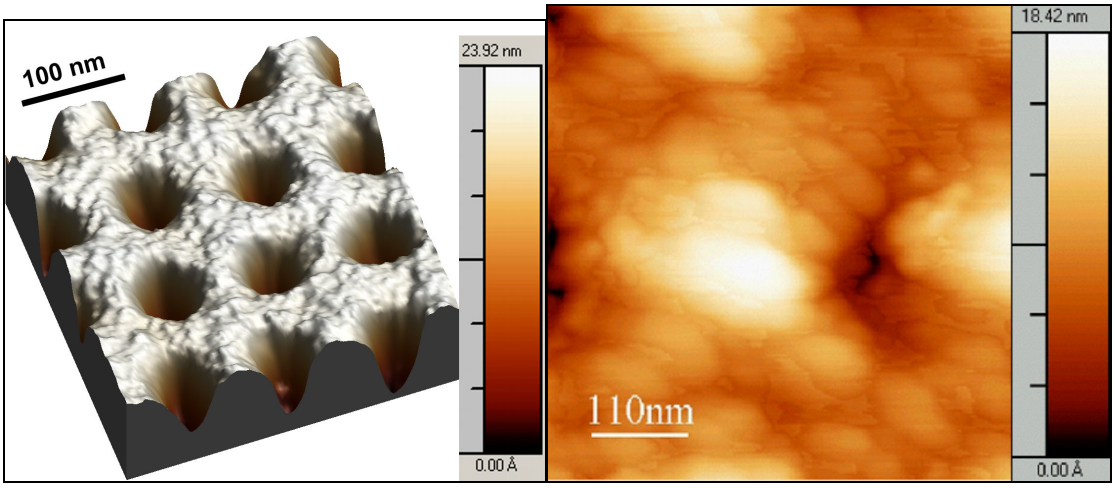

Fig.4-7. AFM image of 950K PMMA film surface after electron beam lithography and development.

The mr-L 6000 stamp have much more smoother shape of fetures even on the 20 nm scale (Fig.4-4). The resist is spun on as an oligomer rather than a polymer and the resulting roughness leads to sufficiently smooth shapes and surfaces in the 20 nm regime. But for sub-5 nm structures the significance of material texture might become relevant. Moreover, the short-term noise of lithography system may also play a significant role. As a low number of incident electrons is needed to create such a small

pattern (around 80 nm^{-1} for writing of 20 nm lines), its fluctuation as well as the fluctuation of incident position may cause significant variation of pattern shape and size. To explore the limit of resolution for mr-L 6000, the low-dose electron beam lithography experiments were made investigating the line edge roughness of obtained features.

Under illumination of mr-L 6000 by electron beam the photo-acid generator (PAG) initiates a chain reactions resulting in cross-polymerisation. It is well known that secondary electrons contribute to the exposure. In this case, the polymerisation will take place also nearby the written structure resulting in the presence of unwanted polymer here and an increase of line-edge roughness. This effect becomes apparent when a very low exposure dose is used. An AFM image of such structure after e-beam exposure and development is shown in Fig.4-8, where an array of single pixel lines was written with around 30 electrons per nm. The processing steps were the same as for fabrication of polymer stamps in section 4.2 above: 100 nm thick film of mr-L 6000 was obtained by spin coating on silicon substrate, the film was prebaked for 180 s at 120°C at hot plate, patterns were written by electron beam at 30 kV, after exposure the samples were postbaked for 300 s at 100°C and developed in PGMEA, then followed by near UV flood exposure and hard bake on a hot plate for 300 s at 120°C to improve the thermal and mechanical pattern stability. Samples were kept in dark during whole process.

The line-edge roughness is on the same scale as the line thickness. This is the major factor limiting the resolution, although it may be possible to compensate it in partly by adjusting the PAG concentration. The topology analysis of the surface between written lines (Fig.4-9) shows the presence of patterns with sizes on the 5-9 nm scale. It is assumed that the smallest particles are due to cross-polymerisation caused by

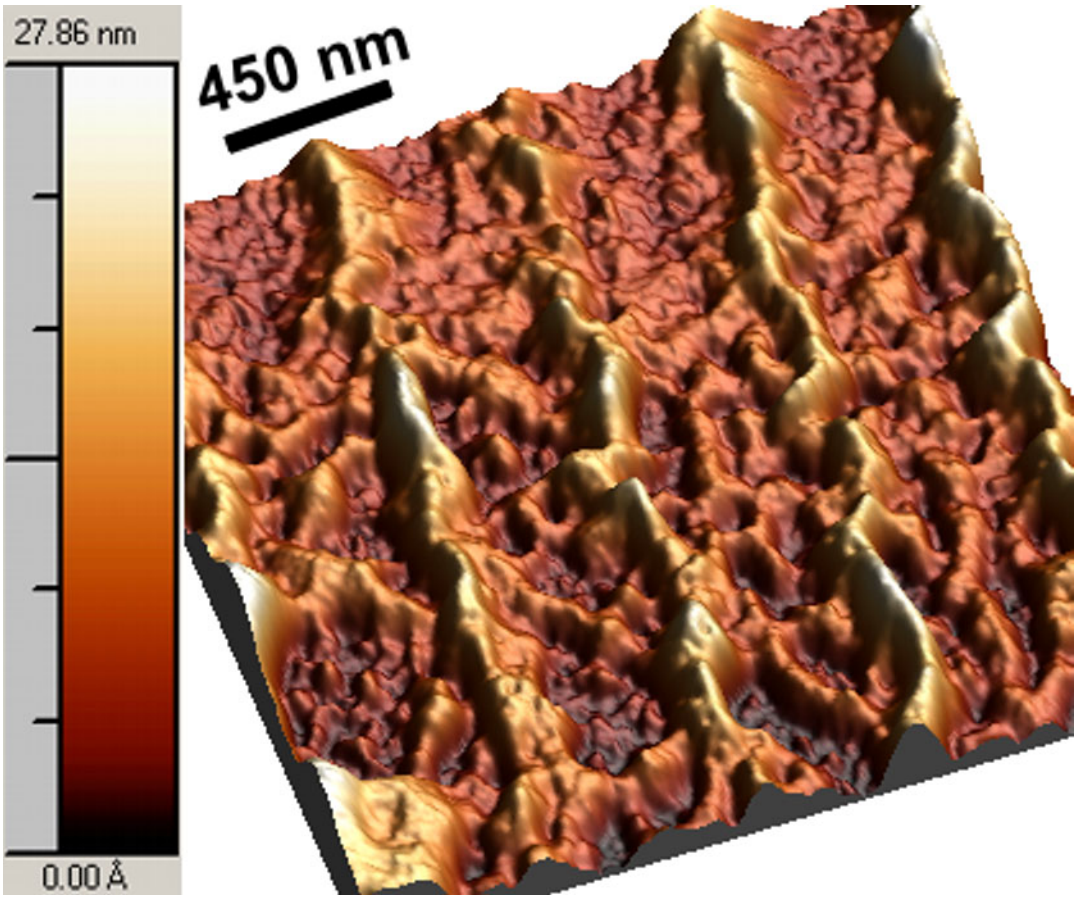

Fig.4-8. AFM image of lines written in mr-L 6000 by electron beam lithography with a low exposure dose. The "roughness" of lines defines the limit of resolution.

only one electron. Of course, this is also a strong limitation to produce safely sub-10 nm stamps. Benefit could be made from using low-energy electron beam. In this case, a small backscattering is expected, as discussed in section 2.3.1, thus leading to a much more flat surface between written patterns. However, at the same time a large forward scattering occurs in the resist and, therefore, requires the use of thinner films to obtain high-density sub-10 nm patterns. This will reduce the aspect ration of features, which cab be written. This approach has not been tested here because of difficulties to spin-coat thin films of mr-L 6000 at this time.

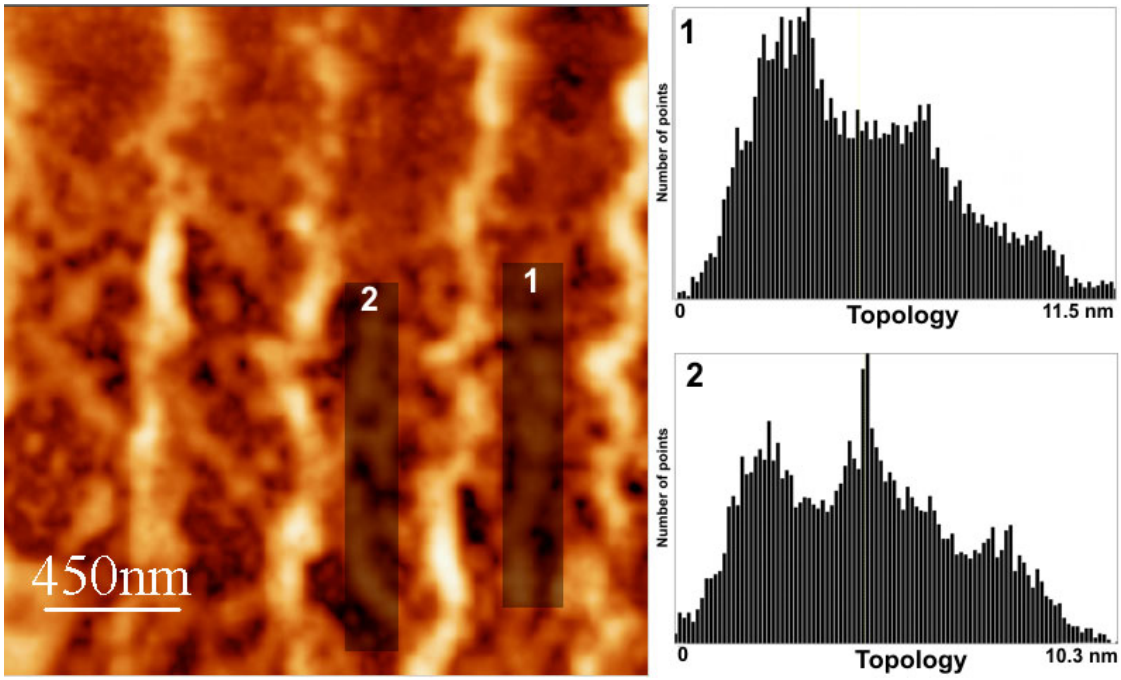

Fig.4-9. AFM topology analysis of areas between lines written in mr-L 6000 by EBL. The presented peaks of about 5 nm and 9 nm above the surface level are due to polymerisation caused by backscattered electrons.

4.4. Summary

If stamps with high density of nm-features are needed, the metal on silicon stamps are a good choice. These are fabricated by electron beam lithography and metal lift-off. Using the above described processes, stamps containing features with sizes down to 20 nm can be reproducibly fabricated. Moreover, a reliable lift-off can be performed for metal thickness up to three fourth of the resist thickness. The problem of critical dimension becomes a serious bottleneck, if fabricating stamps with sub-20 nm features. The polymer and metal properties come into play, and conventional lift-off methods are not generally successful when trying to achieve sub-10 nm structures. As an alternative, directly written polymer stamps can be used. The fabrication process does not involve metal lift-off, while material properties looks very promising on the

scale below 20 nm. Moreover, the use of polymer stamps offers the possibility for low-cost reproduction of master stamp.

Chapter 5. Printing results

In this chapter, results of imprinting on micro- and nano-scale using number of polymers that demonstrate the quality of the replicated structures and their fidelity towards the stamp, are presented.

We start with a basic model of nanoimprint process considering the squeezing flow, which is a simplest approach to describe NIL, and the mechanical properties of polymers. These are helpful for the understanding of printing parameters required to optimize the NIL process and will certainly contribute to define the potentials and limitations of NIL.

5.1. NIL model

In NIL the stamp is placed on the top of the polymer film, which is heated above its glass transition temperature. When pressure is applied, the polymer is forced to flow into the cavities of stamp. A simple model for this process is the model of squeezing

flow: the polymer is considered as an ideal viscous liquid between two parallel disks separated by a distance of $2h_0$ corresponding to the thickness of polymer layer. The application of a force F leads to the squeezing flow of the polymer. A quasi steady state solution is given by the Stefan equation, which expresses the force in terms of disk radius R, the motion of both disks dh/dt and the polymer viscosity η_0 as:

$$F = -\frac{3\pi R^4}{4h_0^3}\frac{dh}{dt}\eta_0, \qquad (1)$$

The strong dependence of the force on the disk radius, $F \propto R^4$, and the fluid thickness, $F \propto h_0^{-3}$, indicates that very large forces are required to obtain polymer motion in thin films and over large transport distances. The polymer viscosity enters only linearly into Eq.(1), but for polymers it usually decreases by orders of magnitude with increasing temperature. The viscosity of polymers could be considered as independent of shear rate at small shear rates, ~10^{-1}-10^{1} s^{-1}, which are typical for nanoimprinting [12]. The usual NIL process uses a constant pressure and the quantity of interest is the time dependent penetration depth as given by the motion of the mould and substrate, dh/dt, which can be computed from Eq.(1):

$$\frac{1}{h_1^2} - \frac{1}{h_0^2} = \frac{16Ft}{3\pi R^4\eta_0} \text{ or } t_{1/2} = \frac{9\pi R^4\eta_0}{16Fh_0^2} \qquad (2)$$

where $t_{1/2}$ is the time needed to reduce polymer thickness by 50%. One can be seen that the size of elevated stamp feature influences strongly the printing time. It is therefore worthwhile to reduce the size of elevated features as much as possible. After polymer filled stamp cavities completely, the motion of stamp practically stops and it is not possible to thin any longer the remaining layer. Another consequence is that printing time and or printing pressure can be reduced considerably by using materials, which have the viscosity much lower than polymers, for example, alphy sexithiophen [12] and

diphenyl-(4-vinyl-phenyl)-amine (see section 5.2.2 below) can be successfully printed with μm-features without remaining of residual layer.

A certain limitation of the present model is the printing of small features, i.e., compared with the size of a polymer molecule. Since in reality the flow caused by the elevated stamp feature is not independent of the surrounding features, the flow (or velocity profile) is more complex and, in general, process parameters may differ strongly from those given by Eq.(1) and (2). More important seems to be the build-up of stress or, in other words, the elastic deformation of single polymer chains, which can be "frozen" in the polymer during the NIL. This is discussed in more details below.

A good control of the nanoimprint process of small features requires understanding of the underlying mechanical properties of polymers. The combination of viscous and elastic behaviour in a polymer is not a simple superposition of both contributions, but brings about a new phenomenon named anelasticity [30]. It becomes apparent in the observation that part of the deformation, although being reversible, requires some time to establish itself.

To illustrate the different contributions to the deformation the response of a polymer to external force is discussed hereinafter. The immediate deformation of the polymer corresponds to its elastic response. The elastic contribution to the deformation is fully recovered upon unloading of the polymer. A second contribution corresponds to the viscous response of the system to external stress. The viscous behaviour is irreversible and its contribution to the overall deformation can be determined from the recovery curve. Finally, there is a retarded deformation, which requires some time to establish itself and is fully recovered some time after unloading of the polymer. The occurrence of a retarded deformation shows that visco-elasticity is more than a simple superposition of viscous and elastic contributions. These retarded deformations are

frequently addressed as anelastic behaviour and are related to the flexibility of the macromolecules. Polymers combine viscous, elastic and anelastic properties and this behaviour is generally addressed as "visco-elasticity". The relative weights of the three contributions to the overall deformation depend on the type of polymer and particularly on the temperature. It is clear, that an understanding of the temperature dependence is essential to control the imprint process since only irreversible deformations are desired in nanoimprint lithography.

With respect to the mechanical behaviour of amorphous polymers, there are two important points to be considered: (i) the conformational changes of the chain that allow for both local motions of short chain segments and motions of entire chains are thermally activated processes and therefore will take place on typical time scales which depend strongly on the temperature, and (ii) the formation of a temporary network of large, entangled chains. Especially interesting is the temperature dependence of the mechanical behaviour of polymers, but the response of a polymer to external forces depends strongly on the temperature-dependent time scales of the different motions.

At low temperatures the conformational changes are very sluggish, taking place on time scales of hours to years. The mayor contribution to the response comes from the elongation of the atomic distances within and between the macromolecules and the response to external forces corresponds to that of an ideal elastic body. The amorphous polymer shows the behaviour of a truly glassy, hard and brittle material. This region is referred to as the *glassy region* (see Fig.5-1).

At temperatures near the glass temperature short range motions of chain segments due to conformational changes will take place on time scales, which lay in a range accessible to the experiment. With increasing temperature the energy barrier for conformational changes related to such motions will be crossed more frequently and

local motions will become faster. However, the temperature is not sufficiently high to permit the motion of entire chains within the experimental time scales. Hence, a temporary network of entangled chains has to be considered. Under applied external forces the chain segment fixed between two entanglement points will extend due to local conformational changes. To establish this extension some time is required and the overall deformation will exhibit a retarded contribution. This region is called the *transition region*.

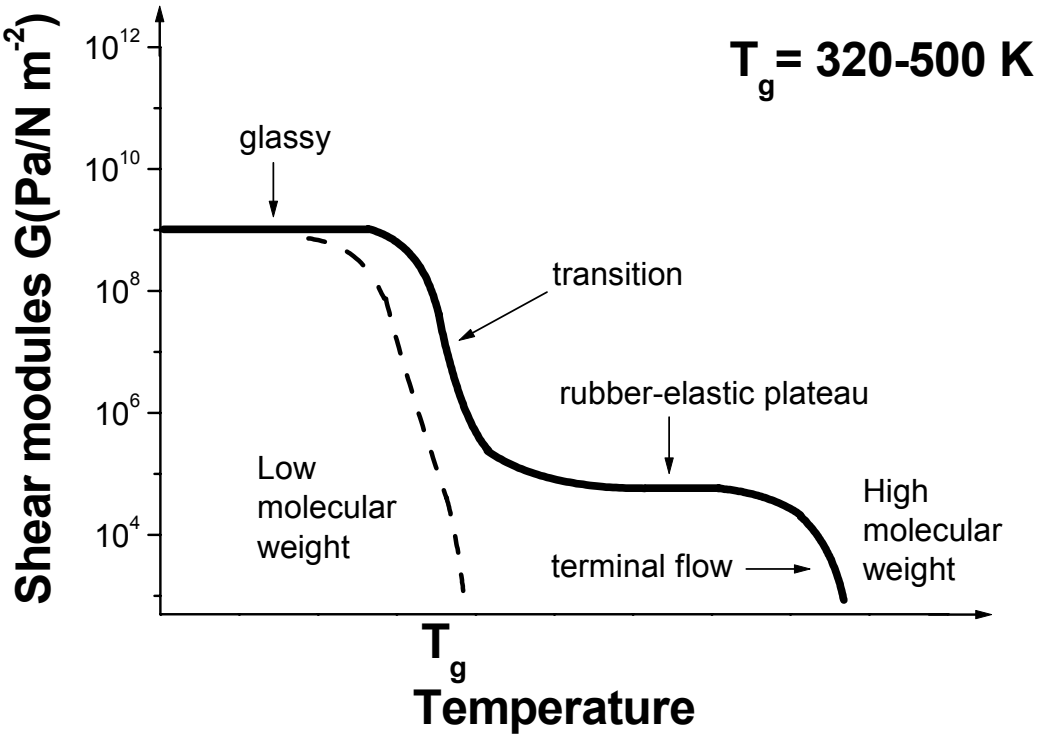

Fig.5-1. The temperature dependence of Shear modulus of polymers with different molecular weight.

The region following the transition region with increasing temperature is the *rubber-elastic region*. In this region the temperature is sufficiently high enabling local motions of chain segments to take place on very short time scales, whereas at the same

time entire chains remain fixed by the temporary network of entanglements. On application of external forces to the polymer, e.g. pressure, the changes in conformation are fast enough to allow for the extension of chain segments fixed between entanglement points and, as a consequence, large deformations are observed.

Finally, the *region of terminal flow* is reached at higher temperatures. Now, even the motion of entire chains takes place on time scales within the time window of the experiment and the polymer flows by chain sliding. This region is of particular interest for nanoimprinting because this behaviour within the experimental time scale is mainly described by irreversible flow, which is the desired behaviour for pattern transfer (Fig.5-2). A polymer melt at sufficiently high temperature will basically exhibit a viscous flow, except when the external forces change in time scale shorter than the time required by the chains to slide across the entanglement points.

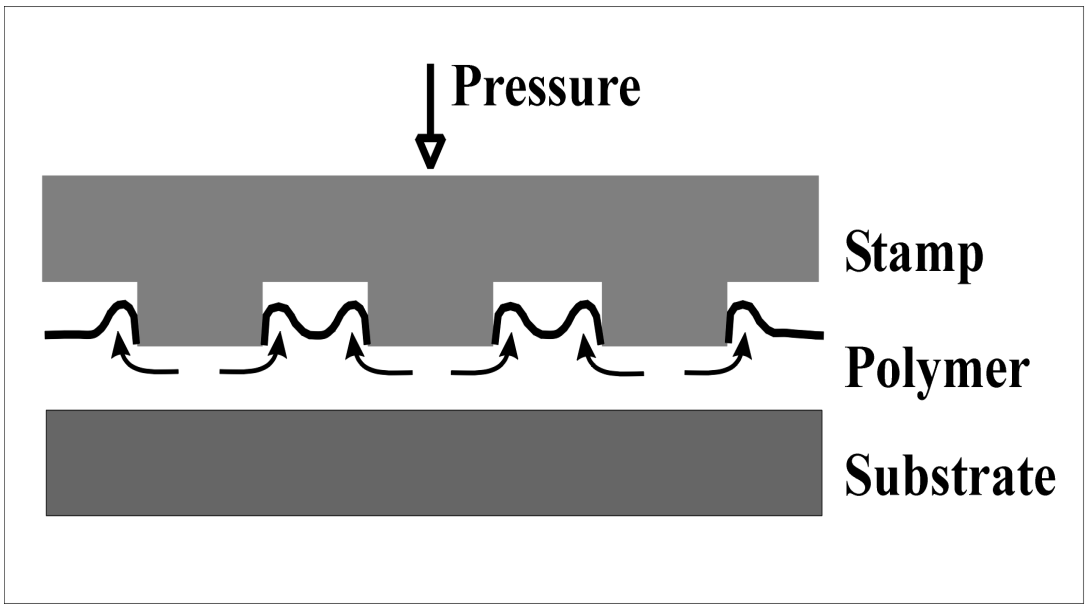

Fig.5-2. Schematics depicting polymer flow during nanoimprinting.

The following consideration has some important consequences for the nanoimprinting process: even in the terminal flow region the action of restoring forces,

which tend to recover the initial shape of the polymer, has to be taken into account. These forces will act on the mould and may cause adhesive-like behaviour during the separation of the stamp from the polymer.

Another important point is the dependence on molecular weight (MW). Since the glass transition temperature depends strongly on local motions due to conformational changes, it is expected that the glass transition temperature does not depend strongly on the molecular weight. On the other hand, the number of entanglements per chain depends on the molecular weight of the polymer and, therefore, it might be expected that at a given temperature a polymer of low molecular weight will flow easier than one with a high molecular weight. For a high molecular weight polymer an extended rubber-elastic plateau is expected.

The choice of appropriate polymers for nanoimprinting can be aided by considering the mechanical behaviour discussed here. Good flow behaviour and antiadhesive properties are essential for nanoimprinting, characteristics exhibited by several commercially available polymers.

5.2. Imprinting polymers

5.2.1. Process development

The choice of material to be printed depends strongly on the target application. For example,

(a) a good etch selectivity is needed when producing an etch mask;

(b) control of critical dimension down to 10 nm is necessary for applications in electronics and optoelectronics;

(c) the functionality of polymers is an advantage offered the possibility for one-step device fabrication (i.e. a printed polymer to be used as a device itself, like optical gratings and waveguides);

(d) low glass transition temperature, if less demanding conditions are needed, like for developments in optics, sensors and biological applications;

(e) long term mechanical stability is essential.

Thus, before nanoimprint lithography become a serious candidate as fabrication technique, printing of a range of polymers have to be demonstrated in order to explore its potentials and limitations. This, as well as the involving of new polymers, is the subject of this work.

Candidates for NIL are: poly methyl methacrylate (PMMA), polysterene (PS) and Teflon (PTFE). PMMA is widely available in a broad range of molecular weights. It is a standard resist for EBL and, therefore, interesting cross-links between imprint and e-beam lithographies could arise. Polystyrene is an attractive material because of it chemical properties with respect to etching in CF_4 plasma, the etching rate of which is about 2 time less than one of PMMA. Moreover, PS has a higher refractive index, which offers the possibility of relatively easy fabrication of optical devices like polymer waveguide on silicon dioxide substrate. Teflon is a particular interesting material because it is chemically inert, its very low surface energy, high thermal stability in comparison to other polymers, low refractive index (~1.3), optical transparency from the infrared to the ultraviolet and its low dielectric constant (~1.9) and dissipation factor. The application of amorphous Teflon as a dielectric can significantly reduce

delay, crosstalk and dissipation of interconnects. Other applications in biomedicine or biochemistry can be envisaged, which makes use of chemical inert fluoropolymers. For example, their strong hydrophobic character in combination with a hydrophilic substrate may allow a selective chemistry, thus offering a nano-patterned surface with hydrophobic and hydrophilic reservoirs and nano-reactors. Some important parameters of these polymers concerning its printability are shown in Table 1 in Section 2.1.

First printing experiments were performed using a 600K PMMA. Usually, the polymer layer thickness has to be larger than stamp relief thickness. A 490 nm thick film of PMMA was spun coated onto a silicon substrate and baked out at 150°C for 30 min. The stamp used is a silicon or silicon dioxide stamp containing features with sizes from 10s of μm down to 200 nm having relief thickness of 360 nm supplied by VTT[1]. Experiments were carried out using a printing temperature of 190°C, i.e. 95°C above the glass transition temperature, at an imprint pressure of 100 bar, the temperature at which the stamp was separated from the sample was 95°C. An example of two printed gratings with period of 800 nm and 8 μm are shown in Fig.5-3. The μm and sub-μm patterns are replicated with a good fidelity and complete filling of cavities can be seen over the whole area of 2 cm x 2 cm. Features with sizes on the scale of few 10s of nanometre are not replicated sufficiently into the given polymer in these experiments, as shown in Fig.5-4 comparing images of stamp (left) and imprint (right). This is possible due to the large molecule size of polymer (typically 60-100 nm for given PMMA) and will be discussed in details below.

[1] VTT Centre for Microelectronics, Finland was a partner within the join EU Project CHANIL (IST-1999-13415)

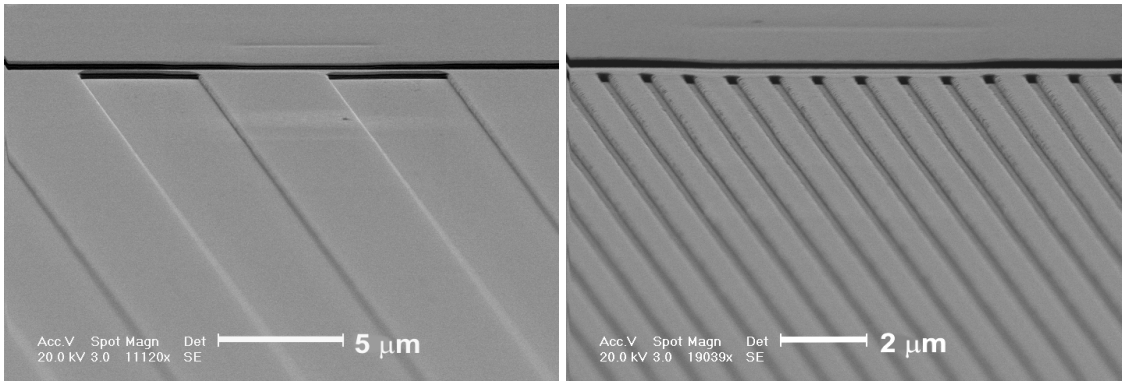

Fig.5-3. SEM micrographs of two gratings with periods of (left) 8 μm and (right) 800 nm imprinted into PMMA with molecular weight of 600K.

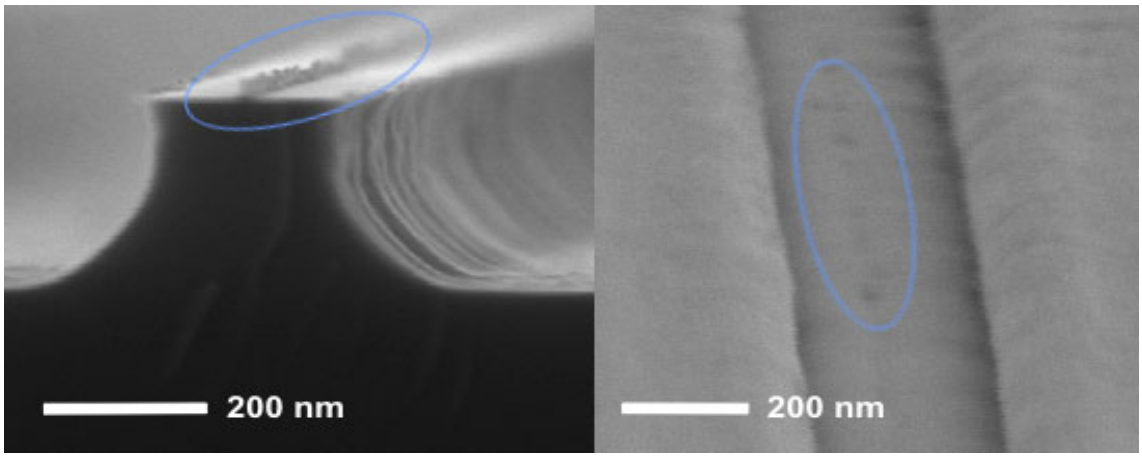

Fig.5-4. SEM micrographs of a silicon stamp (left) and its corresponded imprint into 600K PMMA (right). The small features at the top of the ridge of the stamp are not replicated sufficiently.

The polystyrene used in experiments is BASF 168N with molecular weight of approximately 230K. A 3.3% solution of PS in benzol was spun onto a silicon substrate at 2000 rpm leading to a thickness of approximately 600 nm. Printing of PS with a silicon stamp exhibit very strong adhesion between the stamp and substrate leading to a impossibility to separate them from each other. The problem can be solved using an anti-adhesion coating, as is discussed in section 5.3 below. Surprisingly, silicon dioxide stamps exhibit no adhesion when printing polystyrene. A set of experiments yielded improvements in process optimisation such as decreasing the printing temperature down

to 170°C and determining a best separation temperature of the stamp from substrate to be 115°C, which is 5°C above glass transition temperature. Thus, we found that PS can be printed under less demanding conditions, which may be important for optical applications, in shorter heating and cooling time, which will increase throughput. Moreover, PS demonstrated very good pattern replication fidelity down to sub-nm scale. An example of 4 µm lines imprinted into polystyrene is shown in Fig.5-5, where even features of nm-scale thickness at the top of the lines are good replicated.

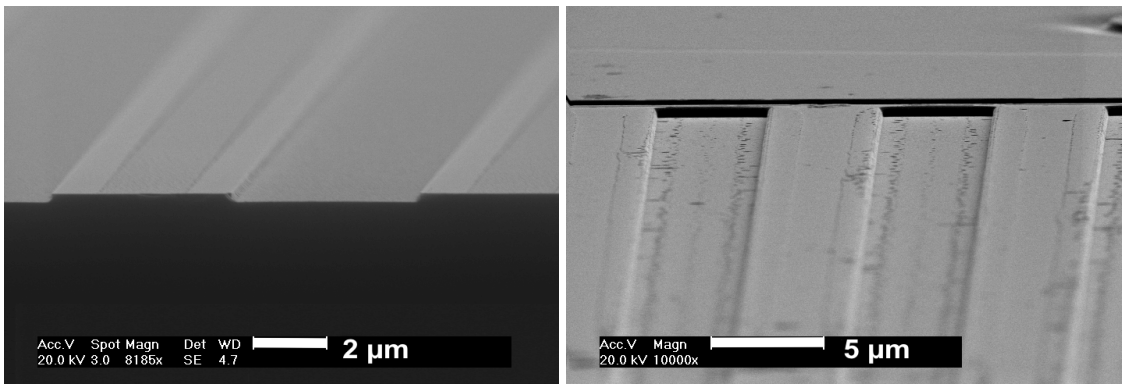

Fig.5-5. SEM micrographs of a silicon dioxide stamp (left) and its imprint made into polystyrene (right).

Teflon® AF1601S (Dupont, Wilmington) is provided as a solution of amorphous fluoropolymer dissolved in Fluoroinert® FC-75 (3M). A 3% solution of Teflon® AF was spun onto the Si substrate at 3000 rpm leading to a thickness of approximately 400 nm. Then the samples were annealed at 200°C for 15 minutes to evaporate the solvent. The glass transition temperature (T_g) of Teflon® AF1601S is approximately 160°C. Imprints were performed at printing temperatures up to 240°C. Although at 220°C Teflon shows already a sufficient polymer flow to fill the stamp cavities completely, the restoring forces are still strong enough to cause adhesion-like behavior during separation of the stamp from polymer. This results in partial polymer pulling as shown in Fig.5-6, left, which is an example of printed negative columns of 800 nm diameter.

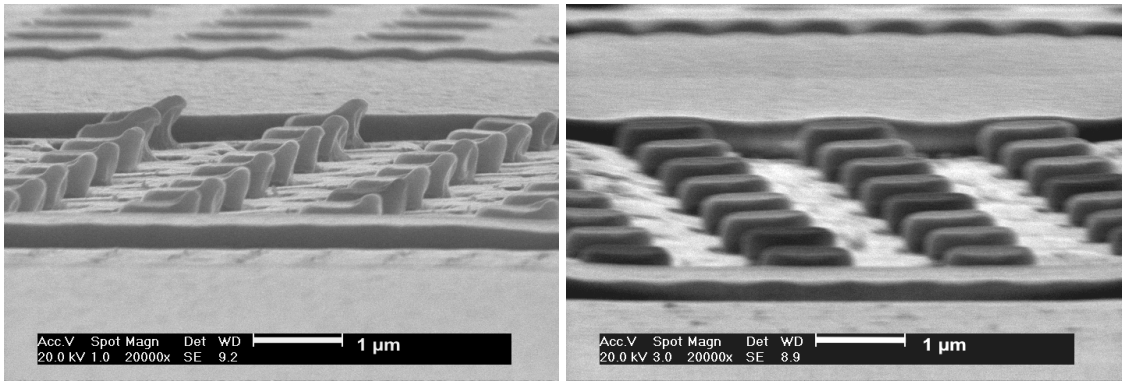

Fig.5-6. SEM micrographs of columns of 800 nm diameter printed in amorphous Teflon at printing temperature of 220°C (left) and 240°C (right). Polymer pulling was observed when printing at 220°C.

5.2.2. New printable materials

The first candidate to be tested for its capability to be patterned by nanoimprint lithography is mr-L6000, which is a newly developed UV- and electron beam resist [15,31]. Of especially interest is the printing of mr-L6000 using a stamp made from the same material, as described in section 4.2 above, which offers the possibility of low-cost stamp fabrication by printing a second, and potentially a third, stamp generation from a master stamp.

NIL on mr-L6000 can be performed at low printing temperature, because this resist has the glass temperature in range of 25-60°C, depending of the modification, and low molecular weight. Therefore imprints were done at temperature between 70 and 100°C, and a pressure of 40 bar applied for 2 min. An example of a mr-L6000 film printed with a mr-L6000 stamp containing 80 nm lines is shown in Fig.5-7. No adhesion in first five imprints was observed. After printing a UV flood exposure for 2 min and a hard bake on a hot plate for 300 s at 120°C followed to improve the thermal and mechanical pattern stability in order to use the printed sample as a stamp.

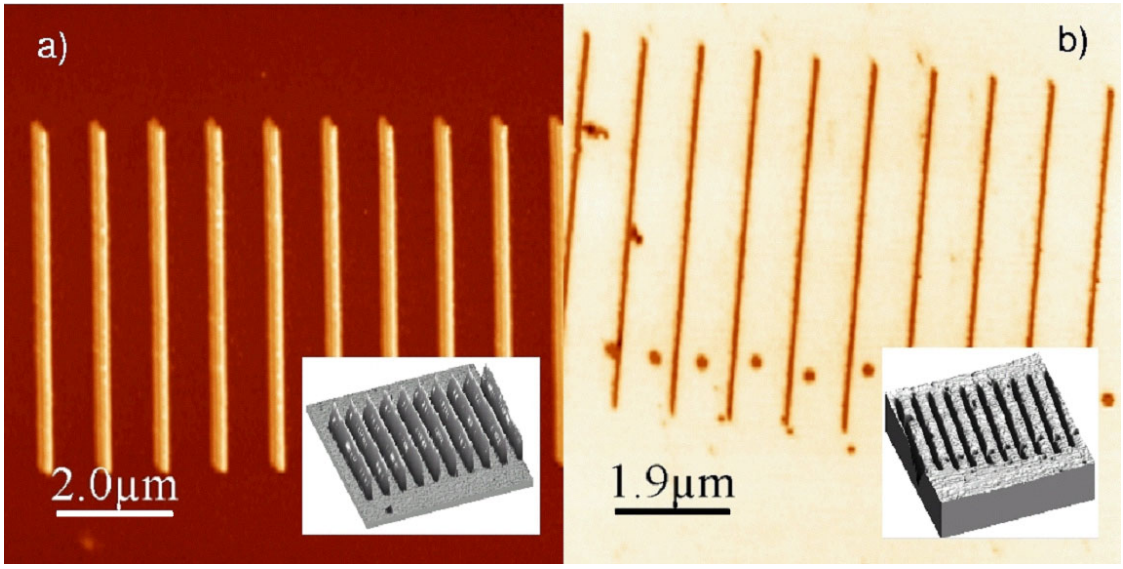

Fig.5-7. AFM images of a mr-L6000-on-Si stamp directly structured by electron beam lithography, hardened by UV exposure and hard bake (left) and of a print of a mr-L6000 film made with this stamp (right).

Other promising materials are semiconducting polymers, like diphenyl-(4-vinyl-phenyl)-amine (arylamine polymer). It can be spun onto silicon dioxide substrate as a monomer followed by flash UV exposure in order to polymerise it in part and in that way tune the viscosity. The viscosity should be sufficiently low for good imprinting and, on the other hand, sufficiently high to prevent structure recovery after pressure release. Given that the glass transition temperature of the oligomer after first UV-flashing is still below room temperature, this material can be successfully printed at room temperature. If the initial film thickness is less than stamp relief thickness, no residual layer is left after imprinting µm features (Fig.5-8). A new process was developed [32], which allows the direct patterning of functional semiconducting polymers in the 100 nm range without the need for a high temperature cycling, further processing steps or irradiation during the processing, i.e. no need for transparent stamp as in Step-and-Flash Imprint Lithography [5].

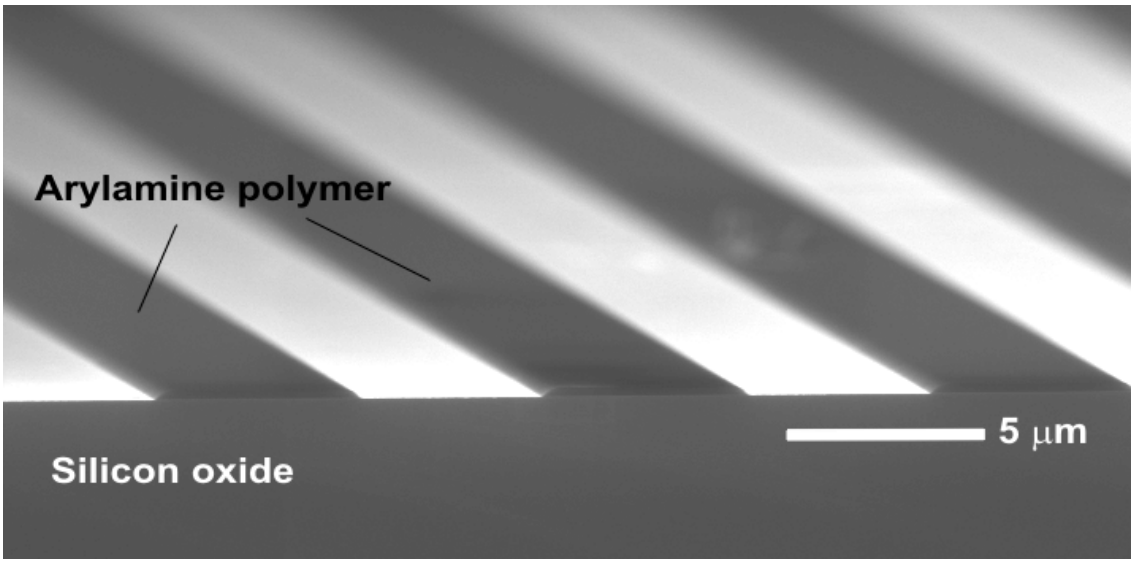

Fig.5-8. SEM micrograph of 4 μm wide lines imprinted into a 180 nm thick diphenyl-(4-vinyl-phenyl)-amine. No residual layer is left after printing at room temperature at a pressure of 100 bar applied for 3 min.

5.2.3. Printing small features

Much of the physics of thin polymer films in the extreme regime used in nanoimprint lithography, like printing high-density nm-features, is still poorly understood. On the one hand, the main mechanism behind forming a pattern in a polymer by printing is ascribes to irreversible viscous flow as shown above (see Fig.5-2). In this context, when printing large features, i.e., features with lateral size much larger than typical size of the polymer molecule, polymer flow should occur over large distance, thus requiring higher temperature and pressure or longer printing time. If these process conditions are satisfactory, large feature, i.e., μm down to few hundreds of nm, can be precisely replicated into polymer by filling the cavities completely (Fig.5-9, left). When the stamp consists of small periodic pattern, i.e., compared to the size of polymer molecule, the polymer flow during imprinting occurs over short distances. Thus, printing small periodic features seems to be easier than printing large pattern. Since polymer flow is understood to take place by chains sliding across the

entanglement points, when size of printed features decreases and becomes comparable with the size of the polymer molecule, the presence of entanglement points will more influential. The polymer between small patterns will not be displaced, but compressed. This means that the elastic response becomes dominant, the stress will freeze during cooling below the glass transition temperature and the polymer will tend to recover after the pressure is released and the stamp is removed. This is illustrated in Fig.5-9 (right) showing an AFM image of 950K PMMA layer after printing with a stamp containing 60 nm high dots of 50 nm diameter. The imprint depth and the diameter of hole have become smaller as a result of the mechanical recovery of the polymer. This is likely to be a major mechanism limiting both the resolution and the control of critical dimension in nanoimprint lithography. Since the number of entanglement points per polymer chain depends on the molecular weight, it is expected that low molecular weight polymers will flow easier and time for relaxation of the stress will be shorter. Thus adjusting molecular weight of polymer may be a way to overcome relaxation-limited resolution.

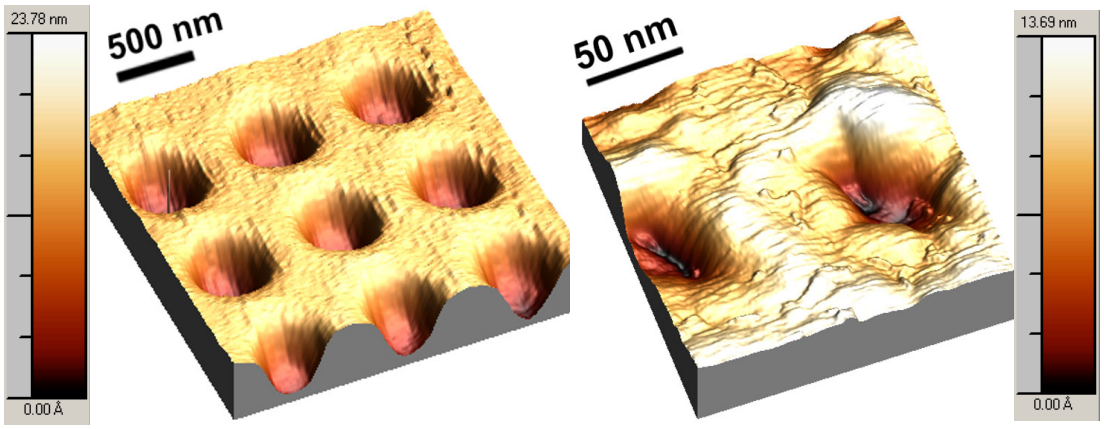

Fig.5-9. AFM images of 400 nm (left) and 50 nm (right) dots imprinted into a 100 nm thick 950K PMMA layer. The mechanical recovery of the polymer becomes apparent for replication of 50 nm structure: the imprint depth and the diameter of the hole have become smaller as a result of the mechanical recovery.

Whereas a good fidelity of printed pattern with sizes down to 20 nm can be achieved using low molecular weight PMMA, the penalty is worse mechanical stability and poor etch resistance. Therefore, in the last years many researchers began to develop new polymers particularly suitable for NIL [14,15,31,33,34]. In this context, the newly developed mr-L6000 described in section 5.2.2 above is a good choice. It is spun on the surface as an oligomer and polymerized after imprint; the minimum resulting roughness leads to sufficiently smooth shapes and surfaces after printing, as shown in Fig.5-10 on the example of printing 30 nm features. These images do not include the tip deconvolution. The convolution effect occurs when sample features are on the same scale as the probe tip used for imaging, which results in an effective broadening of the elevated features. Thus, the AFM pictures of the stamp and imprint do not represent the real shape and size of the pattern, but give information about the roughness of the surface after printing as well as the line-edge roughness of the holes. In all cases the

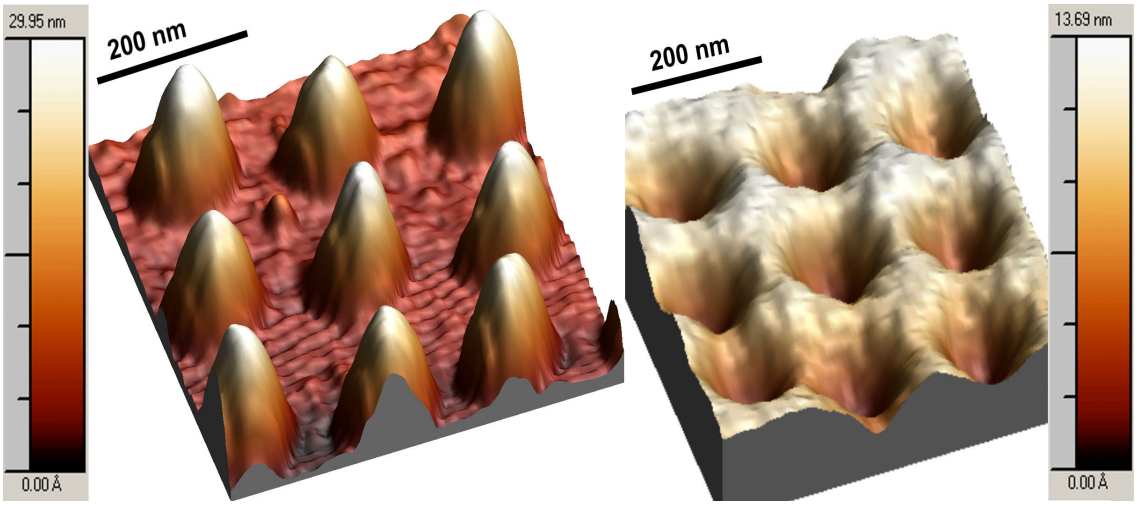

Fig.5-10. AFM images of (left) stamp written in mr-L6000 and (right) an imprint made into the same material using the stamp shown on the left.

lateral size was measured using SEM. It can be clearly seen that the LER as well as the surface roughness are smoother compared to the images of the printed PMMA shown in Fig.5-9. Thus, the mechanical polymer recovery does not seems to be an issue in the time scale of days when printing mr-L 6000.

5.3. Adhesion effects

Since nanoimprinting relies on the contact between stamp and polymer, adhesive behaviour may become apparent. In this case some amount of polymer remains in between the stamp pattern, which is removed together with the stamp during separation. This is illustrated in Fig.5-11, when printing 400 nm lines into PMMA. Thus, as a result of polymer removal, the printed sample cannot be used later on as an etch mask or device. Moreover, an additional cleaning step needs to be included in whole NIL cycle in order to clean the stamp from the rest of polymer. Therefore, it is necessary to put forth an effort to eliminate this problem.

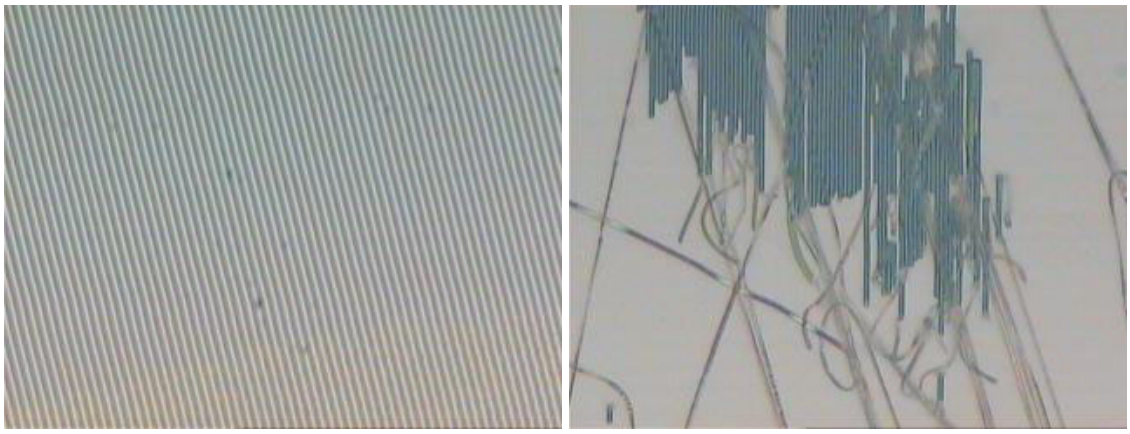

Fig.5-11. Optical image confirmed a successfully printing of 400 nm lines/spaces grating (left) compared to that one after strong adhesion occurs (right).

First of all a good understanding of the physics of adhesion is needed. The adhesion forces on both polymer-substrate and polymer-stamp interfaces have to be taken into account. In general the origin of adhesion can be ascribed to three mechanisms: physical, mechanical and chemical [35]. In case of nanoimprint lithography, these are believed to have a mechanical nature due to interlocking and friction as well as a physical component due to weak interface bonds, while chemical bonds do not become apparent unless no special adhesion agents are used. A desirable situation for nanoimprinting is when the adhesion force between the stamp and printed polymer is smaller than the one between polymer and substrate.

Physical bonds are critical because NIL stamps have patterned surface, which lead to a much higher contact area compared to the substrate contact area. In some cases, like printing polystyrene with a silicon stamp, the adhesion force increases significantly, making it impossible to separate stamp from substrate. Using stamps with a hydrophobic surface, for example silicon dioxide stamps, physical bonds can be easy reduced. A number of experiments show no adhesion when printing using silicon dioxide stamps while silicon stamp exhibit slight up to very heavy sticking to different polymers. A qualitative summary of adhesion behaviour between different stamps and polymers is given in Table 3, where no special measures to prevent adhesion were used. Like silicon dioxide stamps, metal stamps do not exhibit adhesion either. Fig.5-12 shows imprint made with a chromium-on-silicon stamp, containing columns of 400 nm and 100 nm diameter, into PMMA layer. No evidence of adhesion is observed over whole patterned of 1 x 1 mm^2 area.

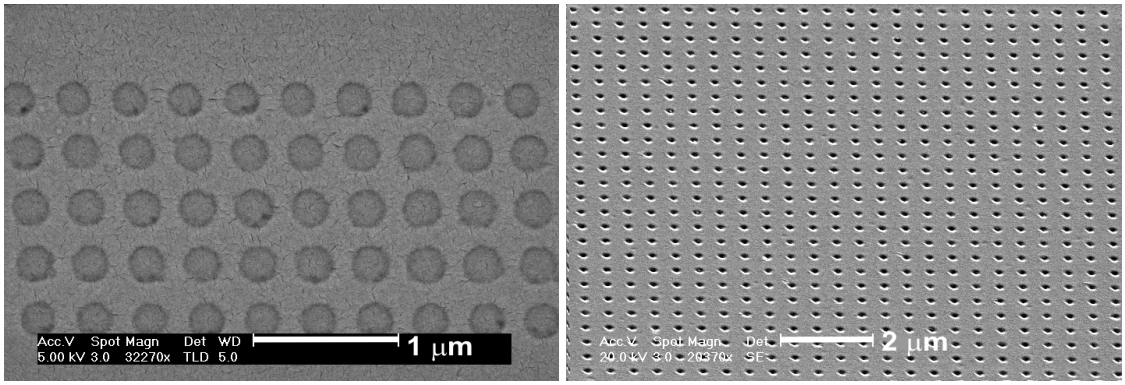

Fig.5-12. A 100 nm thick PMMA film imprinted with Cr-on-Si stamp at 190°C for 10 min. No adhesion is observed over the whole patterned 1 x 1 mm^2 area.

Table 3. Adhesion behaviour without an anti-adhesion layer applied. (---) indicates that the experiment was not made. The data summarize the results of 20 imprints for each combination of stamp and polymer. ("Certain"- heavy adhesion, impossible to separate stamp from substrate; "minimal"- adhesion was observed only over large non-patterned areas; "none"- no adhesion was observed.)

	Silicon	**Silicon oxide**	**Cr-on-Si**	**mr-L6000-on-Si**
PMMA	minimal	none	minimal	---
mr-L6000	---	---	---	minimal
mr-I8030F	minimal	---	---	---
PS	certain	none	---	---

Mechanical-induced adhesion is caused mainly by the friction and interlocking. During imprinting the polymer fills the stamp cavities and, ideally, perfectly conforms them. Thus, if stamp features have very rough sidewalls and undercutting profile, these features will be interlocked with the resist appearing as adhesion-like behaviour (Fig.5-13). Solution of this problem relies on careful specification of the stamp quality, which should indicate smooth surface and vertical sidewalls. These specifications depend strongly of used polymer and stamp design and have to be defined for each particular case individually. More critical is interlocking due to mechanical recovery of polymers. As demonstrated in section 5.2.3 above, this effect becomes apparent when

printing nm-features. If the printing temperature is not sufficiently high or printing time is not long enough for stress relaxation, the stress will be frozen. The restoring forces lead to the clamping of stamp features resulting in adhesion. Such kind of interlocking can be minimized, or even completely eliminated, by choosing appropriate processing parameters. This phenomenological explanation of adhesion mechanism is in agreement with results of [16], where a higher tendency to adhesion of small features was detected even if stamps with anti-adhesion coatings were used.

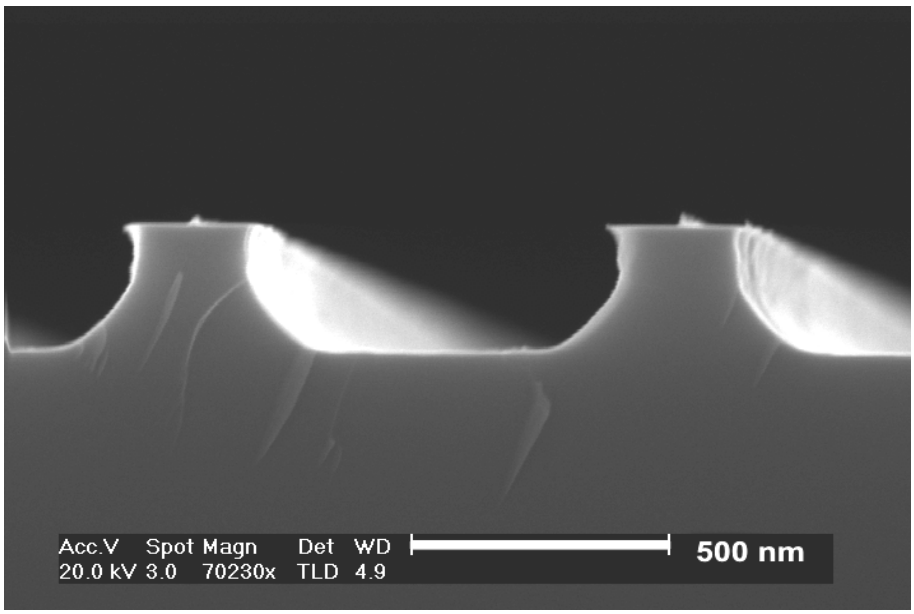

Fig.5-13. SEM micrograph of silicon stamp with undercut etched features. Such profile has a tendency to interlock the polymer resulting in adhesion-like behaviour.

A further reduction of adhesion forces between stamp and polymer can be achieved using anti-adhesion coatings. The main requirements are:

(a) the surface energy should be as low as possible;

(b) anti-adhesion layers thickness should be less compared to the features size to be printed;

(c) the coating must cover the surface completely and

(d) the stability of such coatings with respect to the whole printing cycle is very advantageous.

Suitable materials for anti-adhesion layers have been known for years. Most prevailing among them are fluorinated derivatives and fluorinated polymers like PTFE (Teflon), which are used in a wide range of applications from cooking pans through macroscopic replication technique to microscopic one. These materials have a much lower surface energy compared to those of stamps and polymers to be printed, as shown in Table 4, where values of widely used polymers are given and still need to be completed by values for polymers developed for NIL last years. The deposition of PTFE on micrometer-structured surfaces is well established [36,37]. However, applying a PTFE coating to the stamp in nanoimprinting may have a serious drawback. The polymer character does not make possible the deposition of very thin layers and its inherent surface roughness become apparent (Fig.5-14). This will result in large deviation of shape and size if stamp with nm-features is used. Whereas this can be acceptable, if printed µm- and sub-µm patterns will be used as an etch mask, it is absolutely not suitable for printing nm-features with, e.g., a targeted tolerance below 1%, as is needed for specific applications, like in polymers photonics.

Table 4. Values of surface tension energy for different surfaces [38].

	Surface energy, mJ/m^2
PMMA	41.1
PS	40.7
PTFE	15.6
-CF_2 and –CF_3	15-17
Silicon surface	20-26

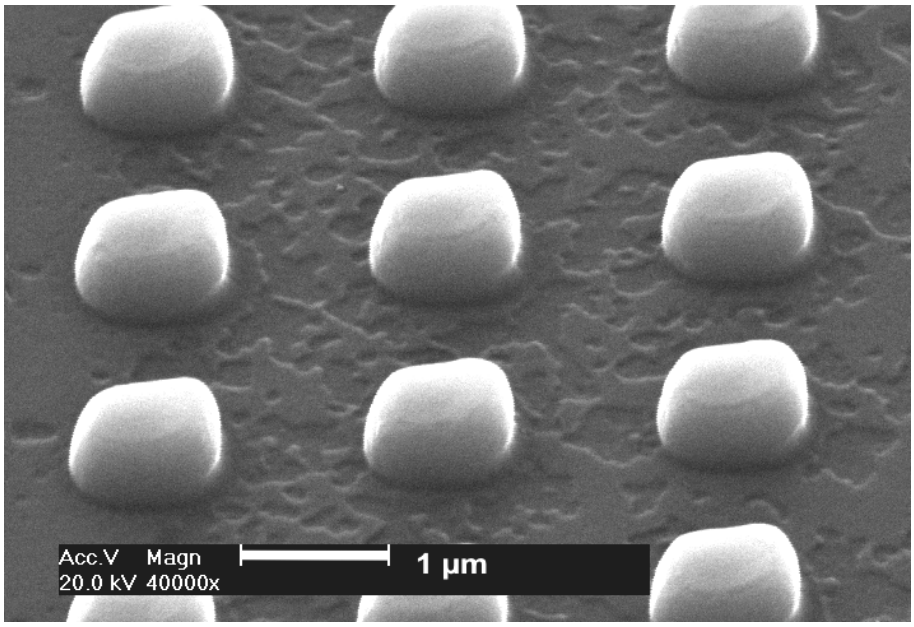

Fig.5-14. SEM image of a polystyrene film imprinted using a Si-stamp with PTFE anti-adhesive layer. No sticking over whole area of 2 x 2 cm^2 was observed. Submicrometer "roughness" features are observed at the bottom of the printed area, which is the replication of the large roughness of PTFE layer on the stamp.

This problem can be avoided using a self-assembled monolayer of fluorinated derivative as an anti-adhesive coating. One example is (heptadecafluoro-1,1,2,2-tetrahydrodecyl)-triethoxysilane. A simple way to prepare such film is by liquid-phase deposition (Fig.5-15, top), which requires the immersion of the stamp in a solution of fluorinated derivative at room temperature followed by blow-drying. While good anti-adhesive properties can be obtained in this way for stamps with patterns on the µm and sub-µm scale, the areas containing small nm-patterns still exhibit adhesion [16,39]. This arises as a result of insufficient wetting of these areas. An improvement can be achieved using a gas-phase deposition (Fig.5-15, bottom). In this coating approach the stamp is placed on a hot plate, a drop of (heptadecafluoro-1,1,2,2-tetrahydrodecyl)-triethoxysilane is deposited close to stamp, then both, stamp and drop, are covered with a Petri dish and baked for 45 min at 120°C. The base group at one end of the molecule provides a chemical bond to the stamp surface, while the ($–CF_3$) group at the other end

provides good anti-adhesion properties since it has low surface energy. Due to the chemical nature of the link between monolayer and surface, such layer has been found to be stable even after a number of printing cycles.

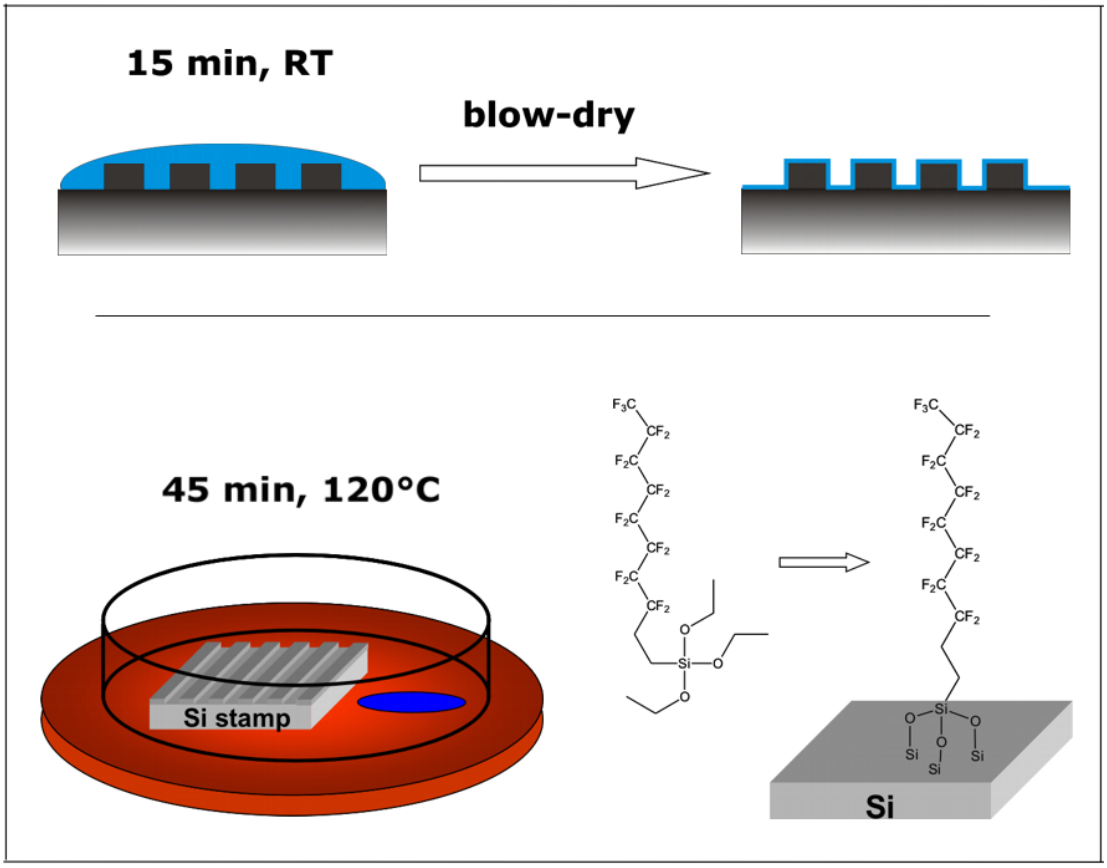

Fig.5-15. Schematics of the liquid-phase (top) and gas-phase (bottom) preparation of anti-adhesion coatings based on the self-assembled monolayer of (heptadecafluoro-1,1,2,2-tetrahydrodecyl)-triethoxysilane. The base group at one end of molecule provides a chemical bond to the stamp surface, while the ($-CF_3$) group at the other end, having low surface energy, provides good anti-adhesion properties.

5.4. Summary

The choice of polymers appropriate for nanoimprinting can be aided by considering the mechanical behaviour discussed here. Good flow behaviour and anti-adhesion properties are essential for NIL. A good understanding of the interdependence

of material viscosity, printing temperature, pressure, its hold time, the rate, at which temperature and pressure increase, layer thickness and size of the stamp features is needed. Such an understanding will certainly contribute to the definition of the potential and limitations of nanoimprint lithography. The molecular weight and polymer recovery were found to be a major limiting factor for resolution and critical dimension. Whereas reliable processes for new polymer developed for NIL, like mr-I8000, mr-I9000 and mr-L6000 series, were established, they are still not explored up to its limits with respect to resolution and printing fidelity on sub-20 nm scale. Adhesion may also become a crucial point when printing nm-feature limiting the potentials of nanoimprinting and will require appropriate preventive measures. Since the use of anti-adhesion layers increases the complexity of whole NIL process and, moreover, its preparation adds to the cycle time thus decreasing throughput, methods based on appropriate choice of materials and process parameters are preferable. In this context, the complement of database of the properties of polymers, in particular the surface energy, developed for NIL last years is needed. Thus, the main challenge is to define a process for a given polymer and application with an acceptable compromise between high throughput, high quality and reliability.

Chapter 6. Evaluation of imprint induced effects on optical properties

Applications in optoelectronics are limited not only to passive devices. Many optoelectronic devices, like semiconductor lasers and light emitting diodes, use technologically important III-V semiconductors GaAs- and InP-related materials as an active layer [40,41,42]. These require fabrication steps with accuracy in nm-range usually involving expensive EBL and RIE. In this context, NIL could be used to pattern a mask to be transferred into a semiconductor multi layer by RIE in order to be used later either electrically or optically. The density of non-radiative recombination centres, as well as internal stresses in the active layer, play a significant role in device performance [43]. Besides both fabrication steps, EBL and RIE, induce damages, avoiding EBL at least one source of damage would be eliminated if NIL does not damage the active layer. In this case, one key question to be answered is to what degree does the process step of nanoimprinting, with its pressure and temperature cycle, affect electrical and optical properties of the semiconductor active layer.

A study of the luminescence and photoluminescence excitation of semiconductor quantum well structures subjected to nanoimprint lithography was undertaken to ascertain if this lithographic technique induces detrimental changes in the properties of the active layers over a range of pressures and temperatures, typically used in printing process.

Photoluminescence (PL) measurements were done comparing integrated intensity, which is an indication of the number of non-radiative recombination centres, energy position and full width at half maximum (FWHM) for each QW. Photoluminescence excitation (PLE) spectra from both samples were obtained in an attempt to determine the presence and magnitude of changes in the internal strain of the printed samples, which is expected to manifest as changes in the splitting between the heavy-hole (hh) and the light-hole (lh) exciton of the different quantum wells.

6.1. Samples

Two multiple quantum well (MQW) structures of lattice-matched MBE-grown GaAs/$Al_{0.3}Ga_{0.7}As$ and MOVPE-grown $Ga_{0.47}In_{0.53}As$/InP were used for optical experiments. Details of the grown process are reported in [44,45]. The samples were designed to consist of three quantum wells of different thickness positioned at different depths (Fig.6-1). Thus, having the emission spectrum with its emission bands coming from different depths within the sample, it is possible to estimate how far into the sample nanoimprint lithography could induce defects, if any.

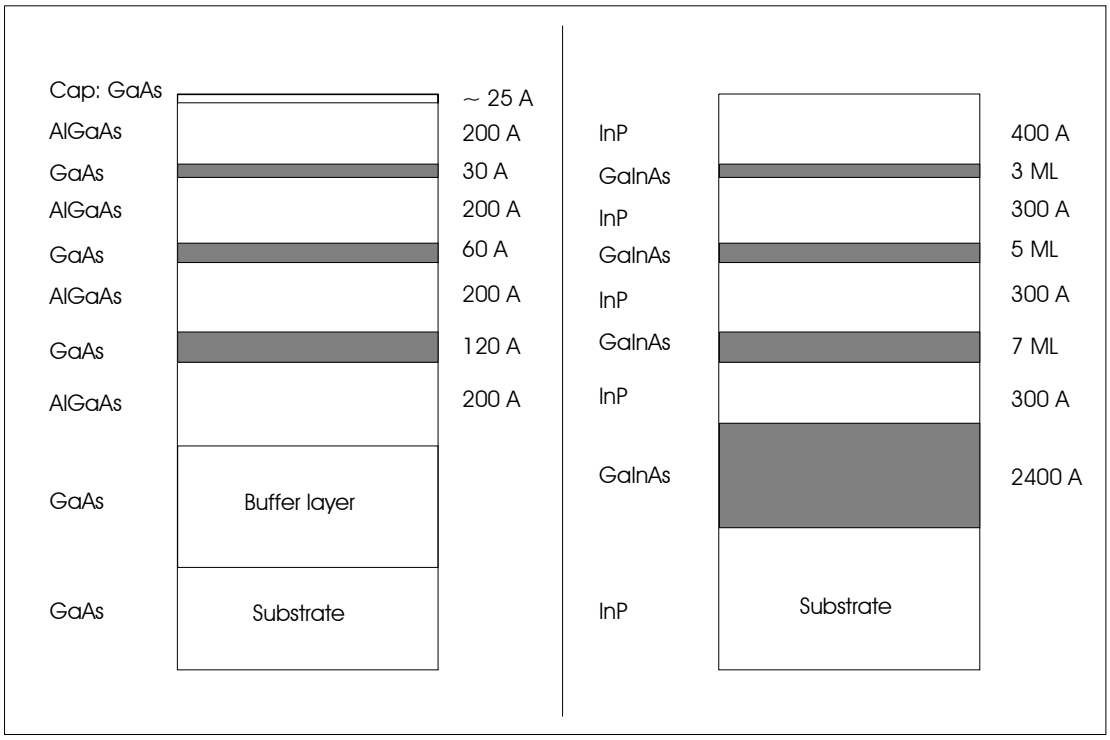

Fig.6-1. Schematic of the cross-section of (left) $Al_{0.3}Ga_{0.7}As$-GaAs and (right) $Ga_{0.47}In_{0.53}As$-InP multiple quantum well structure samples used in the optical investigations.

6.2. Experimental details

For NIL experiments the samples were spin-coated with 600K poly(methyl methacrylate) (PMMA) and baked at 120°C for 10 min. The stamp and the substrate were brought in contact and heated up to the imprint temperature (T_{imp}). The pressure (P_{imp}) is applied and held for several minutes at this temperature. After cool down, the stamp and substrate are separated. Both pressure and imprint temperature were varied in a wide range: up to 200 bar and up to 190°C, respectively. The stamps used were silicon stamps fabricated by UV-lithography and dry etching. The size of structures on stamps ranged from micrometers down to 400 nm. Imprints were made using both an *Obducat Nano-Imprinter* press and hydraulic press.

Photoluminescence (PL) and photoluminescence excitation (PLE) measurements were performed either with a standard lock-in detection based system equipped with the double spectrometer and Ge detector (GaInAs/InP samples) or in a photon counter system equipped with the triple spectrometer and photomultiplier tube (GaAs/AlGaAs samples) with resolution of about 0.6 meV and 0.1 meV, respectively. The arrangement is described in section 3.4.

6.3. PL and PLE results

PL and PLE investigations were carried out on samples before and after imprint. Samples were subjected to the NIL process with printing temperature up to 190°C and printing pressure in the range from 40 bar up to 200 bar. The pressure hold time was typically 5 min. Before measurements, the printed resist was removed in acetone. Measurements were performed at 20K.

In Fig.6-2a typical PL spectra of $Ga_{0.47}In_{0.53}As$/InP MQW structure are shown before (top) and after (bottom) printing with pressure of 200 bar. Peaks at 1.085, 1.133 and 1.247 eV correspond to the emission bands of QWs with 7, 5 and 3 monolayer (ML) nominal thickness, respectively. The full width at half maximum (FWHM) of these peaks is 20, 16 and 9.6 meV, respectively. Within the spectral and intensity resolution of the PL measurements, no significant degradation of the luminescence intensity is observed. The PL intensity of the 3ML emission decreases by about a factor of two, which is not significant in the emission of ultrathin quantum wells. Moreover, neither change in the emission energy position nor in the FWHM is detectable for printed samples compared to the as-grown sample. The PLE spectra of uppermost QW with thickness of 3ML before and after printing are shown in Fig.6-2b, where observed

peaks attributed to the E_{1h}, E_{13h} and E_{2h} [46]. No evidence of strain was found as no changes were detected in the energy separation of the exciton bands after printing.

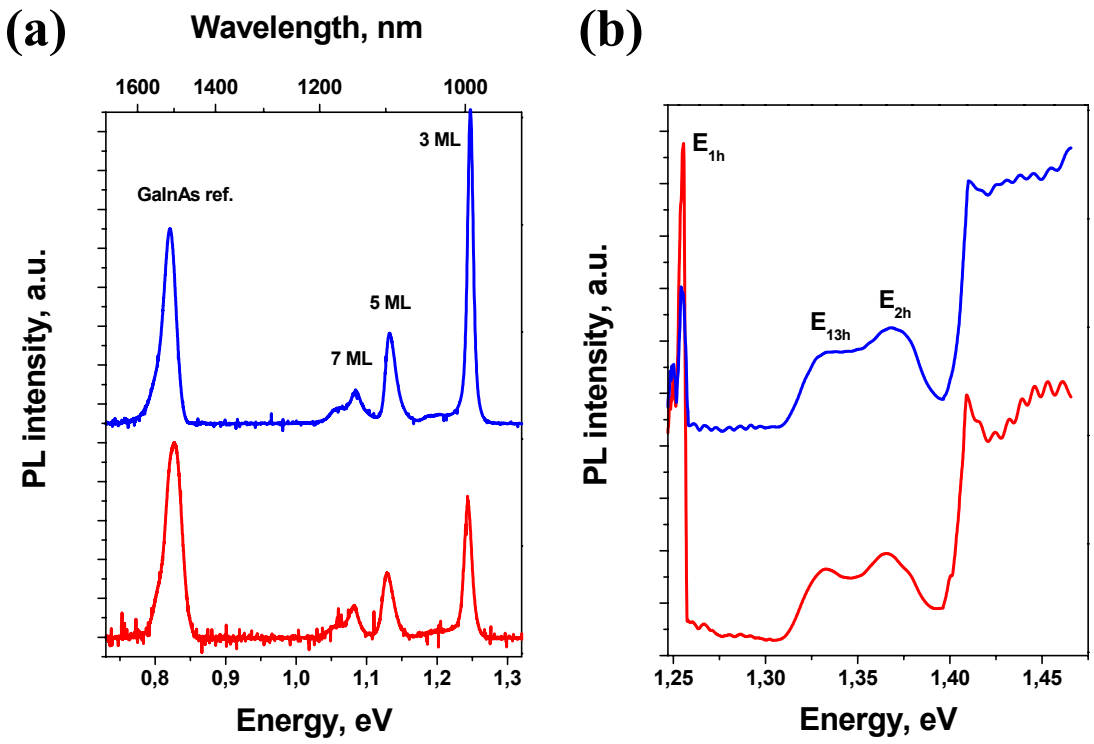

Fig.6-2. (a) PL spectra of the $Ga_{0.47}In_{0.53}As$/InP MQW sample at 20K before (top) and after imprint with pressure of 200 bar (bottom). (b) PLE spectra of the $Ga_{0.47}In_{0.53}As$/InP MQW sample before (top) and after (bottom) imprint. Spectra were excited at the peak energy of the PL emission of the QW with 3 ML thickness (1.247 eV).

Typical PL spectra of GaAs/$Al_{0.3}Ga_{0.7}As$ before and after NIL are shown in Fig.6-3. The peaks at 1.549, 1.613 and 1.731 eV correspond to the emission bands of QWs with nominal thickness of 12, 6 and 3 nm, respectively. No significant changes of luminescence intensities nor emission energies were detected on the samples subjected to the NIL process with pressure up to 200 bar (Fig.6-3a, bottom). Some samples exhibit a dependence of their emission intensity upon excitation power even before printing (dash and solid lines in Fig.6-3b, top). We ascribe this to the presence of non-

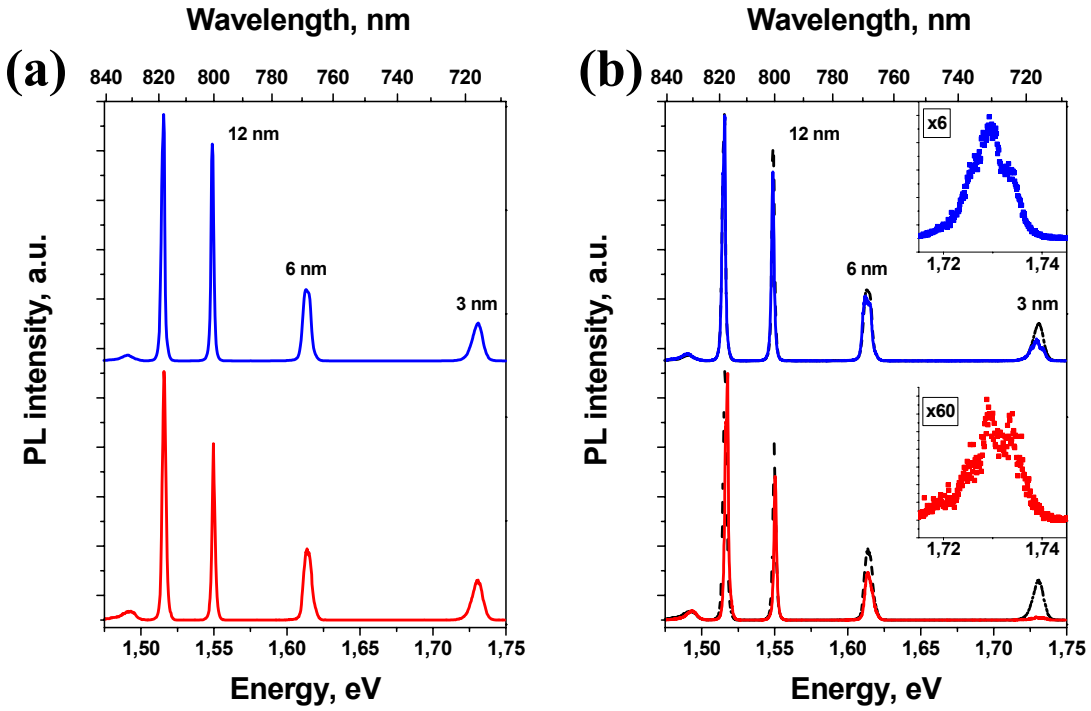

Fig.6-3. PL spectra of the GaAs/$Al_{0.3}Ga_{0.7}As$ QW sample at 20K. (a) Spectra recorded before (top) and after (bottom) imprint with pressure of 200 bar. (b) Spectra of the sample initial containing the considerable number of defects before (top) and after (bottom) printing with pressure of 60 bar. The dash and solid line correspond to the different excitation power. The insets show an expanded part of the spectrum to demonstrate the changes in the emission intensity of the 3 nm quantum well.

radiative defects in the as-grown sample. In this case, a dramatic change in the intensity of the uppermost quantum well (3 nm), placed 20 nm below the surface, and to a lesser degree of the second from the top quantum well (6 nm), placed 40 nm below the surface, after being subjected to NIL at 60 bar is observed (Fig.6-3b, bottom). However, within the resolution of the experiment, no changes in energies were detected (see expanded part of the spectrum in insets to Fig.6-3b). The deeper quantum wells were not affected. The PLE analysis did not yield any difference between samples before and after printing neither samples with or without initial presence of defects. Typical PLE spectra are shown in Fig.6-4 for the 6 nm (left) and the 3 nm (right) quantum wells

before and after printing, where observed peaks attributed to the E_{1h} and E_{2h} [46]. In any case, NIL does not induce additional strains in these semiconductor MQWs.

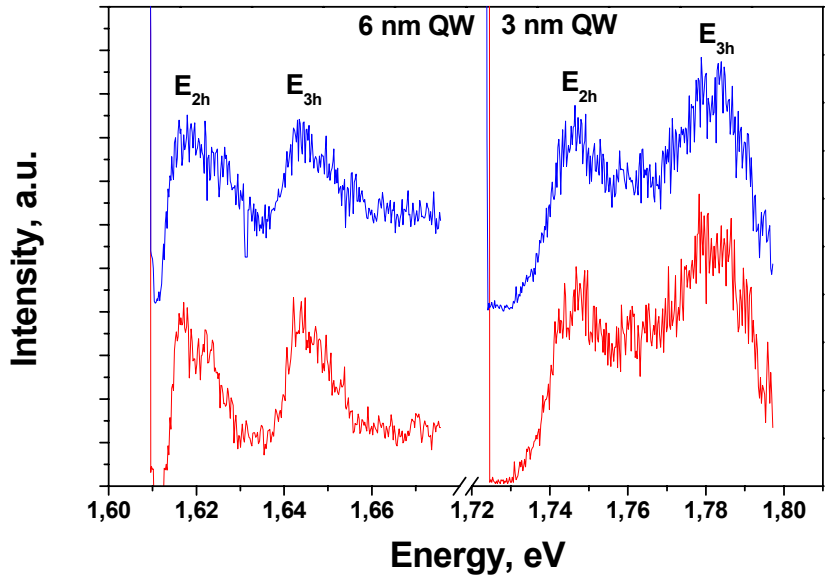

Fig.6-4. PLE spectra of a GaAs/$Al_{0.3}Ga_{0.7}As$ QW sample before (top) and after (bottom) imprint. Spectra were excited at the peak energy of the PL emission of (right) the QW with 3 nm thickness (1.724 eV) and (left) the QW with 6 nm thickness (1.610 eV).

6.4. Electrical properties

Although the following part of the work was not carried out in Wuppertal, it is included here for completeness. Recently, investigations were carried out in Lund University by group of Prof.L.Montelius within the join EU Project CHANIL in order to analyse the effect of NIL upon electrical properties of a two-dimensional electron gas (2DEG) of a MOVPE-grown high mobility $Ga_{0.25}In_{0.75}As$/InP modulation-doped heterostructure (MDHS) [47,48]. Electrons in the 2DEG were confined to a 9 nm thick quantum well located 40 nm below the surface. The magneto transport experiments were performed on the samples before and after printing. Samples were spin-coated

with 950K PMMA and baked at 140°C for 5 min and printed at different pressures up to 80 bar using a Nickel CD stamp. The hold time during printing was 1 min at the selected pressure and temperature. After imprinting the resist was removed in hot acetone and IPA and the sample was blow-dried. For electrical measurements, standard Hall bars with Au/Ge ohmic contacts were fabricated using optical lithography technique. The samples were cooled to 300 mK in darkness and both the longitudinal resistance (Shubnikov de Haas effect) and the Hall resistance (quantum Hall effect) were measured in order to determine the electron mobility and electron concentration of a 2DEG. The current through the structures was about 10 nA r.m.s. (root mean square), i.e., small enough to keep electron heating to a negligible level.

The observed variations of 2DEG mobility after NIL, by 1.5 times, are attributed to the non-uniform mobility over the sample. Transport measurements of the same sample piece before and after NIL were cumbersome since electrical contacts would have to be removed for NIL due to the parallel sample and stamp requirements. Then it was not possible to ascertain if the pressure used in NIL affect the 2DEG mobility by more than a factor of 2-3. On the other hand, the 2DEG electron concentration was around $8.9 \cdot 10^{11}$ cm^2 at 0.3K and was not affected by imprint pressures up to 80 bars. This means, the Lund team concluded, that the pressures used do not induce deep levels, which may trap electrons.

Thus, the investigations of the Lund University team yielded no evidence of deterioration of neither the mobility nor carrier concentration of a two-dimensional electron gas in a modulation-doped $Ga_{0.25}In_{0.75}As/InP$ heterostructure. Electron waveguide devices made using NIL demonstrate a fully functional device, which confirms the negligibly damage induced in the 2DEG during the NIL process [48].

6.5. Summary

GaAs/AlGaAs and GaInAs/InP multiple quantum well structures were studied in order to determine the influence of nanoimprint lithography on the optical properties of device-like semiconductor multilayers. It was found that NIL does not affect the integrated emission intensity, emission energy and strain of samples subjected to pressures up to 200 bar. No evidence was found of strains induced by the NIL process in any of the studied samples over wide range of pressures.

In a separate study at Lund University, the mobility measurements of the 2DEG in a GaInAs/InP MDHS showed large variations, which were attributed to a non-uniformity of mobility over the sample. The carrier concentration of the 2DEG was found to be practically unchanged after NIL.

Based on our work and work of Lund University it is concluded that NIL has the potentials to replace conventional lithography technologies, like electron beam lithography, to define the mask for fabrication of semiconductor opto-electronic devices.

Chapter 7. Imprinted passive optical devices

Polymer optical devices are an interesting alternative to dielectric or semiconductor devices, since they provide for flexible, large area and low-cost fabrication process through the simple spin-coating and further lithography steps. In addition, modifying the chemical structure or doping of the polymer permits tuning of the physical properties in an easier manner compared to semiconductor. A number of polymer-based optical devices have been fabricated and characterised in other laboratories, for example, waveguides for optical interconnections [49], combiners for WDM applications [50], arrayed waveguide grating (AWG) multi-/demultiplexer [51], modulators and switches [52,53,54], filters, attenuators, amplifiers, add/drop multiplexers, photonic crystal waveguides, etc. These devices have definite advantages over semiconductor or widely used today silica-based analogues including: lower switching power, higher wavelength tuning range and the ability to make temperature-independent AWG by matching the positive coefficient of thermal expansion and the negative thermo-optic coefficient of the polymer. Thus, high expectations have been

placed on polymers as the material of choice for cost-efficient optical components and circuits. The main technique to fabricate polymer optical devices remained until recently UV lithography followed by dry etching. Due to the high resolution, low-cost and high throughput, over the last years nanoimprint lithography has become a serious candidate to replace conventional lithography techniques.

The goal of this Chapter is to demonstrate the possibility to fabricate by nanoimprint lithography simple passive polymer-based optical devices. Here results for two types of passive optical devices: gratings and waveguides fabricated by NIL are described. For the latter, the field of sub-wavelength optics is addressed by imprinting of 2D photonic crystal (PC) structures.

7.1. Diffraction grating

A 7 x 7 mm^2 diffraction grating with 1250 lines/mm, i.e. 400 nm lines with 800 nm period, was imprinted 400 nm deep into PMMA. The imprint process is decribed in details in section 5.2.1 A SEM micrograph of a typical imprint is shown in Fig.7-1. It was used as a grating in a 60 cm monochromator setup with a 5 mm entrance hole and a 2 cm exit hole. The grating characterization was done by Dr. J. Seekamp and Dipl.-Phys. T. Maka. The appearance of the imprinted gratings to the naked eye under an optical microscope is shown in Fig.7-2. The image shows the colour play of the grating from violet to red due to the varying incident angle of the incident light, illustrating the disperse properties. The homogeneity of the dispersion over an area of roughly 100 x 100 μm^2 is observed. In Fig.7-3 the full width at half maximum of the peaks is seen to be around 20 nm over a range from the near UV to the near infrared.

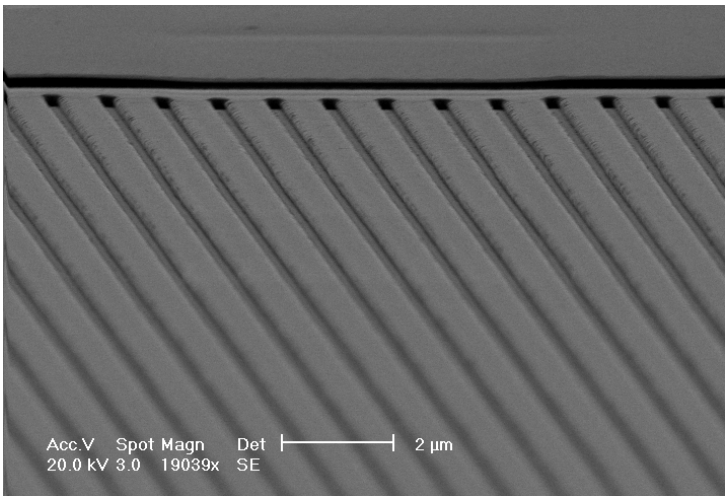

Fig.7-1. SEM micrograph of a grating with 1250 lines/mm imprinted into 400 nm thick PMMA.

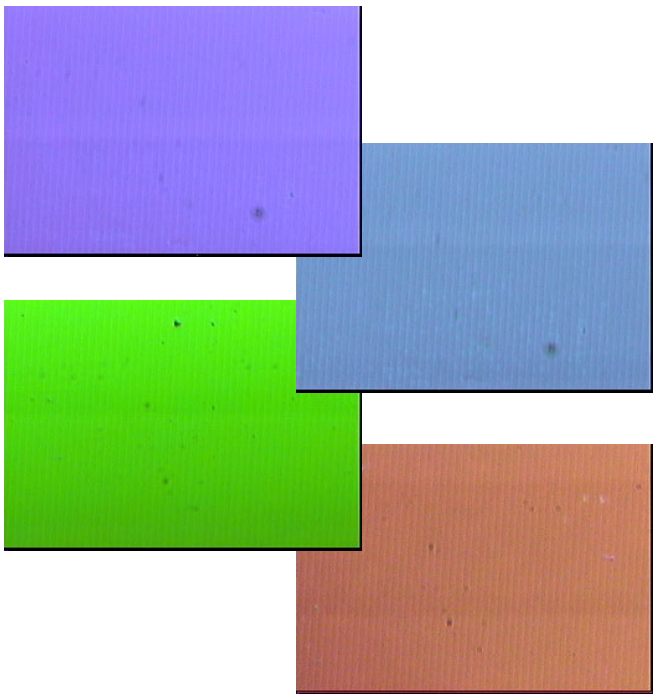

Fig.7-2. Optical microscope photography of imprinted 1250 lines/mm grating with different angle of incident show the homogeneity of the dispersion over an area of roughly 100 x 100 μm^2.

The grating efficiency using the setup is measured to be better than 4% compared to values between 60 and 80% for commercially available holographic gratings. Comparing the position of the peaks with the theoretically expected values given by

$m\lambda = 2d \cdot \cos\phi \sin\theta$ where m as the order of the reflection and the other denominators chosen as in the inset of Fig.7-3 a good agreement is found. For a given angle, the wavelength of the diffracted light was proportional to the line spacing. If the linewidth of the diffracted peaks is attributed to variations of the line spacing alone, this variation would be below 3% of the linewidth. The grating investigated here had a line spacing of 800 nm. Hence, the deviation for this grating was below 24 nm on average.

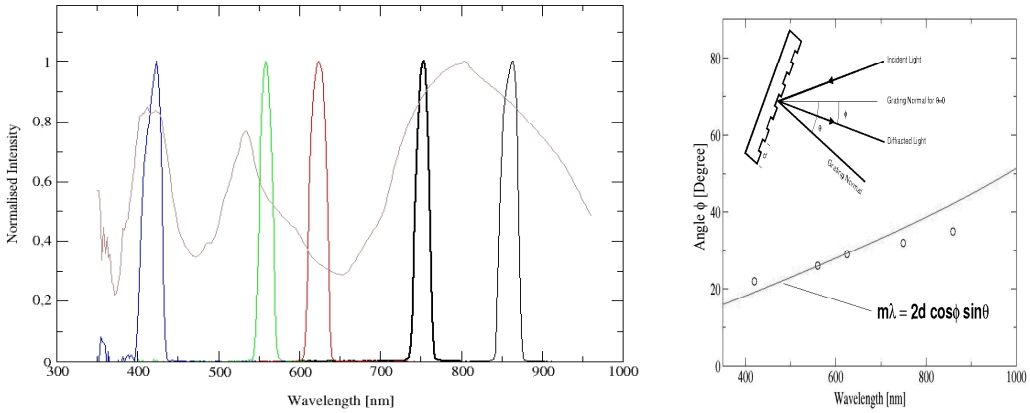

Fig.7-3. (left) Transmission and 0th order reflection characteristics of a printed 7 x 7 mm^2 grating. The coloured lines show a set of transmission lines from UV to the near infrared. The light grey line in the background gives the characteristic for the 0th order reflection. (right) Calculated (solid line) and measured (open circles) wavelength-angle pairs for a printed 7 x 7 mm^2 grating. The inset sketches the geometry used for measurements.

7.2. Waveguides

Two kinds of waveguides were fabricated and tested: a set of 5 mm slab waveguides with 4 µm width and 8 µm period and a Y-branch, which is intended to be a building block of a photonic crystal (PC) waveguide passive device. Both are fabricated by a 400 nm deep printing of polystyrene on silicon dioxide substrate. The fabrication process is described in section 5.2.1. A SEM image of the cross-section of such waveguides is shown in Fig.7-4 (left).

A basic fibre coupling setup was used to characterise these printed waveguides. A monomode fibre with a mode field diameter of about 4 μm was used to couple in 514 nm light from an Ar-laser. The guided light is collected by a multimode fibre of 200 μm core diameter. To obtain the damping coefficient of the waveguide the intensity of the light coupled directly from one fibre to another was compared to that guided by the printed waveguide. Measurements for 5 mm printed rib waveguide including coupling loss give the total loss of 50 dB, which is attributed mainly to the high coupling loss between fibres and polymer waveguide at both entrance and exit. This is clearly observed in the photograph of the Y-branch waveguide in Fig.7-4 (right): a bright spot at the entrance. Nevertheless, the light guiding in the NIL made waveguide is demonstrated, the light at the exit of waveguide can be seen with the naked eye. Moreover, it was shown that such waveguides could be fabricated in one step, i.e., without an additional etching for removal of the residual layer [55]. The numerical simulations claim that the remaining layer thickness, typical for the NIL process, does not affect the quality of confinement in a waveguide.

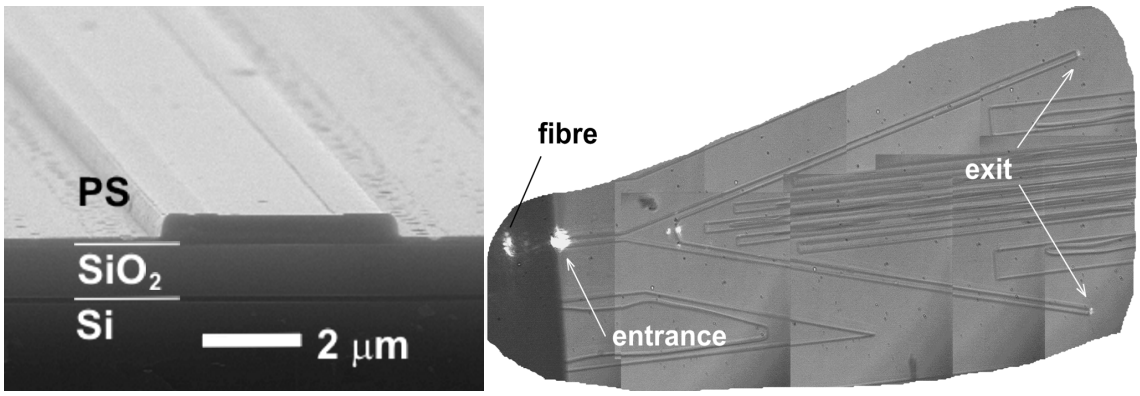

Fig.7-4. (left) Y-branch structure imprinted into polystyrene on silicon dioxide substrate. Light of 514 nm is coupled into the structure from a monomode fibre with a mode field diameter of about 4 μm from the left. The light travels in the waveguide reaching both ends of the branch despite losses at the joint. (right) Cross-section of the waveguide imprinted in polystyrene on silicon dioxide substrate. The imprint depth is 400 nm, the residual layer is less than 100 nm.

The printed Y-branch waveguide was intended for investigations of photonic crystal (PC) structures placed in one of the branches. The future of photonic crystal based applications is unequivocally bright, as for example, highly efficient photonic crystal lasers and extremely bright LEDs, waveguides and the use of photonic crystals for high resolution spectral filtering. Photonic crystals usually consist of dielectric materials that is, materials that serve as electrical insulators or in which an electromagnetic field can be propagated with low loss. Holes are arranged in a lattice-like structure in the dielectric and repeated identically and at regular intervals, a property known as periodicity. If built precisely enough, the resulting crystal will have what is known as a photonic bandgap, a range of frequencies within which a specific wavelength of light is blocked. In addition, it is possible to create energy levels in the photonic bandgap by introducing defects. For example, changing the size of a few of the holes in a photonic crystal is equivalent to breaking the perfect periodicity of the silicon crystal lattice. Thus, although perfect crystals are valuable for fabricating dispersive elements such as superprisms and mirrors, those with defects enable to custom design photonic crystals that allow precise control of the frequencies and directions of propagating electromagnetic waves. This feature makes them especially useful in optical telecommunications. The accuracy needed for fabrication of photonic crystals can be simply estimated as periodicity/50 [56], for example, for PMMA photonic crystal on silicon dioxide substrate at an operating wavelength of 1.55 μm gives the following values: period of 552 nm, the placement accuracy have to be better than 10 nm.

In this work, several stamps with pattern geometry required for realization of photonic crystal were fabricated and imprinted into different polymers. An example of PC structure placed in one arm of Y-branch is shown in Fig.7-5. To combine the

nm-structures with the μm and mm size structures of the Y-branch, a mix-and-match approach was used resulting in stamps of the type depicted in Fig.7-5, top. The stamp was made using a simple design to realize a PC with a band gap in the near infrared. Part of the stamp and an imprint are shown in Fig.7-5, bottom. To form a photonic band gap structure in the visible wavelength range a Cr stamp with 100 nm diameter dots and a 200 nm period in a square lattice was fabricated and printed into PMMA on silicon substrate. Stamp and imprint are shown in Fig.7-6. The characterization of imprinted PC was not finished because of very high coupling losses.

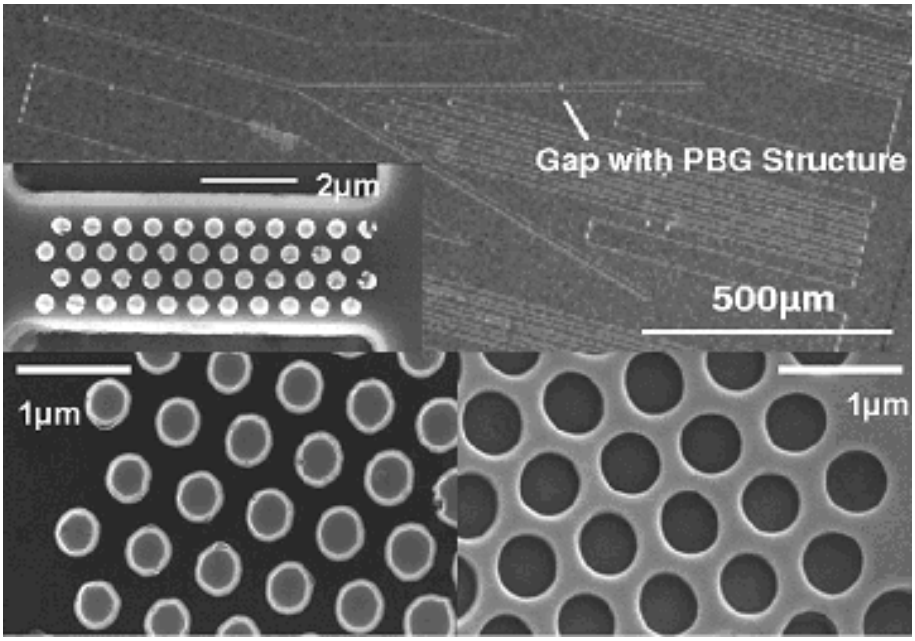

Fig.7-5. (top) Stamp for a Y branch structure with a photonic crystals in the upper arm. (bottom) SEM micrographs of a pattern transfer imprinting of photonic crystals. The 300 nm columns with 120 nm separation between them (left) are successfully printed into PMMA (right).

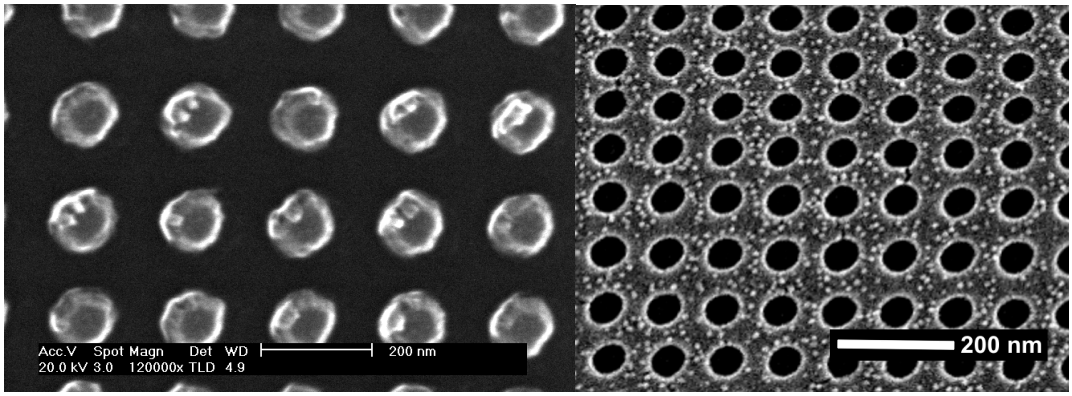

Fig.7-6. Photonic crystal 2D lattice preparation for visible wavelengths. SEM micrograph of a stamp with 100 nm diameter Cr dots and a 200 nm period in a square lattice made on silicon (left) is imprinted into PMMA (right).

7.3. Summary

Polymer optical devices have great prospects for future integrated optical circuit due to their good processibility and integration advantages. In this context, nanoimprint lithography, as a technique relied on the direct polymer patterning, offers the possibility to fabricate passive polymer devices in one step process. In addition, due to the capability for low-cost and high volume production, nanoimprint lithography pretends to be a main technique for future integrated optical circuits, once the printing technology is established for simple polymer optical devices. The pattern transfer for micrometre size structures was found to be accurate to the 10 nm scale, as it was shown in Chapter 5. The feasibility of nanoimprint lithography to fabricate polymer optical devices has been demonstrated here on few examples, such as gratings, waveguides and photonic crystals. At this stage the reliable process to fabricate these devices is developed, as shown in Chapter 4 and Chapter 5 above, and only basic characterization was carried out. Gratings with an area of 7×7 mm^2 showed uniformity better than 3% over whole area. PS rib waveguides is expected to have losses on the acceptable level,

but they were not measured because of high coupling losses. The remaining layer thickness, typical for the NIL process, does not affect the quality of confinement in a PC and even with a remaining layer, a bandgap should be observed, according to the 3D calculations. More detailed experiments to quantify key parameters and compare them with parameters of analogous devices made by UV lithography and RIE are still remaining to be done.

Chapter 8. Conclusions

This thesis deals with the potentials and perspectives of Nanoimprint Lithography for the fabrication of optoelectronic and optical devices. These include the development of processes (fabrication of necessary stamps, printing), appropriate materials, one-step fabrication of passive polymer optical devices, optical properties of semiconductor substrate subjected to the NIL cycle. Since such applications make high demands of accuracy and precision, the especial attention is paid to the material and process issues, which may affect the limitations to the resolution and control of features size.

To fabricate stamps, reliable processes (electron beam lithography and metal lift-off) were developed to achieve high density of 20 nm features with suitable precision and line-edge roughness. The problem of the control of feature size becomes a serious bottleneck, when fabricating stamps with sub-20 nm features. It was shown that the polymer and metal properties come into play, and conventional lift-off methods are not sufficient when trying to achieve sub-10 nm structures. An alternative technique

proposed here is the direct writing of polymer stamps, in particular, using mr-L 6000 on Si. In this case, the fabrication process does not involve metal lift-off, while material properties looks very promising on the scale below 20 nm. Moreover, a low-cost reproduction process can be introduced for such stamps, such as fabrication of second and third stamp generation from the master stamp.

Concerning polymer to be printed, appropriate mechanical characteristics, in particular, good flow behaviour and anti-adhesion properties, are essential for NIL. In this context, the interdependence of the material viscosity, printing temperature, pressure and its hold time, layer thickness and size of the stamp features found as a key factor. The understanding of this interdependence certainly contributes to the definition of the potential and limitations of nanoimprint lithography. The molecular weight and polymer recovery found to be a major limiting factor for resolution and critical dimension. Whereas reliable processes for new polymers developed for NIL, like mr-I8000, mr-I9000 and mr-L6000 series, are partly established, they are still not explored up to its limits with respect to resolution and printing fidelity on the sub-20 nm scale. Adhesion also becomes a crucial point when printing nm-features limiting the potentials of nanoimprinting and requires appropriate preventive measures. As the use of anti-adhesion layers increase the complexity of the whole NIL process and its preparation takes time thus decreasing throughput, methods based on right choice of materials and process parameters are preferable. Thus, the main task is to define a process with a compromise between high throughput, high quality and reliability for a given application.

Nanoimprinting has been demonstrated to be a suitable technique to imprint passive optical devices in organic materials. In this case, polymers have to meet both demands in mechanical properties and optical properties. Polystyrene and mr-L6000 are

some of most appropriate ones for this purpose combining relative high refractive index and good printability. Few devices, such as gratings, waveguides and photonic crystals, for application in visible range were demonstrated during this work.

The investigations carried out during this work prove that NIL does not affect the integrated emission intensity, emission energy and strain of quantum wells substrate subjected to the NIL cycle, if the printing pressure kept below 200 bar and printing temperature below 190°C. No evidence was found of strains induced by the NIL process over a wide range of pressures. Thus, NIL can be safely used to define the mask for fabrication of semiconductor opto-electronic devices, thus replacing conventional lithography technologies, like electron beam lithography.

The outlook for future research in the field of nanoimprint lithography inevitable goes through extending of knowledge in nanorheology, in particular the polymer flow in very thin films (down to few nm), which is of interest when very thin residual layer and very homogeneous polymer thickness over the whole wafer are necessary. A more critical and still widely open research field is the long time stability of imprinted structures. This includes the mechanical recovery, i.e., the knowledge of the elastic energy, which is a measure of elastic deformation remaining in the polymer after printing. A better understanding of stored elastic energy could help not only to predict long-time stability but also to understand better the printing process on the molecular level. Recently, work in this direction started in collaboration with the National Physical Laboratory, UK [57], where the first attempt to measure the distribution of elastic energy in a 200 nm wide and 200 nm high polymer line was made.

Although recently few representative optical applications, like 2D PC for organic laser applications, polarising devices and add-drop filters, were shown to be suitable for the nanoimprint-based fabrication processing, much remains to be done.

This inevitable will include the work to quantify key parameters and compare them with parameters of analogous devices made by UV lithography and RIE. Another prospect is the range of optical devices for standard telecommunication window, where the NIL has great advantages such as the easiness to process suitable polymers. For example, Teflon, which is highly resistant to the electron and photon exposure, can be easily patterned by nanoimprinting. It has the lowest known optical losses in near infrared, thus becoming a good candidate as a material for waveguiding structures operated in the communication wavelength range. In this context, in a follow-on project, Teflon will be used as a cladding layer for buried or embedded waveguides, where NIL will be applied to pattern Teflon layer, followed by filling the grooves with “core” polymer.

Acknowledgments

First of all I would like to thank Prof. Dr. Clivia M. Sotomayor Torres, my supervisor, for the opportunity to carry out this work at her Optical Nanostructures Laboratory, Institute of Materials Science, Dept. of Electrical, Information and Media Engineering, University of Wuppertal, and for her continued interest in my work, support, encouragement and helpful discussions I have gotten in this time.

Thank you very much to Prof. Dr. Ludwig Josef Balk for taking over the second expertise.

I also wish to express my sincere thanks to my colleagues at the Laboratory for the time we spend together, helpful discussions and support. Particular thanks to Dr. Jörg Seekamp, day-to-day supervisor during first years, Dr. Sergei Romanov and Dipl.-Phys. Torsten Maka for valuable help with optical measurements. I am grateful to the partners within join German and international projects: Prof. Jouni Ahopelto from VTT Microelectronics Centre, Finland for supply of stamps, Dr. Karl Pfeiffer from Microresist Technology GmbH, Berlin for polymers and interesting discussion on polymer chemistry, Prof. Lars Montelius from Lund University, Sweden and Prof. Andreas D. Wieck from Ruhr-Universität Bochum for growth of QW samples.

Financial support from the EU/IST project CHANIL (IST-1999-13415) and German Research Council DFG (grant SCHE 580/3-3) is acknowledged.

References

1 S.Y. Chou, P.R. Krauss and P.J. Renstrom, Appl.Phys.Lett., **67**, (1995), 3114-3116

2 T. Haatainen, J. Ahopelto, G. Gruetzner, M. Fink and K. Pfeiffer, Proc. SPIE Vol. **3997**, (2000), 874-880

3 J. Haisma, M. Verheijen, K. van den Heuvel and J. van den Berg, J.Vac.Sci.Technol.B, **14**, (1996), 4124-4128

4 T. Borzenko, M. Tormen, G. Schmidt, L.W. Molenkamp and H. Janssen, Appl.Phys.Lett., **79**, (2001), 2246-2248

5 M. Colburn, S. Johnson, M. Stewart, S. Damle, T. Bailey, B. Choi, M. Wedlake, T. Michaelson, S.V. Sreenivasan, J. Ekerdt and C.G. Willson, Proc. SPIE, Vol. **3676**, (1999), 379-389

6 A. Kumar and G.M. Whitesides, Appl.Phys.Lett., **63**, (1993), 2002-2004

7 D.L. White and O.R. Wood, J.Vac.Sci.Technol.B, **18**, (2000), 3552-3556

8 Z. Yu, W. Wu, L. Chen and S.Y. Chou, J.Vac.Sci.Technol. B, **19**, (2001), 2816-2819

9 B. Heidari, I. Maximov and L. Montelius, J.Vac.Sci.Technol. B, **18**, (2000), 3557-3560

10 H. Schift, C. David, J. Gobrecht, A. D'Amore, D. Simoneta, W. Kaiser and M. Gabriel, J.Vac.Sci.Technol.B, **18**, (2000), 3564-3568

11 M. Otto, M. Bender, B. Hadam, B. Spangenberg and H. Kurz, Microelectronic Engineering, **58**, (2001), 361-366

12 T. Hoffmann, 2003, in book *Alternative Lithography: Unleashing the Potentials of Nanotechnology*, ed. C.M. Sotomayor Torres, (New York: Kluwert Academic / Plenum Publischers), p.25-45

13 T. Haatainen, P. Majander and J. Ahopelto, presented at the 6th EU-MELARI/NID Workshop, 25-28 June 2000, Enschede, The Netherlands

14 H. Schulz, D. Lebedev, H.-C. Scheer, K. Pfeiffer, G. Bleidissel, G. Gruetzner and J. Ahopelto, J.Vac.Sci.Technol.B, **18**, (2000), 3582-3585

15 K. Pfeiffer, M. Fink, G. Ahrens, G. Gruetzner, F. Reuther, J. Seekamp, S. Zankovych, C.M. Sotomayor Torres, I. Maximov, M. Beck, M. Graczyk, L. Montelius, H. Schulz, H.-C. Scheer and F. Steingrueber, Microelectronic Engineering, **61-62** (1), (2002), 393-398

16 Ch. Finder, M. Beck, J. Seekamp, K. Pfeiffer, P. Carlberg, I. Maximov, F. Reuther, E.-L. Sarwe, S. Zankovych, J. Ahopelto, L. Montelius, C. Mayer and C.M. Sotomayor Torres, Microelectronic Engineering, **67-68C**, (2003) 623-628

17 M. Hatzakis, J. Electrochem. Soc. **116**, (1969), 1033-1037

18 M. McCord and M. Rooks, 1997, in book *Handbook of Microlithography, Micromachining and Microfabrication*, ed. P. Rai-Choudhury, (Washington: SPIE Optical Engineering Press), p.139-250

19 S.P. Beaumont, P.G. Bower, T. Tamamura and C.D.W. Wilkinson, Appl.Phys.Lett., **38**, (1981), 436-439

20 L.D. Jackel, R.E. Howard, E.L. Hu, D.M. Tennant and P. Grabbe, Appl.Phys.Lett., **39**, (1981), 268-270

21 W. Chen and H. Ahmed, Appl.Phys.Lett., **62**, (1993), 1499-1501

22 C. Vieu, M. Mejias, F. Ceicenac, G. Gaini and H. Launois, Microelectronic Engin., **35**, (1997), 253-256

23 H.G. Craighead, R.E. Howard, L.D. Jackel and P.M. Mankiewich, Appl.Phys.Lett., **42**, (1983), 38-40

24 S.Y. Chou, M.S. Wei, P.R. Krauss, P.B. Fisher and B.A. Fisher, J.Appl.Phys., **76** (10), (1994), 6673-6675

25 G. Binnig, C.F. Quate and Ch. Gerber, Phys.Rev.Lett., **56**, (1986), 930-933

26 S. Zankovych, T. Hoffmann, J. Seekamp, J-U. Bruch and C.M. Sotomayor Torres, Nanotechnology, **12**, (2001), 91-95

27 A. Yoshida, Y. Kojima, K. Matsuoka, Y. Tomo, I. Shimizu and M. Yamabe, Microelectronic Engineering, **53**, (2000), 313-316

28 M. Kotera, T. Yamada and Y. Ishida, Jpn.J.Appl.Phys., **41**, (2002), 4150-4156

29 T. Nakasigi, A. Ando, R. Inanami, N. Sasaki, K. Sugihara, M. Miyoshi and H. Fujioka, Jpn.J.Appl.Phys., **41**, (2002), 4157-4162

30 G. Strobl, 1997, *The Physics of Polymers: concepts for understanding their structures and behavior*, 2nd Edition (Berlin: Springer)

31 K. Pfeiffer, F. Reuther, M. Fink, G. Gruetzner, N. Roos, H. Schulz, H.-C. Scheer, J. Seekamp, S. Zankovych, C.M. Sotomayor Torres, I. Maximov, L. Montelius and Ch. Cardinaud, Microelectronic Engineering, **67-68C**, (2003), 266-273

32 M. Behl, J. Seekamp, S. Zankovych, C.M. Sotomayor Torres, R. Zentel and J. Ahopelto, Adv.Mater. **14**, (2002), 588-591

33 K. Pfeiffer, M. Fink, G. Bleidiessel, G. Gruetzner, H. Schulz, H.- C. Scheer, T. Hoffmann, C.M. Sotomayor Torres, F. Gaboriau and Ch. Cardinaud, Microelectronic Engineering **53**, (2000), 411-414

34 H. Schulz, H.-C. Scheer, T. Hoffmann, C.M. Sotomayor Torres, K. Pfeiffer, G. Bleidiessel, G. Grützner, Ch. Cardinaud, F. Gaboriau, M.C. Peignon, J. Ahopelto and B. Heidari, J Vac Sci Technol B **18**, (2000), 1861-1865

35 L.-H. Lee, 1980, *Adhesion and adsorption of polymers*, (New York: Plenum Press)

36 R.W. Jaszewski, H. Schift, P. Groning and G. Margaritondo, Microelectronic Engineering, **35**, (1997), 381-384

37 H. Schulz, H.-C. Scheer, F. Osenberg and J. Engemann, Proc.SPIE **3996**, (2000), 244-249

38 J. Brandrup and E.H. Immergut, 1975, *Polymer Handbook*, 2nd Ed., (New York: Willey)

39 T.G.I. Ling, M. Beck, R. Bunk, E. Forsén, J.O. Tegenfeldt, A.A. Zakharov and L. Montelius, Microelectronic Engineering, **67-68**, (2003), 887-892

40 I. Martini, M. Kamp, F. Fischer, L. Worschech, J. Koeth and A. Forchel, Microelectronic Engineering, **57-58**, (2001), 397-403

41 J. Moosburger, M. Kamp, F. Klopf, M. Fischer and A. Forchel, Microelectronic Engineering, **57-58**, (2001), 1017-1021

42 J. Braithwaite, M. Silver, V.A. Wilkinsol, E.P. O'Reilly and A.R. Adams, Appl.Phys.Lett., **67**(24), (1995), 3546-3548

43 Z. Yu, J. Steven, J. Schablitsky and S.Y. Chou, Appl.Phys.Lett., **74**, (1999), 2381-2383

44 D. Reuter, D. Kahler, U. Kunze and A.D. Wieck, Semicond. Sci. Technol. **16**, (2001), 603-607

45 P. Ramvall, N. Carlsson, P. Omling, L. Samuelson, W. Seifert, M. Stolze, and Q. Wang, Appl.Phys.Lett., **68**, (1996), 1111-1113

46 (a) On-line database "*New Semiconductor Materials. Characteristics and Properties: Heterostructures*", http://www.ioffe.rssi.ru/SVA/NSM/; (b) C. Weisbuch and B. Vinter, 1991, *Quantum Semiconductor Structures. Fundamentals and Applications*, (San Diego, CA: Academic Press Inc.)

47 S. Zankovych, I. Maximov, I. Shorubalko, J. Seekamp, M. Beck, S. Romanov, D. Reuter, P. Schafmeister, A.D. Wieck, J. Ahopelto, C.M. Sotomayor Torres and L. Montelius, Microelectronic Engineering, **67-68C**, (2003), 214-220

48 I. Maximov, P. Carlberg, I. Shorubalko, E.-L. Sarwe, W. Seifert, A. Song, H.Q. Xu, L. Montelius and L. Samuelson, paper presented at the 16th Workshop on Compound Semiconductor Devices and Integrated Circuits held in Europe, 21-25.05.2002, Chernogolovka, Russia, p.79

49 M. Hikita, R. Yoshimura, M. Usui, S. Tomaru and S. Imamura, Thin Solid Films, **331**, (1998), 303-308

50 E. Toussaere, N. Bouadma and J. Zyss, Opt.Mater., **9**, (1998), 255-258

51 N. Keil, H.H. Yao and C. Zawadzki, Appl.Phys.B, **73**, (2001), 619-622

52 X. Lu, D. An, L. Sun, Q. Zhou and R.T. Chen, Appl.Phys.Lett., **76**, (2000), 2155-2157

53 N. Ooba, S. Toyoda and T. Kurihara, Jpn.J.Appl.Phys, **39**, (2000), 2369-2371

54 D. Chen, H.R. Fetterman, A. Chen, W.H. Steier, L.R. Dalton, W. Wang and Y. Shi, Appl.Phys.Lett., **70** (25), (1997), 3335-3337

55 J. Seekamp, S. Zankovych, A.H. Helfer, P. Maury, C.M. Sotomayor Torres, G. Böttger, C. Liguda, M. Eich, B. Heidari, L. Montelius and J. Ahopelto, Nanotechnology, **13**, (2002), 581-586

56 M.L. Schattenburg, presented at Symposium and Summer School on Nano and Giga Challenges in Microelectronics, September 12, 2002, Moscow, Russia

57 D.A. Mendels, 11th MEL-ARI/NID Workshop, 5-7 February 2003, Toulouse, France

Annex A. List of publications and presentations appearing during this work

Papers:

I. S. Zankovych., T. Hoffmann, J. Seekamp, J-U. Bruch and C.M. Sotomayor Torres, *Nanoimprint Lithography: Challenges and Prospects*, Nanotechnology, **12**, (2001), 91-95

II. C.M. Sotomayor Torres, K. Pfeiffer, T. Hoffmann, J. Seekamp, S. Zankovych and C. Clavijo Cedeño, *Nanoimprint Lithography: exploring some options*, PHANTOMS Newsletter, No.1, July 2001

III. J. Seekamp, S. Zankovych, A.H. Helfer, P. Maury, C.M. Sotomayor Torres, G. Böttger, C. Liguda, M. Eich, B. Heidari, L. Montelius and J. Ahopelto, *Nanoimprinted Passive Optical Devices*, Nanotechnology, **13**, (2002), 581-586

IV. K. Pfeiffer, M. Fink, G. Ahrens, G. Gruetzner, F. Reuther, J. Seekamp, S. Zankovych, C.M. Sotomayor Torres, I. Maximov, M. Beck, M. Graczyk, L. Montelius, H. Schulz, H.-C. Scheer and F. Steingrueber, *Polymer Stamps for Nanoimprinting*, Microelectronic Engineering, **61-62** (1), (2002), 393-398

V. C. Clavijo Cedeño, J. Seekamp, A.P. Kam, T. Hoffmann, S. Zankovych, C.M. Sotomayor Torres, C. Menozzi, M. Cavallini, M. Murgia, G. Ruani, F. Biscarini, M. Behl, R. Zentel and J. Ahopelto, *Nanoimprint lithography for organic electronics*, Microelectronic Engineering, **61-62** (1), (2002), 25-31

VI. C.M. Sotomayor Torres, S. Zankovych, J. Seekamp, A.P. Kam, C. Clavijo Cedeño, T. Hoffmann, J. Ahopelto, F. Reuther, K. Pfeiffer, G. Bleidiessel, G. Gruetzner, M.V. Maximov and B. Heidari, *Nanoimprint Lithography: an alternative nanofabrication approach*, Materials Science and Engineering C, **23**, (2003), 23-31

VII. S. Zankovych, I. Maximov, I. Shorubalko, J. Seekamp, M. Beck, S. Romanov, D. Reuter, P. Schafmeister, A.D. Wieck, J. Ahopelto, C.M. Sotomayor Torres and L. Montelius, *Nanoimprint-induced Effects on Electrical and Optical Properties of Quantum Well Structures*, Microelectronic Engineering, **67-68C**, (2003), 214-220

VIII. K. Pfeiffer, F. Reuther, M. Fink, G. Gruetzner, P. Carlberg, I. Maximov, L. Montelius, J. Seekamp, S. Zankovych, C.M. Sotomayor Torres, H. Schulz and H.-C. Scheer, *A comparison of thermally and photochemically cross-linked polymers for nanoimprinting*, Microelectronic Engineering, **67-68C**, (2003), 266-273

IX. Ch. Finder, M. Beck, J. Seekamp, K. Pfeiffer, P. Carlberg, I. Maximov, F. Reuther, E.-L. Sarwe, S. Zankovych, J. Ahopelto, L. Montelius, C. Mayer and C.M. Sotomayor Torres, *Fluorescence microscopy for quality control in nanoimprint lithography*, Microelectronic Engineering, **67-68C**, (2003), 623-628

X. M. Behl, J. Seekamp, S. Zankovych, C.M. Sotomayor Torres, R. Zentel and J. Ahopelto, *Towards plastics electronics: Patterning semiconducting polymers by Nanoimprint Lithography*, Advanced Materials, **14**, (2002), 588-591

Conference presentations:

I. *Electron Beam Lithography for Optical Applications***,** S. Zankovych, J. Seekamp, J-U. Bruch, L. Bruchhaus and C.M. Sotomayor Torres, NATO ARW/Spring School on Nano-optoelectronics, 21-27 May 2000, Kiev, Ukraine.

II. *Nanoimprint Lithography with 30 nm resolution*, S. Zankovych, J. Seekamp, V. Zuev, C.M. Sotomayor Torres and J. Ahopelto, 6th MEL-ARI/NID Workshop, 25-28 June 2000, Enschede, Netherlands.

III. *Nanoimprinted Optical Devices: Exploring Properties and Potential for Integrated Optics*, J. Seekamp, S. Zankovych, T. Maka, C.M. Sotomayor Torres, G. Böttger, C. Liguda, M. Eich, B. Heidari, L. Montelius and J. Ahopelto, Trends in Nanotechnology Conference TNT2000, 16-20 October 2000, Toledo, Spain.

IV. *Nanoimprinting: Potentials for Integrated Optics and Bioapplications*, J. Seekamp, S. Zankovych, T. Maka, C.M. Sotomayor Torres and J. Ahopelto, 7th MEL-ARI/NID Workshop, 7-9 February 2001, Barcelona, Spain.

V. *Nanoimprinting of a UV- and electron beam-sensitive polymer and investigation of possible damage by nanoimprinting*, S. Zankovych, J. Seekamp, C. Clavijo Cedeno, C.M. Sotomayor Torres, J. Ahopelto, K. Pfeiffer, D. Reutera and A. Wieck, 8th MEL-ARI/NID Workshop, 4-6 July 2001, Wuerzburg, Germany

VI. *Nanoimprint Lithography as a Flexible nm-Accurate Fabrication Technique*, S. Zankovych, J. Seekamp, C. Akbayir, C. Clavijo-Cedeno, T. Maka, C.M. Sotomayor Torres, 1st Materialwissenschaftliches Forum, 9 November 2001, Wuppertal, Germany

VII. *Nanoimprint Lithography for Optical Applications*, S. Zankovych, J. Seekamp, T. Maka, C.M. Sotomayor-Torres, G. Böttger, C. Liguda, M. Eich, B. Heidari, L. Montelius and J. Ahopelto, Workshop on Nanoimprint Lithography, 16-17 January, 2002, Lund, Sweden

VIII. *NIL as a Promising Technique Towards Nano-electronic Device Fabrication*, C. Clavijo-Cedeño, J. Seekamp, A.P. Kam, T. Hoffmann, S. Zankovych, C.M. Sotomayor Torres, F. Biscarini, M. Murgia, M. Behl, R. Zentel and J. Ahopelto, Workshop on Nanoimprint Lithography, 16-17 January, 2002, Lund, Sweden

IX. *Challenges for Nanoimprint Lithography below 100 nm*, J. Seekamp, S. Zankovych, C.E. Clavijo Cedeño, A.P. Kam, F. Bulut, C.M. Sotomayor Torres, K. Pfeiffer, M. Fink, G. Ahrens, G. Gruetzner and F. Reuther, Workshop on Nanoimprint Lithography, 16-17 January, 2002, Lund, Sweden

X. *Adhesion effects in nanoimprinting*, S. Zankovych, J. Seekamp, C.M. Sotomayor Torres, I. Maximov, M. Beck, L. Montelius, H. Schulz, N. Roos, H.-C. Scheer, Ch. Finder, C. Mayer, K. Pfeiffer, F. Reuther, M. Fink, G. Gruetzner, J. Ahopelto and T. Haatainen, Nanoimprint and Nanoprint Technology NNT 2002, 11-13 December, 2002, San Francisco, CA USA

XI. *Development and characterisation of resists for low temperature nanoimprint lithography*, K. Pfeiffer, F. Reuther, J. Seekamp, H.-C. Scheer, M. Fink, S. Zankovych, C.M. Sotomayor Torres, H. Schulz, L. Montelius, C. Mayer, J. Ahopelto, Ch. Cardinaud and G. Gruetzner, Nanoimprint and Nanoprint Technology NNT 2002, 11-13 December, 2002, San Francisco, CA USA

XII. *Effects of Nanoimprint Lithography on Electrical and Optical Properties of GaInAs/InP and AlGaAs/GaAs Quantum Well Structures*, I. Maximov, S. Zankovych, I. Shorubalko, M. Beck, W. Seifert, J. Seekamp, S. Romanov, D. Reuter, P. Schafmeister, A.D. Wieck, Ch. Cardinaud, G. Gruetzner, C. Mayer, J. Ahopelto, H.-C. Scheer, C.M. Sotomayor Torres and L. Montelius, Nanoimprint and Nanoprint Technology NNT 2002, 11-13 December, 2002, San Francisco, CA USA

XIII. *Nanoimprinted Active and Passive Devices*, I. Maximov, P. Carlberg, M. Beck, D. Wallin, J. Seekamp, S. Zankovych, T. Haatainen, J. Salmi, E-L. Sarwe, H.-C. Scheer, Ch. Cardinaud, G. Gruetzner, F. Reuther, K. Pfeiffer, C.M. Sotomayor Torres, J. Ahopelto and L. Montelius, Nanoimprint and Nanoprint Technology NNT 2002, 11-13 December, 2002, San Francisco, CA USA

XIV. *Fluorescence Microscopy as a New Method for Quality Control in Nanoimprint Lithography*, Ch. Finder, M. Beck, J. Seekamp, K. Pfeiffer, P. Carlberg, I. Maximov, F. Reuther, E.-L. Sarwe, S. Zankovych, J. Ahopelto, C.M. Sotomayor Torres, L. Montelius and C. Mayer, Nanoimprint and Nanoprint Technology NNT 2002, 11-13 December, 2002, San Francisco, CA USA

XV. *Technology of Nanoimprint Stamps with Sub-100 nm Features*, I. Maximov, M. Beck, E-L. Sarwe, S. Zankovych, P. Carlberg, H.-C. Scheer, Ch. Cardinaud, G. Gruetzner, F. Reuther, K. Pfeiffer, C.M. Sotomayor Torres, T. Haatainen, J. Salmi, J. Ahopelto and L. Montelius, Nanoimprint and Nanoprint Technology NNT 2002, 11-13 December, 2002, San Francisco, CA USA

XVI. *Mechanical Properties of NIL Polymer Lines*, D.-A. Mendels, S. Zankovych and C.M. Sotomayor Torres, Nanoimprint and Nanoprint Technology NNT 2002, 11-13 December, 2002, San Francisco, CA USA

XVII. *Nanoimprint-Induced Effects on Electrical and Optical Properties of Quantum Well Structures*, S. Zankovych, J. Seekamp, S. Romanov, C.M. Sotomayor Torres, I. Maximov, I. Shorubalko, M. Beck, L. Montelius, D. Reuter, P. Schafmeister, A.D. Wieck and J. Ahopelto, DPG Frühjahrstagung des Arbeitskreises Festkörperphysik, 24-28 March, 2003, Dresden, Germany

Talks:

I. *Nanoimprint Lithography with 30 nm resolution*, S. Zankovych, 6th MEL-ARI/NID Workshop, 25-28 June 2000, Enschede, Netherlands

II. *Nanoimprint Lithography*, S. Zankovych, 1. Nanotechnologie Workshop des IMW, 21-23 March 2001, Travemünde, Germany.

III. *Nanoimprinting of a UV- and electron beam-sensitive polymer and investigation of possible damage by nanoimprinting*, S. Zankovych, 8th MEL ARI/NID Workshop, 4-6 July 2001, Wuerzburg, Germany

IV. *Nanoimprint-induced Effects on Electrical and Optical Properties of Quantum Well Structures*, S. Zankovych, MNE 2002, 16-19 September, 2002, Lugano, Switzerland

V. *Fluorescence microscopy for quality control in nanoimprint lithography*, S. Zankovych, MNE 2002, 16-19 September, 2002, Lugano, Switzerland

VI. *Potentials of nanoimprint lithography for optical applications*, S. Zankovych, Seminar at Lehrstuhl für angewandte Festkörperphysik (Prof.Dr.A.D. Wieck), Ruhr-Universität Bochum, 7 February, 2003, Bochum, Germany